An experimental and modeling study of carbon nanomaterial membranes, bacterial growth, and their interactions towards Pb(II) removal from wastewater

An experimental and modeling study of carbon nanomaterial membranes, bacterial growth, and their interactions towards Pb(II) removal from wastewater

By:
Cassandra Chidiac, B.Eng

A Thesis Submitted to the School of Graduate Studies
in Partial Fulfillment of the Requirements for the Degree
Master of Applied Science

McMaster University
August 2020

McMaster University MASTER OF APPLIED SCIENCE (2020) Hamilton, Ontario (Chemical Engineering)

TITLE: An experimental and modeling study of carbon nanomaterial membranes, bacterial growth, and their interactions towards Pb(II) removal from wastewater

AUTHOR: Cassandra Chidiac, B.Eng (McMaster University)
SUPERVISORS: Dr. Charles de Lannoy and Dr. Younggy Kim
NUMBER OF PAGES: 86

Abstract

Pb(II) removal is imperative due to its inherent toxicity at low levels and its tendency to accumulate in ecosystems. Conductive carbonaceous nanomaterials (CCNs), such as carbon nanotubes (CNTs) and carbon nanofibers (CNFs), have recently gained the interest of researchers due to their superior properties and ease of functionalization. The aim of this study is to utilize CCNs for Pb(II) removal within membrane technology and bioremediation strategies.

Membranes have shown promise in their treatment abilities, producing excellent effluent quality while reducing plant footprints. The integration of CNTs within membrane technology provides an opportunity to couple its removal capacity with Pb(II) removal that exhibits regeneration capabilities. However, membrane fouling can be problematic for membrane longevity and regeneration. CNTs have also shown to be capable of mitigating fouling via electrostatic repulsion and pollutant degradation. However, little work has been conducted on its fabrication. In this work, CNTs were incorporated with poly(vinyl) alcohol (PVA) in thin film composites, where the effects of PVA chain length and degree of crosslinking were investigated. It was found that a pseudo-optimal coating can be obtained using 31-50kDa PVA with 10% crosslinking. This combination lead to a highly permeable, hydrophilic surface with good electrical conductivity that exhibited a molecular weight cut off of 2000kDa.

Biosorption has shown promise in Pb(II) removal in the lab scale but its large-scale use is hindered from rapid saturation of binding sites and low regeneration abilities. Exoelectrogens were proposed as reactive biosorbents to couple biosorption with bioreduction in an attached growth configuration. CCNs were investigated as bacterial scaffolds, where their efficacy and Pb(II) dosage concentration was studied. It was found that CNFs were superior in removing Pb(II), exhibiting Pb(II) concentrations $\leq$0.10 ppm where removal increased when Pb(II) dosage increased from 0.5 to 5ppm. SEM-EDX analysis provided evidence that bioreduction dominated Pb(II) removal. A long-term study was further conducted using CNFs, revealing its robustness in long term removal over suspended growth reactors with a sustained removal of $\approx$ 80%. A numerical model was further proposed which exhibited a goodness of fit with an R^2 of 0.92. This model confirmed that bioreduction dominated Pb(II) removal and revealed biofilm thickness and Monod kinetics to be the main influential parameters on Pb(II) removal.

Acknowledgements

First and foremost, I would like to thank both of my supervisors, Dr. Charles de Lannoy and Dr. Younggy Kim for their guidance and encouragement in the duration of my Masters. I really appreciate both always making themselves available to me and fostering in my growth in professionalism and academia during my time at McMaster. I would further like to extend gratitude to Monica Han, who would always help me in the lab when needed. I am also grateful to my supervisory committee member, Dr. Carlos Felipe for his time and expertise.

I would further like to express my gratitude to my lab members as well as to all my friends I have made during my time McMaster, who always supported me throughout my journey. I would like to extend this further to Hyejin Lee, who was truly a mentor to me and always provided me with guidance during my Masters. Lastly, I would like to express my appreciation to both my parents Samir and Terry Chidiac. Thank you for your love and encouragement throughout my Masters. Your constant support truly aided in my journey and I would not be where I am today without both of you. I am honored to have both of you as role models.

Table of Contents

Lists of Figures

List of Tables

1.0 Introduction

1.1 Pb(II) Sources, Hazards and Conventional Treatments

The release of Pb(II) into the environment is ubiquitous due to its wide use in industries, such as metal plating, batteries, mining operations, and electrical cables (Brink et al., 2019; Colantonio and Kim, 2016). Concerns around its release stems from its level of toxicity. Pb(II) has been listed by the USA Environmental Protection Agency (EPA) as one of the hazardous inorganic wastes that is both mutagenic and teratogenic. Specifically, Pb(II) can cause neurodegenerative impairment, renal failure, reproductive failure and even cancer, where its detrimental effects are further exaggerated in children (Naik and Dubey, 2013). Even at low concentrations (<10mg/L, ppm) Pb(II) interrupts endocrine activities in vulnerable species and can eradicate ecosystems at >1000ppm (Brink et al., 2019). Due to its devastating effects, the world health organization (WHO) has limited its discharge into environments to levels of <0.01ppm (Naik and Dubey, 2013).

Its inherent properties of non-biodegradability and stability make Pb(II) removal difficult from environments (Colantonio and Kim, 2016). Conventional methods that have been used to remove Pb(II) are chemical precipitation, ion-exchange, membrane filtration and electrochemical methods (Fu and Wang, 2010). Chemical precipitation can remove Pb(II) economically but produces toxic sludge that in turn creates difficulties in its disposal. Similarly, ion-exchange has the capacity to remove Pb(II) but its use is hindered due to the strong acids required for resin regeneration which is problematic in terms of secondary pollution. Membrane filtration and electrochemical methods both efficiently remove Pb(II) but are found to be too costly in terms of operational and capital costs. Thus, there is a present need to find both an economical and efficient mode to treat Pb(II) contaminated waters.

1.2 Conductive Carbonaceous Nanomaterials for Pb(II) Removal

Conductive carbonaceous nanomaterials (CCNs), such as carbon nanotubes (CNTs) and carbon nanofibers (CNFs), have gained the attention of researchers due to their excellent properties of good electrical conductivity, high porosity, high surface area and excellent mechanical properties (Mohamed, 2016; Shan et al., 207). Through their ease of functionalization via acid treatments and doping, CCNs' use has been universalized, ranging from sensors to biomedical applications (Nikoleli et al., 2018). The focus of this research is to implement CCNs' within membrane technologies and bioremediation methods to improve their efficiencies in removing Pb(II) from water sources. Further, a tangential goal of this research was to use numerical modelling for CCNs in bioremediation removal of Pb(II). CCNs may convolute the mechanisms involved which complicate the full understanding of the system at hand. Numerical modelling may be a solution to decouple mechanisms and gain a full understanding of the proposed systems. The following sections will highlight the efficacy these materials have shown in the respective fields and constructed models that are useful in predicting bioremediation of Pb(II) using CCNs.

1.3 Conductive Carbonaceous Nanomaterials in Membrane Technology

1.3.1 Membrane Technology and its potential in Pb(II) removal

In recent years, membrane filtration has been highlighted as both an economical and efficient method for cleaning a wide variety of water sources. This technology uses low pressures to drive water flow through a membrane which acts as a physical barrier for feed contaminants (Formoso et al., 2017). Typically, the membrane used is a porous structure which separates the feed constituents based on size-exclusion, rejecting organics and other contaminants from the influent. A schematic of this membrane filtration process can be seen in Figure 1. Within the realm of membrane filtration, ultrafiltration (UF) has peaked the interest of researchers due to its relatively high permeability and ability to produce excellent effluent quality (Bai et al., Dudchenko et al., 204; Zhang and Vecitis, 2014). Further, it has been found to handle feed quality fluctuations while reducing conventional wastewater treatment plants' footprint via replacing the typical processes used (i.e. coagulation, sedimentation, and granular filtration).

In addition to creating an effective mode to treat waters, membrane technology provides a viable surface for the implementation of CCNs. Specifically, the implementation of CNTs to UF membranes may provide an efficient mode to couple the treatment capabilities of UF with the excellent Pb(II) adsorption properties exhibited with CNTs. CNTs are rolled up sheets of graphene which exhibit continuous sp^2 hybridized bonds along their lengths. Their popularization in Pb(II) removal stems from their high surface area, chemical inertness, and ease of functionalization. Further, acid treated CNTs are well known in literature to have high affinity for Pb(II) through their intrinsic mechanisms of surface complexation, electrostatic interaction, and ion-exchange (Gupta et al., 2015).

Not only do CNTs create a surface with excellent Pb(II) adsorption abilities, it also provides a surface that can be regenerated in an environmentally benign process. A study conducted by Ganzoury et al., has shown that expensed CNTs can be regenerated using electrochemical methods, showing 90% recovery over 4 consecutive adsorption cycles (Ganzoury et al, 2020). This can alleviate the costs of these adsorbents while creating a closed-loop process that avoids the addition of harmful chemicals. Thus, implementing CNTs as adsorbents for Pb(II) in membrane technology may create a treatment method that can produce excellent effluent quality while providing an environmentally friendly and efficient means of removing Pb(II).

1.3.1 Current Challenges in Membrane Technology

Although this technology provides a viable method to produce excellent effluent quality while simultaneously removing Pb(II), the prevalence of membrane fouling may be problematic. Membrane fouling can be problematic as it can reduce the CNT networks' conductivity as well as the membrane longevity. Thus, to preserve the regeneration abilities proposed for Pb(II) removal as well as the membrane's lifetime, the hurdle of membrane fouling must be addressed. As seen by Figure 1, membrane fouling involves the deposition of dissolved and suspended particles/colloids within the surface or pores of the membrane (Ahmed et al., 2016; Formoso et al., 2017; Lalia et al., 2015; Lee et al., 2004). Fouling occurs within three distinct processes. First there is pore constriction due to small particles passing through the membrane and subsequently adsorbing onto the pores. This in turn,

reduces the pore size and increases water flow resistance. Subsequently, the second phase of pore blocking commences due to their physical blockage as particles continue to adhere onto them. Eventually, this leads to the third stage of fouling which involves the formation of a cake layer. This cake layer is produced from the accumulation of deposited macromolecules and colloids on the membrane surface which in turn creates a dense gel layer. This final fouling stage causes a severe increase in water resistance which often leads to membrane replacements.

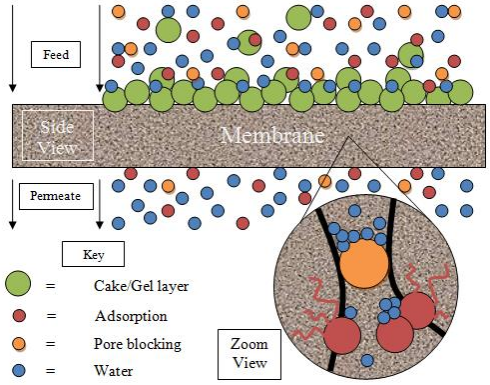

Figure 1. Schematic of membrane filtration along with the fouling mechanisms involved (Verona et al, 2013).

In addition to particle deposition, biofouling can be problematic in UF technology. Due to the advective transport of organics as well as nutrients, bacteria can easily adhere onto the membrane and thrive (Hong et al., 2008). Once adhered, the bacteria have the capacity to produce extra polymeric substance (EPS), a sticky product that promotes further cell adherence and eventually the formation of biofilms on the membrane surface. Biofilms impose irreversible membrane damage, shortening their lifetime and inherently increasing their operational and maintenance costs. Thus, there is a present need to find an active solution which can both reduce organic and bacterial adherence onto the membrane surface, so it may be used as an active means of removing Pb(II) and other water contaminants.

1.3.2 CNTs as Electrically Conductive Membranes in Membrane Technology

CNTs as electrically conductive membranes (ECMs) have also been the interest of researchers as an efficient method to reduce membrane fouling due to their fast electron transport, high surface area, antimicrobial properties and fast water transport abilities (Bai et al., 2015; de Lannoy et al., 2012; de Lannoy et al., 2013; Hong et al., 2008; Lalia et al., 2015; Sun et al., 2012; Yeung et al., 2020; Yi et al., 2018). CNTs as ECMs can alleviate membrane fouling via adjusting the surface charge of the membrane and in turn minimizing particle and bacterial deposition. This can be accomplished by pollutant degradation as well as electrostatic repulsion and H_2(g) bubbling on the membrane when positive and negative potentials are applied, respectively (de Lannoy et al., 2013; Yang et al., 2018). An applied potential can further induce antifouling mechanisms through the promotion of local pH changes and the production of radicals and hydrogen peroxide, as these create unsuitable conditions for bacteria (Hong et al., 2008). The main antifouling removal mechanisms invoked by ECMs can be visualized in Figure 2.

Extensive research has been employed to show the efficacy of CNT networks in reducing fouling while aiding in membrane rejection and selectivity. For instance, in the work by Yi et al. CNT coatings were implemented on polyether sulfone (PES) supports to show its efficacy in recovering permeate fluxes after filtering soybean oil-in-water emulsion (Yi et al., 2018). After 120 minutes, the permeate flux of the thin film was 2.02 and 11.43 times than that of the poly(vinyl) difluoride (PVDF) and PES support membranes, respectively. Furthermore, backflushing operations were imposed to show the films' resistance to irreversible fouling. This revealed that the coated membranes could recover a flux that was 1.49 and 7.71 times than that of PVDF and the PES support membranes. Dudchenko et al. used CNT networks to show the thin films' capability to prevent fouling from alginic acid compared to its support membrane comprised of polysulfone (PS) (Dudchenko et al., 2014). It was shown that with the thin film coating reduced the transmembrane pressure by 24% and 51% when -3V and -5V were applied, respectively. This was found to be attributed to the strong electrostatic repulsive forces created on the thin film. Further, -5V further eliminated fouling when Ca^{2+} was added, which normally forms a gelatinous mass on membranes when in contact with alginic acid. In terms of biofouling, Ronen et al. revealed the CNT thin film's capacity to prevent biofouling on the membranes (Yi et al., 2018). Specifically, it was shown that an applied voltage of 1V and 1.5V could detach 71% and 86% of bacteria present. This was attributed to the thin film's capability to increase the bacterial mobility on the membrane surface while producing the antimicrobial product, hydrogen peroxide.

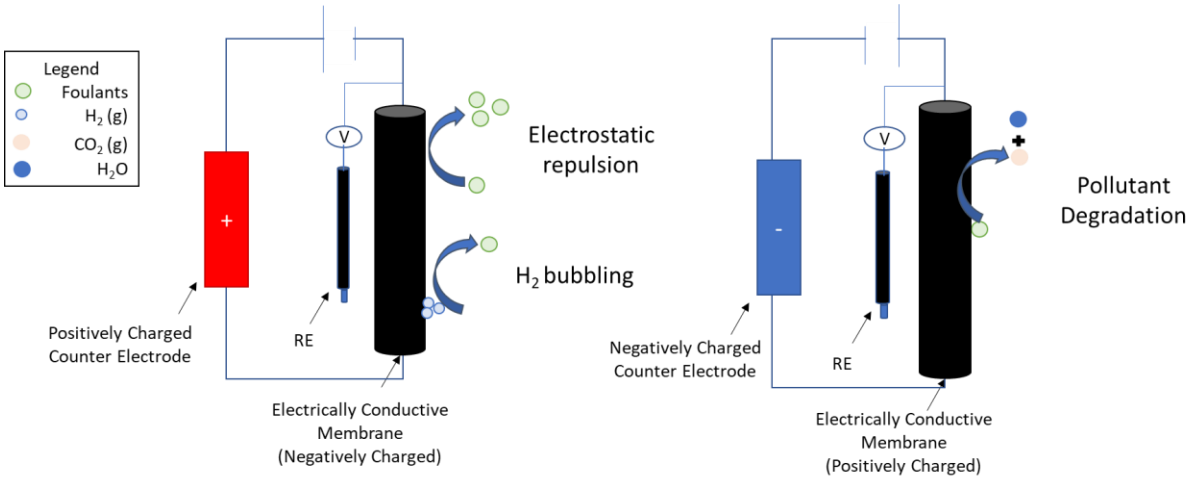

Figure 2. Electrically conductive membranes' main antifouling mechanisms on UF membranes when applied under negative and positive potentials.

1.3.3 Current Efforts on CNT-PVA Thin Films' Fabrication

To improve the antifouling mechanisms of the membranes, the fabrication of the ECMs must be optimized. The first consideration made in the aforementioned studies is the synthesis of CNTs as conductive thin films on polymeric supports. This was imperative as this mode of fabrication prevents the leaching of CNTs into receiving waters, which would in turn cause health hazards (Zhang and Vecitis, 2014). CNTs were further implemented as composites using the integration of the polymer, poly(vinyl) alcohol (PVA) for

stabilization. The synthetization of CNT thin films can be difficult due to their inherent hydrophobicity, inducing quick aggregation of the nanomaterials when introduced to polar solvents. One promising method to overcome this downfall is noncovalent polymer wrapping on the CNT lengths (Fujigaya and Nakashima, 2015; Bilalis et al., 2014). Specifically, it has been shown that the PVA can wrap around the CNT lengths through π-CH interactions and improve its overall hydrophilicity through the exposure of its hydroxyl groups. The improved hydrophilicity allows for the creation of stable suspensions that eases CNT vacuum deposition onto polymeric supports. Additionally, the exposure of its hydroxyl groups provides a more hydrophilic surface that can reduce the adherence of hydrophobic foulants, while providing an additional opportunity for the network to be crosslinked.

Although the synthesized CNT-PVA network has proven its efficacy in preventing fouling, little work has been put forward in optimizing its properties. The beginning works was conducted by de Lannoy et al. who first pioneered the CNT-PVA thin film crosslinked with succinic acid (de Lannoy et al., 2012). In this work, the thin film's conductivity, hydrophilicity, permeability, and rejection was optimized by investigating the impact of CNT:PVA weight ratio and curing time. This study highlighted that increasing curing time increased conductivity by invoking a greater degree of crosslinking and that the hydrophilicity of the thin film decreased with decreasing CNT:PVA mass ratio. Overall, it was found that a weight ratio of CNT:PVA of 1:10 with a curing time of 20 minutes lead to the most optimal membrane based on the metrics previously mentioned. Building on this work, Halali and de Lannoy used the previously optimized conditions and further investigated the effect of crosslinker lengths and degree of crosslinking on the network (Halali and de Lannoy, 2019). It was found that longer crosslinkers at a higher degree of crosslinking improved the overall permeance of the membrane, where only crosslinking length improved its conductivity. Lastly, it was found that these impacts had no baring on the membrane hydrophilicity.

1.4 Conductive Carbonaceous Nanomaterials for Bioremediation of Pb(II)

1.4.1 Bioremediation's Challenges and Advancements in Pb(II) Removal

In recent years, biosorption has caught the attention of researchers as a viable and economical solution to remove Pb(II) (Hörstmann et al., 2020). Biosorption entails the use of live or reconditioned biomasses as natural adsorbents that can remove Pb(II) through their intrinsic mechanisms of ion-exchange, electrostatic interactions, and complexations with their cell wall functional groups (Singh et al., 2020). The multitude of studies conducted have proven that these biosorbents have a high sorption capacity for Pb(II) in the lab-scale (Mohapatra et al., 2019; Singh et al., 2020). However, the regeneration and pilot scale studies of these materials have been found to be problematic. For instance, the few studies conducted on biosorbents' regeneration have shown that strong acids such as HCl and HNO_3 are required to recover just 60-80% of their initial sorption capacities with diminishing returns (Martin-Lara et al., 2011; Cechinel et al., 2017; Tran and Chao, 2018; Pandey et al., 2015). The use of these acids also further causes secondary pollution. Furthermore, the few studies conducted from pilot scales have shown that biosorbents' binding sites becomes quickly saturated within a few minutes to hours from the reduced

retention times, eliminating further Pb(II) removal and possibly causing the desorption of Pb(II) back into treated waters (Singh et al, 2020).

The use of exoelectrogenic bacteria as live, reactive biosorbents may alleviate the challenges associated with biosorption. Exoelectrogens encompasses a class of bacteria capable of transferring electrons extracellularly onto a variety of substrates using their pili or electron shuttles (Logan et al., 2019). Typically, these bacteria are used as catalysts in microbial fuel cells (MFCs) and in microbial electrolysis cells (MECs) to drive the production of electricity or H_2 depending if operated under open circuit, aerobic conditions or under an applied voltage aerobically or anaerobically, respectively (Logan et al., 2007;Logan et al., 2008). However, it was found by Colantonio and Kim that these bacteria have the capacity to use Pb(II) as their terminal electron acceptor when operated in MECs under anaerobic, open circuit conditions (Colantonio and Kim, 2016). Specifically, it was found that the MECs had a higher capacity of removing Pb(II) when the applied voltage was turned off, resulting in 83% of Pb(II) removal compared to the 57% removal observed at 0.6V. It was found that once exoelectrogens were deactivated with ethanol treatment, Pb(II) removal halted, proving the removal came from the exoelectrogens themselves.

From the measured anode potentials, it was found that exoelectrogens have the capacity to gain energy for growth by dumping their electrons on Pb(II) and reducing it to metallic Pb. This is advantageous as the bioconversion of Pb(II) to metallic Pb transforms the metal to a less mobile state which inherently lowers its cytotoxic effects. This same bioreduction phenomenon was also reported by a study conducted by Brink et al. which used Pb-resistance bacteria from industrial waste to remove 80ppm of Pb(II) in batch reactors (Brink et al., 2019). Overall, these reactors could achieve up to 76% removal of the Pb(II), where XPS confirmed the occurrence of bioreduction. It was found that the bacterial enzymes acted as catalysts to reduce the thermodynamic barrier and in turn allow for Pb(II) to be bioreduced to metallic Pb. Although there are limited studies on the bioreduction of Pb(II) itself, the occurrence of Cr(VI) and U(VI) bioreduction by the action of exoelectrogens is well reported in literature (Liu et al., 2002; Konishi et al., 2005; Tran and Chao, 2018; Iravani and Varma, 2020; Li et al., 2020; Wang et al., 2015; Thacher et al., 2015; Tekerlekopoulou et al., 2013).

1.4.2 Integration of Conductive Carbonaceous Nanomaterials in Bioremediation Removal of Pb(II)

Building on the shown bioreduction capacities of exoelectrogens, it is proposed to use these bacteria as reactive biosorbents to alleviate the challenges currently faced in the biosorption removal of Pb(II). Specifically, it is proposed to use these bacteria in an attached growth configuration utilizing conductive carbonaceous nanomaterials (CCNs). The use of CCNs such as carbon nanotubes (CNTs) and carbon nanofibers (CNFs) is proposed as their flexible structures have been shown to have high efficiency in capturing bacteria in solution (Akasaka and Watari, 2008). By these CCNs capturing bacteria, Pb(II) removal can be improved by: (1) enhancing direct electron transfer and (2) biofilm formation. The sp^2 hybridized bonds along the CCNs structures allow for fast electron transport along their lengths. This property along with their excellent Pb(II) adsorption capabilities, will allow them to co-adsorb Pb(II) with exoelectrogens and facilitate electron transfer between them

(Mahar et al., 2019),(Upadhyayula et al., 2009). This phenomenon was observed when CNTs were implemented in hydrogel beads to facilitate electron transfer between exoelectrogenic bacteria (*Geobacter, Pseudomonas* and *Bacillus*) and U(VI). The study conducted by Wang et al., showed that the incorporation of CNTs improved reduction rates from 53.6% to 98.4% through its promotion of electron transfer (Wang et al., 2015). The idea of electron shuttling was further realized in a study conducted by Thacher et al., which showed the electron shuttling capabilities of humic acids with the exoelectrogen, *Shewanella spp.* in a Cr(VI) reduction study. Specifically, this research group showed that through the electron shuttling abilities of humic acids, the reduction rate of Cr(VI) to Cr(III) could be increased from $6.1h^{-1}$ to $9.9h^{-1}$ (Thacher et al., 2015).

Moreover, the incorporation of biofilms on CCNs have been proven to further enhance the bioremediation of metals. Biofilms form from the adsorption of bacteria onto a substrate and the subsequent production of extra polymeric substance (EPS), causing a cascade of bacterial adsorption on the surface. It has been found that this polymeric matrix keeps cells close to one another, enhancing their inter-cellular communications and allowing for them to act in a coordinated manner. This has shown to improve cells resistance to toxic metals and their removal of Pb(II) in several studies (Black et al., 2014; Igiri et al., 2018; Tekerlekopoulou et al., 2013). Thus, the use of CCNs in an attached growth configuration with exoelectrogenic bacteria should yield a novel mode to remove Pb(II) that exhibits additional benefits compared to the conventional biosorption methods used presently.

1.5 Numerical Modeling in Bioremediation of Heavy Metals

Numerical modelling is proposed for the CCN attached growth reactors, as these materials convolute the removal mechanisms involved. As seen by Figure 3, the proposed reactor intrinsically combines the mechanisms: biosorption, bioreduction and CCN adsorption. This can be problematic for the full understanding of the system at hand which in turn is necessary for its optimization. The construction of a model that captures the transport and removal of Pb(II) as it propagates through the biofilm may be a viable solution to understand the mechanisms involved. Similar approaches have been carried out in Cr(VI) and U(VI) bioreduction studies for understanding removal trends, kinetics, and system optimization. For instance, Lin used a predictive model to investigate the causes for temporal variations in Cr(VI) removal when using *E.coli* grown on ceramic beads. The model further realized the reactor's kinetics which is necessary when considering its upscale (Lin, 2013). Similarly, Chirwa and Wang modelled the prevalence of cell inactivation in a pure culture biofilm when subjected to high Cr(VI) loading (Chirwa and Wang, 2004). This allowed the researchers to understand the removal capacity and kinetics of the reactor under different operational conditions.

Thacher et al. modelled Cr(VI) bioreduction using *Shewanella spp.* in aquifers. A sensitivity analysis identified the main influential parameters that determined the dynamic removal of Cr(VI) in the system (Thacher et al., 2015). Specifically, it revealed the significance of biomass concentration and Monod kinetics, while uncovering the insignificant role biofilm thickness had on its removal. Further, a reactive model constructed for an aquifer in Oak ridge, allowed researchers to establish the significance of sorption and desorption effects on U(VI) removal on site (Luo et al, 2007). By revealing

the significance of this phenomenon, the removal of U(VI) may be better controlled. Overall, predictive models have aided in researchers understanding of their designed reactors' kinetics and removal mechanisms that is useful in their optimization and upscale. It is therefor proposed to construct a model from a theoretical standpoint as a predictive tool for understanding the removal mechanisms of Pb(II) and the key parameters involved.

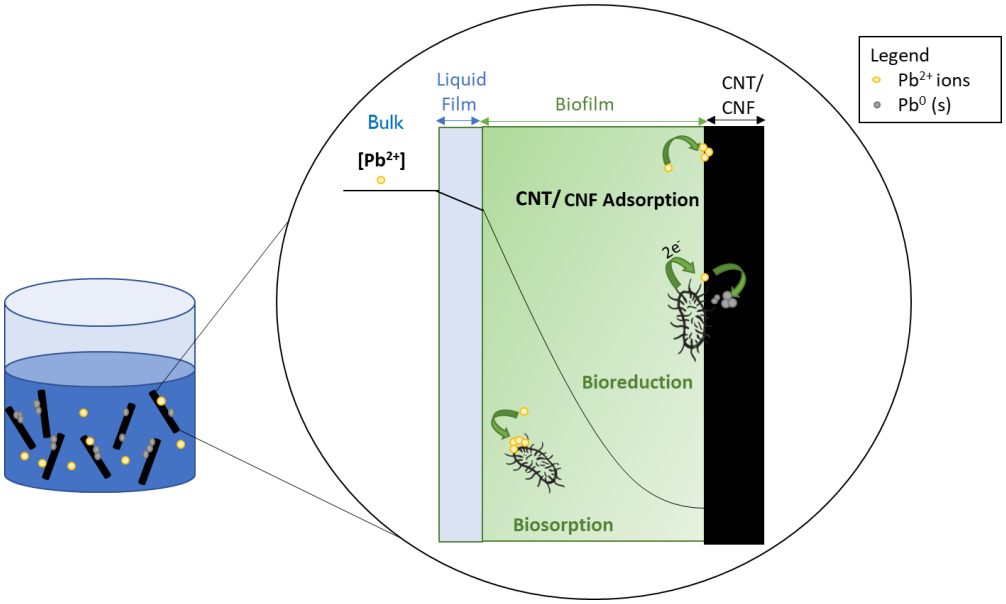

Figure 3. The schematic for the proposed CCN attached growth reactor with the predicted removal mechanisms and Pb concentration.

1.6 Research Objectives

The overall research objective of this study is to show the efficacy of CCNs in both membrane and bioremediation technologies that may alleviate current challenges faced in removing Pb(II). The following subsections will highlight the objectives for each chapter of the thesis.

1.6.1 Chapter 2 Objectives

The second chapter of this thesis used CNTs as CCNs in conductive thin film coatings to enhance antifouling properties of UF membranes. This was deemed necessary to utilize these thin films' as an active means for Pb(II) removal, as foulants would progressively eliminate their removal and regeneration abilities. To promote antifouling properties of the CNT networks, they were implemented with PVA for a stabilized network. The overall goals of this sections were to investigate the impact of PVA chain length and degree of crosslinking on the membrane's antifouling properties (i.e. electrical conductivity, water permeance and hydrophilicity).

1.6.2 Chapter 3 Objectives

The third chapter investigated CCNs' efficacy as bacterial scaffolds in the bioremediation removal of Pb(II). The goals involved in this study were: to determine if CCNs can enhance bioremediation removal of Pb(II), to investigate the efficacy of different CCNs on Pb(II)

removal, to understand the effect Pb(II) dosage concentration has on removal and to understand Pb(II) removal mechanisms within the proposed reactor.

1.6.3 Chapter 4 Objectives

The fourth chapter of this thesis employed CNFs as bacterial scaffolds to assess its efficacy in long term Pb(II) removal under multiple Pb(II) dosages. It also assessed the feasibility of numerical modelling as a predictive tool in determining the removal mechanisms involved in the reactor. The goals of this chapter were: to show the efficacy of the proposed CNF attached growth design for long term removal of Pb(II) in comparison to suspended growth reactors; to use numerical modelling to understand the removal mechanisms involved in the attached growth reactor; use the fitted model to predict the fate and removal of Pb(II) as it transports through the biofilm in the short and long term; and to perform a sensitivity analysis on model parameters to gain a further understanding on key parameters that can aid in the system's optimization.

1.7 References

Ahmed, F., Lalia, B. S., Kochkodan, V., Hilal, N., & Hashaikeh, R. (2016). Electrically conductive polymeric membranes for fouling prevention and detection: A review. Desalination, 391, 1–15. https://doi.org/10.1016/j.desal.2016.01.030

Akasaka, T., & Watari, F. (2009). Capture of bacteria by flexible carbon nanotubes. Acta Biomaterialia, 5(2), 607–612. https://doi.org/10.1016/j.actbio.2008.08.014

Bai, L., Liang, H., Crittenden, J., Qu, F., Ding, A., Ma, J., Du, X., Guo, S., & Li, G. (2015). Surface modification of UF membranes with functionalized MWCNTs to control membrane fouling by NOM fractions. Journal of Membrane Science, 492, 400–411. https://doi.org/10.1016/j.memsci.2015.06.006

Bilalis, P., Katsigiannopoulos, D., Avgeropoulos, A., & Sakellariou, G. (2014). Non-covalent functionalization of carbon nanotubes with polymers. RSC Adv., 4(6), 2911–2934. https://doi.org/10.1039/c3ra44906h

Black, R., Sartaj, M., Mohammadian, A., & Qiblawey, H. A. M. (2014). Biosorption of Pb and Cu using fixed and suspended bacteria. Journal of Environmental Chemical Engineering, 2(3), 1663–1671. https://doi.org/10.1016/j.jece.2014.05.023

Brink, H. G., Hörstmann, C., & Peens, J. (2019). Microbial Pb(II)-precipitation: the influence of oxygen on Pb(II)-removal from aqueous environment and the resulting precipitate identity. International Journal of Environmental Science and Technology, 17(1), 409–420. https://doi.org/10.1007/s13762-019-02502-4

Cechinel, M. A. P., Mayer, D. A., Mazur, L. P., Silva, L. G. M., Girardi, A., Vilar, V. J. P., de Souza, A. A. U., & Guelli U. de Souza, S. M. A. (2018). Application of ecofriendly cation exchangers (Gracilaria caudata and Gracilaria cervicornis) for metal ions separation and recovery from a synthetic petrochemical wastewater: Batch and fixed bed studies. Journal of Cleaner Production, 172, 1928–1945. https://doi.org/10.1016/j.jclepro.2017.11.235

Colantonio, N., & Kim, Y. (2016). Lead(II) Removal at the Bioanode of Microbial Electrolysis Cells. ChemistrySelect, 1(18), 5743–5748. https://doi.org/10.1002/slct.201601539

de Lannoy, C. F., Jassby, D., Davis, D. D., & Wiesner, M. R. (2012). A highly electrically conductive polymer–multiwalled carbon nanotube nanocomposite membrane. Journal of Membrane Science, 415–416, 718–724. https://doi.org/10.1016/j.memsci.2012.05.061

de Lannoy, C.-F., Jassby, D., Gloe, K., Gordon, A. D., & Wiesner, M. R. (2013). Aquatic Biofouling Prevention by Electrically Charged Nanocomposite Polymer Thin Film Membranes. Environmental Science & Technology, 47(6), 2760–2768. https://doi.org/10.1021/es3045168

de Lannoy, C.-F., Soyer, E., & Wiesner, M. R. (2013). Optimizing carbon nanotube-reinforced polysulfone ultrafiltration membranes through carboxylic acid functionalization. Journal of Membrane Science, 447, 395–402. https://doi.org/10.1016/j.memsci.2013.07.023

Dudchenko, A. V., Rolf, J., Russell, K., Duan, W., & Jassby, D. (2014). Organic fouling inhibition on electrically conducting carbon nanotube–polyvinyl alcohol composite ultrafiltration membranes. Journal of Membrane Science, 468, 1–10. https://doi.org/10.1016/j.memsci.2014.05.041

Formoso, P., Pantuso, E., De Filpo, G., & Nicoletta, F. (2017). Electro-Conductive Membranes for Permeation Enhancement and Fouling Mitigation: A Short Review. Membranes, 7(3), 39. https://doi.org/10.3390/membranes7030039

Fu, F., & Wang, Q. (2011). Removal of heavy metal ions from wastewaters: A review. Journal of Environmental Management, 92(3), 407–418. https://doi.org/10.1016/j.jenvman.2010.11.011

Fujigaya, T., & Nakashima, N. (2015). Non-covalent polymer wrapping of carbon nanotubes and the role of wrapped polymers as functional dispersants. Science and Technology of Advanced Materials, 16(2), 024802. https://doi.org/10.1088/1468-6996/16/2/024802

Ganzoury, M. A., Chidiac, C., Kurtz, J., & de Lannoy, C.-F. (2020). CNT-sorbents for heavy metals: Electrochemical regeneration and closed-loop recycling. Journal of Hazardous Materials, 393, 122432. https://doi.org/10.1016/j.jhazmat.2020.122432

Halali, M. A., & de Lannoy, C.-F. (2019). The Effect of Cross-Linkers on the Permeability of Electrically Conductive Membranes. Industrial & Engineering Chemistry Research, 58(9), 3832–3844. https://doi.org/10.1021/acs.iecr.8b05691

Hong, S. H., Jeong, J., Shim, S., Kang, H., Kwon, S., Ahn, K. H., & Yoon, J. (2008). Effect of electric currents on bacterial detachment and inactivation. Biotechnology and Bioengineering, 100(2), 379–386. https://doi.org/10.1002/bit.21760

Hörstmann, C., Brink, H. G., & Chirwa, E. M. N. (2020). Pb(II) Bio-Removal, Viability, and Population Distribution of an Industrial Microbial Consortium: The Effect of Pb(II) and Nutrient Concentrations. Sustainability, 12(6), 2511. https://doi.org/10.3390/su12062511

Igiri, B. E., Okoduwa, S. I. R., Idoko, G. O., Akabuogu, E. P., Adeyi, A. O., & Ejiogu, I. K. (2018). Toxicity and Bioremediation of Heavy Metals Contaminated Ecosystem from Tannery Wastewater: A Review. Journal of Toxicology, 2018, 1–16. https://doi.org/10.1155/2018/2568038

Iravani, S., & Varma, R. S. (2020). Bacteria in Heavy Metal Remediation and Nanoparticle Biosynthesis. ACS Sustainable Chemistry & Engineering, 8(14), 5395–5409. https://doi.org/10.1021/acssuschemeng.0c00292

Kim, H. J. (2009). Book Review: Microbial Fuel Cells. By Bruce E. Logan. Chemical Engineering & Technology, 32(6), 858. https://doi.org/10.1002/ceat.200990026

Lalia, B. S., Ahmed, F. E., Shah, T., Hilal, N., & Hashaikeh, R. (2015). Electrically conductive membranes based on carbon nanostructures for self-cleaning of biofouling. Desalination, 360, 8–12. https://doi.org/10.1016/j.desal.2015.01.006

Lee, N., Amy, G., Croué, J.-P., & Buisson, H. (2004). Identification and understanding of fouling in low-pressure membrane (MF/UF) filtration by natural organic matter (NOM). Water Research, 38(20), 4511–4523. https://doi.org/10.1016/j.watres.2004.08.013

Li, Y., Wang, H., Wu, P., Yu, L., Rehman, S., Wang, J., Yang, S., & Zhu, N. (2020). Bioreduction of hexavalent chromium on goethite in the presence of Pseudomonas aeruginosa. Environmental Pollution, 265, 114765. https://doi.org/10.1016/j.envpol.2020.114765

Lin, Y.-H. (2013). Modeling chromium(VI) reduction by Escherichia coli 33456 using ceramic pearl as a supporting medium. International Journal of Environmental Science and Technology, 11(7), 1887–1896. https://doi.org/10.1007/s13762-013-0392-z

Liu, C., Gorby, Y. A., Zachara, J. M., Fredrickson, J. K., & Brown, C. F. (2002a). Reduction kinetics of Fe(III), Co(III), U(VI), Cr(VI), and Tc(VII) in cultures of dissimilatory metal-reducing bacteria. Biotechnology and Bioengineering, 80(6), 637–649. https://doi.org/10.1002/bit.10430

Liu, C., Gorby, Y. A., Zachara, J. M., Fredrickson, J. K., & Brown, C. F. (2002b). Reduction kinetics of Fe(III), Co(III), U(VI), Cr(VI), and Tc(VII) in cultures of dissimilatory metal-reducing bacteria. Biotechnology and Bioengineering, 80(6), 637–649. https://doi.org/10.1002/bit.10430

Logan, B. E., Call, D., Cheng, S., Hamelers, H. V. M., Sleutels, T. H. J. A., Jeremiasse, A. W., & Rozendal, R. A. (2008). Microbial Electrolysis Cells for High Yield Hydrogen Gas Production from Organic Matter. Environmental Science & Technology, 42(23), 8630–8640. https://doi.org/10.1021/es801553z

Logan, B. E., Rossi, R., Ragab, A., & Saikaly, P. E. (2019). Electroactive microorganisms in bioelectrochemical systems. Nature Reviews Microbiology, 17(5), 307–319. https://doi.org/10.1038/s41579-019-0173-x

Mahar, F. K., He, L., Wei, K., Mehdi, M., Zhu, M., Gu, J., Zhang, K., Khatri, Z., & Kim, I. (2019). Rapid adsorption of lead ions using porous carbon nanofibers. Chemosphere, 225, 360–367. https://doi.org/10.1016/j.chemosphere.2019.02.131

Martín-Lara, M. A., Blázquez, G., Ronda, A., Rodríguez, I. L., & Calero, M. (2012). Multiple biosorption–desorption cycles in a fixed-bed column for Pb(II) removal by acid-treated olive stone. Journal of Industrial and Engineering Chemistry, 18(3), 1006–1012. https://doi.org/10.1016/j.jiec.2011.11.150

Mohapatra, R. K., Parhi, P. K., Pandey, S., Bindhani, B. K., Thatoi, H., & Panda, C. R. (2019). Active and passive biosorption of Pb(II)using live and dead biomass of marine bacterium Bacillus xiamenensis PbRPSD202: Kinetics and isotherm studies. Journal of

Environmental Management, 247, 121–134. https://doi.org/10.1016/j.jenvman.2019.06.073

Naik, M. M., & Dubey, S. K. (2013). Lead resistant bacteria: Lead resistance mechanisms, their applications in lead bioremediation and biomonitoring. Ecotoxicology and Environmental Safety, 98, 1–7. https://doi.org/10.1016/j.ecoenv.2013.09.039

Nkhalambayausi-Chirwa, E. M., & Wang, Y.-T. (2004). Modeling hexavalent chromium removal in aBacillus sp. fixed-film bioreactor. Biotechnology and Bioengineering, 87(7), 874–883. https://doi.org/10.1002/bit.20196

Pandey, A., Bera, D., Shukla, A., & Ray, L. (2007). Studies on Cr(VI), Pb(II) and Cu(II) adsorption–desorption using calcium alginate as biopolymer. Chemical Speciation & Bioavailability, 19(1), 17–24. https://doi.org/10.3184/095422907x198031

Singh, S., Kumar, V., Datta, S., Dhanjal, D. S., Sharma, K., Samuel, J., & Singh, J. (2020). Current advancement and future prospect of biosorbents for bioremediation. Science of The Total Environment, 709, 135895. https://doi.org/10.1016/j.scitotenv.2019.13589

Sun, X., Wu, J., Chen, Z., Su, X., & Hinds, B. J. (2012). Fouling Characteristics and Electrochemical Recovery of Carbon Nanotube Membranes. Advanced Functional Materials, 23(12), 1500–1506. https://doi.org/10.1002/adfm.201201265

Tekerlekopoulou, A. G., Tsiflikiotou, M., Akritidou, L., Viennas, A., Tsiamis, G., Pavlou, S., Bourtzis, K., & Vayenas, D. V. (2013). Modelling of biological Cr(VI) removal in draw-fill reactors using microorganisms in suspended and attached growth systems. Water Research, 47(2), 623–636. https://doi.org/10.1016/j.watres.2012.10.034

Thacher, R., Hsu, L., Ravindran, V., Nealson, K. H., & Pirbazari, M. (2015). Modeling the transport and bioreduction of hexavalent chromium in aquifers: Influence of natural organic matter. Chemical Engineering Science, 138, 552–565. https://doi.org/10.1016/j.ces.2015.08.011

Tran, H. N., & Chao, H.-P. (2018). Adsorption and desorption of potentially toxic metals on modified biosorbents through new green grafting process. Environmental Science and Pollution Research, 25(13), 12808–12820. https://doi.org/10.1007/s11356-018-1295-9

Upadhyayula, V. K. K., Deng, S., Mitchell, M. C., & Smith, G. B. (2009). Application of carbon nanotube technology for removal of contaminants in drinking water: A review. Science of The Total Environment, 408(1), 1–13. https://doi.org/10.1016/j.scitotenv.2009.09.027

Verona, D., Semião, A., & Antizar - Ladislao, B. (2013). Membrane Fouling & Flux Decline - Harvesting Microalgae with Ultrafiltration Membranes. Harvesting Microalgae with Ultrafiltration Membranes. https://sites.google.com/site/algaeultrafiltration/current-issues/fouling-and-flux-optimisation

Wang, W., Feng, Y., Tang, X., Li, H., Du, Z., Yi, A., & Zhang, X. (2015). Enhanced U(VI) bioreduction by alginate-immobilized uranium-reducing bacteria in the presence of carbon nanotubes and anthraquinone-2,6-disulfonate. Journal of Environmental Sciences, 31, 68–73. https://doi.org/10.1016/j.jes.2014.11.005

Yang, Y., Qiao, S., Jin, R., Zhou, J., & Quan, X. (2018). Fouling control mechanisms in filtrating natural organic matters by electro-enhanced carbon nanotubes

hollow fiber membranes. Journal of Membrane Science, 553, 54–62. https://doi.org/10.1016/j.memsci.2018.02.012

Yeung, R., Zhu, X., Gee, T., Gheen, B., Jassby, D., & Rodgers, V. G. J. (2020). Single and binary protein electroultrafiltration using poly(vinyl-alcohol)-carbon nanotube (PVA-CNT) composite membranes. PLOS ONE, 15(4), e0228973. https://doi.org/10.1371/journal.pone.0228973

Yi, G., Chen, S., Quan, X., Wei, G., Fan, X., & Yu, H. (2018a). Enhanced separation performance of carbon nanotube–polyvinyl alcohol composite membranes for emulsified oily wastewater treatment under electrical assistance. Separation and Purification Technology, 197, 107–115. https://doi.org/10.1016/j.seppur.2017.12.058

Yi, G., Chen, S., Quan, X., Wei, G., Fan, X., & Yu, H. (2018b). Enhanced separation performance of carbon nanotube–polyvinyl alcohol composite membranes for emulsified oily wastewater treatment under electrical assistance. Separation and Purification Technology, 197, 107–115. https://doi.org/10.1016/j.seppur.2017.12.058

Zhang, Q., & Vecitis, C. D. (2014). Conductive CNT-PVDF membrane for capacitive organic fouling reduction. Journal of Membrane Science, 459, 143–156. https://doi.org/10.1016/j.memsci.2014.02.017

2.0 Optimizing Carbon-Nanotube Poly(vinyl) Alcohol Thin Film Composites Through a Design of Experiments

Abstract

Membrane technology has shown to be robust in maintaining excellent effluent quality while reducing treatment plants' footprints. Implementing carbon nanotubes (CNTs) in membrane technology provides a viable method to couple membranes' removal capacity with Pb(II) removal while exhibiting regeneration capabilities. However, membrane fouling has been found to be problematic in the membranes' longevity and regeneration abilities. CNTs as conductive thin films have shown ability in mitigating fouling via electrostatic repulsion and pollutant degradation. However, little work has put forth in the fabrication of these conductive thin films. This study used a design of experiments (DOE) to investigate the antifouling properties of CNT-poly(vinyl) alcohol (PVA) thin films under varying PVA chain lengths and degree of crosslinking. The DOE revealed a strong correlation among water permeance and electrical conductivity with PVA chain length and degree of crosslinking ($R^2 \geq 0.87$) while a poor correlation was found for hydrophilicity ($R^2 = 0.44$). Based on the results from the constructed DOE, it was found that 31-50kDa PVA with 10% crosslinking created a pseudo-optimal thin film composition that was hydrophilic, highly electrically conductive and exhibited a large water permeance. This membrane also showed to have the capacity to aid in membrane's rejection abilities through its secondary porous barrier, exhibiting a molecular weight cut off of 2000kDa. Overall, this study founded DOE models that provides further insight on influential parameters that impact CNT-PVA antifouling properties which in turn can be used to improve membranes' longevity and regeneration abilities in Pb(II) removal.

2.1 Introduction

2.1.1 Background

In recent years, membrane filtration has been highlighted as both an economical and efficient method for cleaning a wide variety of water sources. This technology uses low pressures to drive water flow through a membrane which acts as a physical barrier for feed contaminants (Formoso et al., 2017). Typically, the membrane used is a porous structure which separates the feed constituents based on size-exclusion, rejecting organics and other contaminants from the influent. Within the realm of membrane filtration, ultrafiltration (UF) has peaked the interest of researchers due to its relatively high permeability and ability to produce excellent effluent quality (Bai et al., Dudchenko et al., 204; Zhang and Vecitis, 2014). Further, it has been found to handle feed quality fluctuations while reducing conventional wastewater treatment plants' footprint via replacing the typical processes used (i.e. coagulation, sedimentation, and granular filtration).

In addition to creating an effective mode to treat waters, membrane technology provides a viable surface for the implementation of CCNs. Specifically, the implementation of CNTs to UF membranes may provide an efficient mode to couple the treatment capabilities of UF with the excellent Pb(II) adsorption properties exhibited with CNTs. CNTs are rolled up sheets of graphene which exhibit continuous sp^2 hybridized bonds along their lengths. Their popularization in Pb(II) removal stems from their high surface area, chemical inertness, and ease of functionalization. Further, acid treated CNTs are well known in literature to have high affinity for Pb(II) through their intrinsic mechanisms of surface complexation, electrostatic interaction, and ion-exchange (Gupta et al., 2015).

Not only do CNTs create a surface with excellent Pb(II) adsorption abilities, it also provides a surface that can be regenerated in an environmentally benign process. A study conducted by Ganzoury et al., has shown that expensed CNTs can be regenerated using electrochemical methods, showing 90% recovery over 4 consecutive adsorption cycles (Ganzoury et al, 2020). This can alleviate the costs of these adsorbents while creating a closed-loop process that avoids the addition of harmful chemicals. Thus, implementing CNTs as adsorbents for Pb(II) in membrane technology will create a treatment method that can produce excellent effluent quality while providing an environmentally friendly and efficient means of removing Pb(II).

Although this technology provides a viable method to produce excellent effluent quality while simultaneously removing Pb(II), the prevalence of membrane fouling may be problematic. Membrane fouling can be problematic as it can reduce the CNT networks' conductivity as well as the membrane longevity. Thus, to preserve the regeneration abilities proposed for Pb(II) removal as well as the membrane's lifetime, the hurdle of membrane fouling must be addressed. Membrane fouling involves the deposition of dissolved and suspended particles/colloids within the surface or pores of the membrane (Ahmed et al., 2016; Formoso et al., 2017; Lalia et al., 2015; Lee et al., 2004). In addition to particle deposition, biofouling can also be problematic in UF technology. Due to the advective transport of organics as well as nutrients, bacteria can easily adhere onto the membrane and thrive (Hong et al., 2008). Once adhered, the bacteria have the capacity to produce extra polymeric substance, a sticky product that promotes further cell adherence and eventually

the formation of biofilms on the membrane surface. Biofilms impose irreversible membrane damage, shortening their lifetime and inherently increasing their operational and maintenance costs. Thus, there is a present need to find an active solution which can both reduce organic and bacterial adherence onto the membrane surface, so it may be used as an active means of removing Pb(II) and other water contaminants.

CNTs as electrically conductive membranes (ECMs) have also been the interest of researchers as an efficient method to reduce membrane fouling due to their fast electron transport, high surface area, antimicrobial properties and fast water transport abilities (Bai et al., 2015; de Lannoy et al., 2012; de Lannoy et al., 2013; Hong et al., 2008; Lalia et al., 2015; Sun et al., 2012; Yeung et al., 2020; Yi et al., 2018). CNTs as ECMs can alleviate membrane fouling via adjusting the surface charge of the membrane and in turn minimizing particle and bacterial deposition. This can be accomplished by pollutant degradation as well as electrostatic repulsion and H_2(g) bubbling on the membrane when positive and negative potentials are applied, respectively (de Lannoy et al., 2013; Yang et al., 2018). An applied potential can further induce antifouling mechanisms through the promotion of local pH changes and the production of radicals and hydrogen peroxide, as these create unsuitable conditions for bacteria (Hong et al., 2008).

Extensive research has been employed to show the efficacy of CNT networks in reducing fouling while aiding in membrane rejection and selectivity. For instance, in the work by Yi et al. CNT coatings were implemented on polyether sulfone (PES) supports to show its efficacy in recovering permeate fluxes after filtering soybean oil-in-water emulsion (Yi et al., 2018). After 120mins, the permeate flux of the thin film was 2.02 and 11.43 times than that of the poly(vinyl) difluoride (PVDF) and PES support membranes, respectively. Furthermore, backflushing operations were imposed to show the films' resistance to irreversible fouling. This revealed that the coated membranes could recover a flux that was 1.49 and 7.71 times than that of PVDF and the PES support membranes. Dudchenko et al. used CNT networks to show the thin films' capability to prevent fouling from alginic acid compared to its support membrane comprised of polysulfone (PS) (Dudchenko et al., 2014). It was shown that with the thin film coating reduced the transmembrane pressure by 24% and 51% when -3V and -5V were applied, respectively. This was found to be attributed to the strong electrostatic repulsive forces created on the thin film. Further, -5V further eliminated fouling when Ca^{2+} was added, which normally forms a gelatinous mass on membranes when in contact with alginic acid. In terms of biofouling, Ronen et al. revealed the CNT thin film's capacity to prevent biofouling on the membranes (Yi et al., 2018). Specifically, it was shown that an applied voltage of 1V and 1.5V could detach 71% and 86% of bacteria present. This was attributed to the thin film's capability to increase the bacterial mobility on the membrane surface while producing the antimicrobial product, hydrogen peroxide.

To improve the antifouling mechanisms of the membranes, the fabrication of the ECMs must be optimized. The first consideration made in the aforementioned studies is the synthesis of CNTs as conductive thin films on polymeric supports. This was imperative as this mode of fabrication prevents the leaching of CNTs into receiving waters, which would in turn cause health hazards (Zhang and Vecitis, 2014). CNTs were further implemented as

composites using the integration of the polymer, poly(vinyl) alcohol (PVA) for stabilization. The synthetization of CNT thin films can be difficult due to their inherent hydrophobicity, inducing quick aggregation of the nanomaterials when introduced to polar solvents. One promising method to overcome this downfall is noncovalent polymer wrapping on the CNT lengths (Fujigaya and Nakashima, 2015; Bilalis et al., 2014). Specifically, it has been shown that the PVA can wrap around the CNT lengths through π-CH interactions and improve its overall hydrophilicity through the exposure of its hydroxyl groups. The improved hydrophilicity allows for the creation of stable suspensions that eases CNT vacuum deposition onto polymeric supports. Additionally, the exposure of its hydroxyl groups provides a more hydrophilic surface that can reduce the adherence of hydrophobic foulants, while providing an additional opportunity for the network to be crosslinked.

Although the synthesized CNT-PVA network has proven its efficacy in preventing fouling, little work has been put forward in optimizing its properties. The beginning works was conducted by de Lannoy et al. who first pioneered the CNT-PVA thin film crosslinked with succinic acid (de Lannoy et al., 2012). In this work, the thin film's conductivity, hydrophilicity, permeability, and rejection was optimized by investigating the impact of CNT:PVA weight ratio and curing time. This study highlighted that increasing curing time increased conductivity by invoking a greater degree of crosslinking and that the hydrophilicity of the thin film decreased with decreasing CNT:PVA mass ratio. Overall, it was found that a weight ratio of CNT:PVA of 1:10 with a curing time of 20 minutes lead to the most optimal membrane based on the metrics previously mentioned. Building on this work, Halali and de Lannoy used the previously optimized conditions and further investigated the effect of crosslinker lengths and degree of crosslinking on the network (Halali and de Lannoy, 2019). It was found that longer crosslinkers at a higher degree of crosslinking improved the overall permeance of the membrane, where only crosslinking length improved its conductivity. Lastly, it was found that these impacts had no baring on the membrane hydrophilicity.

2.1.2 Problem Statement

Although the previously mentioned studies provide further insight on the individual parameter's influence on the thin film's performance, they have not touched upon the effect of PVA chain length antifouling properties. This is an imperative parameter as this will in turn effect the overall retention of the polymer which affects the membrane's hydrophilicity. Further, since PVA hydroxyl groups are required for crosslinking with succinic acid, its retention will inherently affect how the network will be crosslinked, making degree of crosslinking a noteworthy parameter to investigate. The goal of this study is to conduct a design of experiment (DOE) as an efficient way to investigate the effects of PVA chain length and degree of crosslinking while yielding models that will aid in a better understanding on how these parameters influence the thin film's antifouling properties (i.e. conductivity, hydrophilicity and permeance).

2.2 Materials and Methods

2.2.1 Design of Experiments Parameters

This DOE investigated the effects of PVA chain length (i.e. molecular weight, MW) and degree of crosslinking, where their investigated ranges are summarized in Table 1.

Table 1. Summary of design of experiment parameters investigated and their tested ranges.

Investigated Parameter	Low range value tested (-)	High range value tested (+)
PVA Chain Length (i.e. molecular weight)	13-23kDa	31-50kDa
PVA degree of crosslinking	0%	10%

As seen in Table 1, PVA MW was varied between 13-23kDa and 31-50kDa and degree of crosslinking was varied between 0 and 10%. All crosslinking reactions were carried out using succinic acid as it has been identified in literature as an effective crosslinker in CNT networks (de Lannoy et al., 2010; Halali and de Lannoy, 2019).

2.2.2 Materials

f-SW/DW CNTs (CNTs, carboxyl functional content 2.73wt%, purity >90%, length 5-30μm and outer diameter 1-4nm) were purchased from Cheap-Tubes USA. Sodium dodecyl sulfate (SDS, MW = 288.4 g/mol) and PVA (30-50kDa or 13-23kDa, 98-99% hydrolyzed) were purchased from Sigma-Aldrich (Canada). Succinic acid (MW = 118g/mol) and hydrochloric acid (38wt%) were purchased from Alfa Aesar (India) and Anachemia (Canada), respectively. Polyether sulfone (PES) ultrafiltration (UF) membranes (30nm pore size, 47mm diameter) were purchased from Sterlitech USA.

2.2.3 Fabrication of Carbon Nanotube Poly(vinyl) Alcohol Thin Film Composites

Fabrication of CNT-PVA network began with creating a CNT-PVA batch. This batch comprised of 75mg of CNTs in 100mL DI water which was stirred at 600RPM for 10 minutes and then subsequently ultrasonicated at 40% amplitude for 30 minutes effective time using a microtip (1/4”). 112.5mg of SDS was added to 100mL DI water and stirred for 10 minutes at 600RPM prior to being added to the sonicated CNT batch suspension in a 1:1.5 wt/wt ratio. After the addition of SDS, the CNT and SDS suspension was stirred for 10 minutes at 600RPM and then sonicated at 40% amplitude for 1hr effective time. In a separate batch, a 500mg/mL PVA suspension was prepared by dissolving PVA in DI water overnight at elevated temperatures (100°C, 600RPM). The dissolved PVA suspension was then added to the CNT-SDS suspension in 1:10 CNT:PVA mass ratio. The CNT-SDS-PVA suspension was then sonicated for 1hour effective time at 40% amplitude for the creation of a stable CNT-PVA network. In instances where the CNT-PVA network was crosslinked, succinic acid was added in sufficient amounts to allow for 10% of the network to undergo crosslinking. This reaction was catalyzed with 2M HCl for a duration of 24hours. A schematic of the crosslinked network can be seen in Figure S.1c.

The stabilized suspensions were then pressure deposited as thin films on pristine PES UF membranes. To ensure membranes were fully wetted prior to CNT deposition, the pristine PES membranes were stored in DI water overnight at ambient temperatures. Thin films

were then deposited with 3mg of CNTs onto the active side of the PES membranes using a well-documented vacuum filtration method (de Lannoy et al., 2010; Halali and de Lannoy, 2019). The coated membranes were then cured in an oven at 100°C for 1hour and then let to cool at room temperature for 20 minutes before. The membranes were then stored in DI overnight before characterization methods were carried out. Figure S.1a and S.1b presents a pristine PES membrane and one with a thin coat of the CNT-PVA network, respectively. Each thin film composite combination was created in triplicates to capture any variability in membrane fabrication.

2.2.4 Characterization of CNT-PVA thin film composites: pure water flux, conductivity, and contact angle

Three metrics were used to characterize the CNT-PVA thin film composite: water permeance, contact angle and conductivity. Water permeance experiments were carried out using a dead-end flow cell (Sterlitech stainless steel) as shown in Figure 4a. In this method, membranes were first compressed under high pressure (100psi) for 1 hour as a pre-treatment before testing commenced. This pre-treatment was selected to ensure that the membrane pores do not compress when undergoing testing and thus to mitigate hysteresis effects. After pre-treatment, pure water flux tests were carried out using pressures: 10, 20, 30, 40, 50 and 60psi. At each tested pressure, the permeate volume was measured every 10 seconds for a total time of 1 minute. This was repeated three times to capture measurement error. Pure water flux was then correlated to permeance by normalizing it by the cross-sectional area of the membrane and pressure in the following equation,

$$J = \frac{V}{t \times A \times \Delta p} \quad (1)$$

where J represents permeance (L/hr/m^2/bar), V is the collected water volume (L) during time duration t (hr), A represents filtration cross sectional area (m^2) and p represents tested pressure (bar).

Contact angle was used as a metric for the thin films' hydrophilicity. It was measured by first air-drying the membrane over night and then using a high-speed contact angle measurement instrument (OCA35) seen in Figure 4b. This instrument works by dropping 5µL of DI water onto the thin film surface using a microneedle tip where a video software captures the droplet being dispensed and spreading on the surface. This allowed an image to be taken of the water droplet as it touched the thin film thus allowing for its angle to measured from the surface. This procedure was carried out three times per membrane to capture any measurement variability.

The last metric used to assess the performance of the thin film composite was conductivity. Membranes were first air dried overnight before conductivity was measured using a four-point conductivity probe. Its four-point needle probes are presented in a square configuration as depicted by Figure 4c where the needles measure the surface potential of the thin films by interacting with the CNT layer-air interface and through the consideration of the paired probes resistance. Through these considerations, the device provides a measurement as sheet resistance. Through the knowledge of the thickness of the thin film, the sheet resistance was correlated to resistivity by:

$$resistivity\ (\Omega\, m) = resistance\ \left(\frac{\Omega}{sq}\right) x\ thickness(m) \quad (2)$$

and thus conductivity

$$conductivity\ (\frac{S}{m}) = \frac{1}{resistivity\ (\Omega\, m)} \quad (3).$$

Multiple measurements were taken along different areas of the thin film to capture the variability along the network.

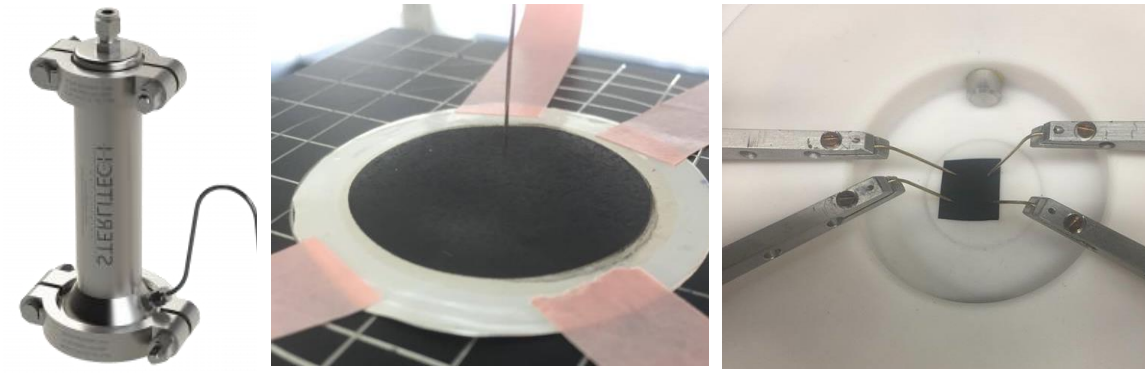

(a) (b) (c)

Figure 4. a) Sterlitech dead-end flow cell set-up used for pure water flux measurements, b) OCA35 high-speed contact angle instrument used to measure thin film hydrophilicity and c)four-point probe set-up for measuring thin film conductivity.

2.2.5 Rejection Tests

The most optimal thin film and the pristine PES membrane were used for further rejection experiments. Rejection experiments were carried out with a dead-end flow cell that was operated under crossflow via inducing mixing conditions (250RPM) and 10psi pressure. The model organic compound that was studied was poly(ethylene oxide) (PEO) under different molecular weights (300, 600 and 2000kDa), where a known feed concentration was introduced into the flow cell (250ppm). The permeate PEO concentration was measured by a total organic carbon (TOC) analyzer. By knowing the permeate concentration in relation the feed, the total rejection of the thin film composite can be calculated through the following equation,

$$Rejection\ (\%) = \left(1 - \frac{[Permeate]}{[Feed]}\right) x\ 100\% \quad (4).$$

Once the rejection values were calculated and plotted, the molecular weight cut off was found by assessing what molecular weight corresponded to a 90% rejection.

2.2.5 Statistical Analysis of Experimental Results

All experimental results were inputted into MiniTab18 which contains a DOE factorial function that performed all statistical analysis, outputting all predictive models and parameters (i.e. p and t-values) as well as interaction plots between parameters.

2.3 Results and Discussion

2.3.1 The Effect of Poly(vinyl) Alcohol Chain Length and Degree of Crosslinking on Water Permeance

The first metric investigated was water permeance. Water permeance was deemed a critical parameter as although CNT-PVA thin films prevent fouling on membranes it can also act as a barrier for water flux if it is not synthesized as a porous network. This in turn leads to

greater pumping costs and a reduction of throughput. Thus, permeance was tested for each CNT-PVA combination where the results are summarized in Figure 5a. As seen in Figure 5a, the greatest water permeance was observed for the CNT network which contained 31-50kDa PVA with crosslinking followed by 13-23kDa with no crosslinking, 13-23kDa with crosslinking and 31-50kDa without crosslinking, respectively. Figure 5a also reveals that there is no statistical difference when the small chained PVA (13-23kDa) is crosslinked, as indicated by the overlapping error bars.

To further understand the impact of PVA MW and degree of crosslinking on water permeance, the results were inputted into Minitab18 to obtain the predictive model,

$$\log(Permeance) = 2.41 - 1.90 \times 10^{-5}\, x_1 - 0.0885\, x_2 + 4.00 \times 10^{-6} x_1 x_2 \qquad (5)$$

where x_1 represents PVA MW (kDa) and x_2 represents degree of crosslinking (%). This model exhibited a strong logarithmic correlation as suggested by its R^2 value of 0.87. All parameters were found to be statistically significant ($p < 0.05$) except for PVA MW but since the interaction term (x_1x_2) had a p-value < 0.05 the term was kept in the model. To understand which parameters are most influential on permeance, each parameter's t-values were plotted and can be observed in Figure 5b. t-values' magnitudes provides a metric for which model parameters are most influential on the outcome parameter. The t-values shown in Figure 5b reveal that crosslinking created the most impact on permeance followed by the interaction factor (x_1x_2) and PVA MW, respectively. This result can be explained by the fact that crosslinking branches CNTs apart and thus improves porosity. Enhanced porosity means that there will be more void spaces and thus less resistance to water flow as it moves through the CNT network. Conversely, PVA MW had the least amount of impact on water permeance. Although its size determines its retention, it has no influence on the overall porosity of the thin film which is the governing parameter for water flow resistance (de Lannoy et al., 2010; Halali and de Lannoy, 2019).

The interaction factor term can be better interpreted through Figure 5c. Figure 5c shows that crosslinking has the most impact when used with high MW PVA (i.e. long chained). Since longer chained PVA can likely wrap around the entirety of the CNTs' lengths, crosslinking them will in turn branch out the CNTs to create a porous network. If the smaller chained PVA is too short to wrap the CNTs lengths, crosslinking will only partially branch out neighbouring CNTs. It may also be due to leaching of PVA from the network, resulting in less polymer available to be crosslinked. Figure 5c also shows that without crosslinking, longer chained PVA reduces permeance. Since longer chained PVA exhibits a larger radius of gyration, it will have a greater retention in the CNT network. PVA retention without crosslinking reduces water flow because of its inherent adhesive properties when cured. These adhesive properties of PVA makes it act like a glue in the network and in turn create an additional non-porous barrier to water flow. Similarly, shorter chained PVA may experience leaching from the CNT network due to its small radius of gyration. The leaching of PVA will prevent the creation of a non-porous barrier from forming and in turn allow for permeance to be enhanced by the CNT's excellent water transport properties.

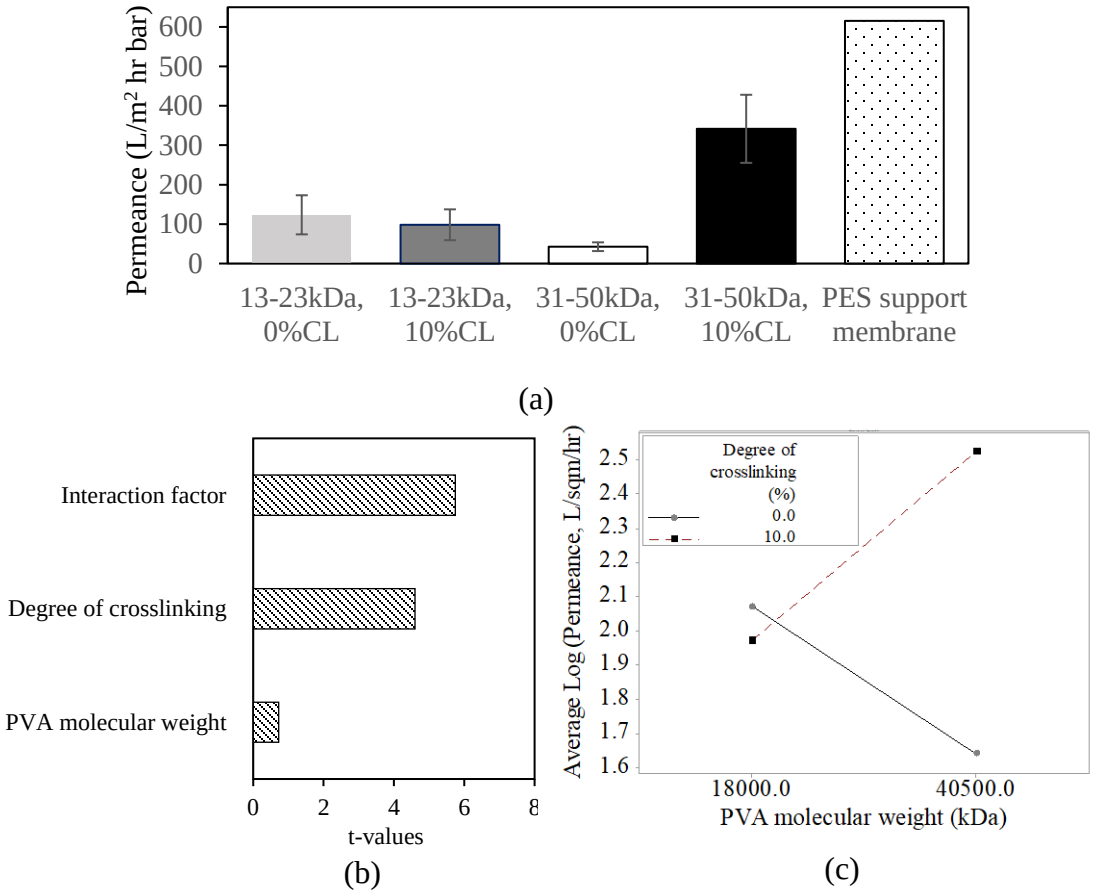

Figure 5. (a) The effect of different molecular weight PVA and degree of crosslinking on permeance, where CL represents degree of crosslinking and the error bars represent standard deviation , (b) the calculated t-values for each model parameter and (c) the interaction plot depicting the influence of degree of crosslinking with PVA molecular weight on average permeance.

2.3.2 The Effect of Poly(vinyl) Alcohol Chain Length and Degree of Crosslinking on Contact Angle

Contact angle was used as a metric for the thin films' hydrophilicity. Contact angle measures the hydrophilicity of the thin films by measuring the spread of a water droplet on its surface. If the thin film is hydrophilic, water will spread more readily across its surface to reduce surface tension, creating a smaller contact angle and vise versa. Hydrophilicity is a critical parameter as invoking a more hydrophilic surface reduces fouling through the reduction of hydrophobic forces between the thin film and organic foulants.

Figure 6a displays the contact angle measurements obtained for each CNT-PVA combination. The pristine PES membrane measurement was not included as its hydrophilic properties allowed for water to spread instantaneously once introduced to its surface, creating a contact angle of 0°. Thus, any increase in hydrophobicity is introduced from the CNTs themselves. Figure 6a reveals that the smallest contact angle was achieved for the

31-50kDa with crosslinking followed by the 31-50kDa without crosslinking, 13-23kDa with crosslinking and 13-23kDa without crosslinking, respectively. It can also be seen that only PVA MW impacted the thin films' hydrophilicity as insignificant changes in contact angle were observed when CNTs were crosslinked.

To further investigate how contact angle is impacted by PVA MW and degree of crosslinking, the following predictive model was constructed in MiniTab18,

$$\text{contact angle} = 61.27 - 0.000411x_1 + 0.018x_2 - 0.000008x_1x_2 \quad (6)$$

where x_1 represents PVA MW (kDa) and x_2 represents degree of crosslinking (%). The t-values from the obtained model is presented in Figure 6b which show that PVA MW had a greater impact on contact angle overall all other parameters. These t-values are also supported by the model parameters' p-values which confirm that the only statistically significant parameter ($p < 0.05$) was PVA MW. The interaction plot presented in Figure 6c is also in accordance with the reported p-values as the parallel lines shown indicate that crosslinking has no baring on the overall thin films' contact angle.

As previously mentioned, increasing the PVA MW allows for greater retention of the polymer. Greater retention of PVA inherently means that there will be more hydrophilic groups in the CNT network which in turn creates smaller contact angles. Degree of crosslinking does not affect contact angle because crosslinking only allows for more connections between CNTs. Since increasing connections between CNTs does not affect PVA retention in the thin film, the hydrophilicity of the CNT network will therefor not change. This finding is in accordance with Halili and de Lannoy's study which found that introducing different crosslinkers to CNT networks exhibited no impact on contact angle (Halali and de Lannoy, 2019).

Thus, degree of crosslinking and the interaction term were removed from the model and it was refitted to the following form,

$$contact\ angle = 61.9 - 4.82\ x\ 10^{-4}x_1 \quad (7).$$

However, the model exhibited a poor goodness of fit as indicated by its R^2 value of 0.44. This weak correlation is likely due to the dependency that contact angle has with surface roughness. It has been shown that a surface composed of the same material with increased roughness will have a smaller contact angle than that seen if it were a smoother surface. Thus, future experiments should incorporate surface roughness into the model to assess whether a stronger correlation can be obtained.

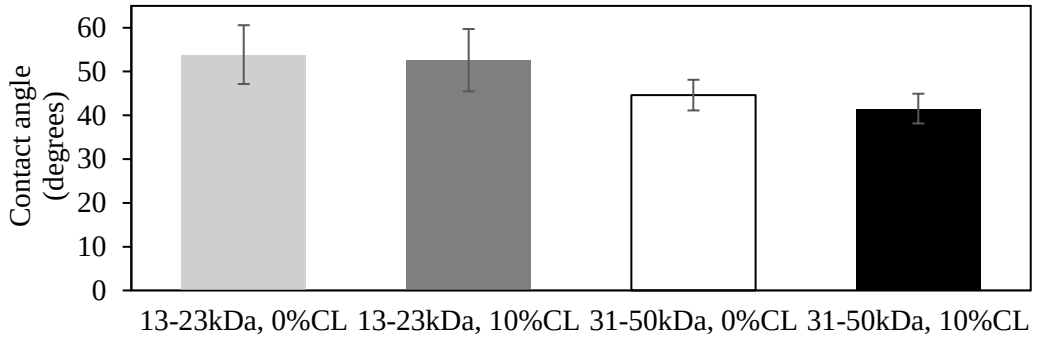

(a)

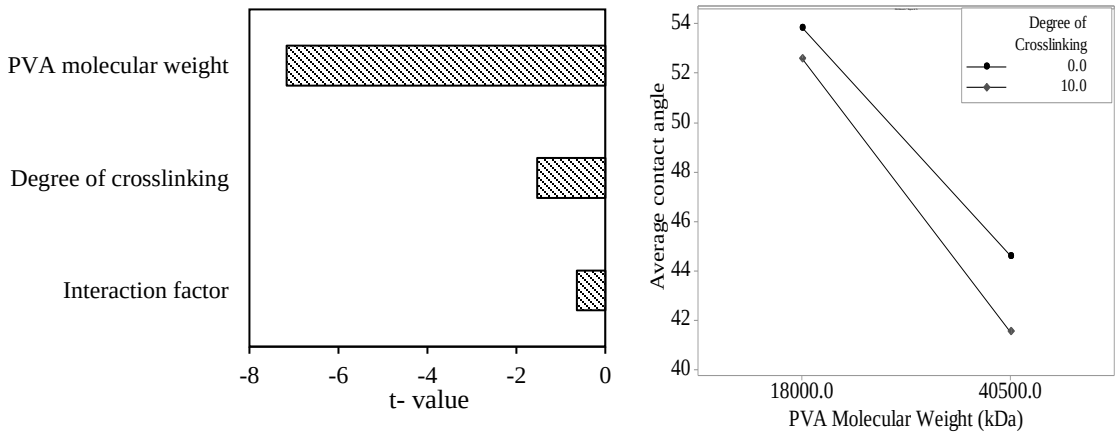

(b) (c)

Figure 6. (a)The effect of PVA molecular weight and degree of crosslinking on CNT-PVA thin film's contact angle, (b) the calculated t-values for each model parameter and (c) the interaction plots between PVA MW and degree of crosslinking for contact angle. Error bars shown represent standard deviation

2.3.3 The Effect of Poly(vinyl) Alcohol Chain Length and Degree of Crosslinking on Conductivity

The last metric investigated was conductivity as it measures the thin films capacity to conduct electron flow and thus hold a surface charge. This property is what gives the thin films the capability of organic degradation and electrostatic repulsion abilities. Figure 7a shows the surface conductivity for the different CNT PVA thin films, where 31-50kDa PVA with crosslinking exhibited the greatest surface conductivity followed by 13-23kDa with crosslinking, 13-23kDa without crosslinking and 31-50kDa without crosslinking, respectively. To understand the relationship between conductivity with PVA MW and degree of crosslinking the following predictive model was constructed

$$conductivity = 99140 - 4520x_1 - 2.12x_2 + 0.286x_1x_2 \quad (8)$$

where x_1 is PVA MW (kDa) and x_2 is degree of crosslinking (%). All parameters were found to be statistically significant ($p < 0.05$) and the model demonstrated a goodness of fit with an R^2 of 0.98.

Each parameters t-values were plotted in Figure 7b to assess which parameters are most influential on surface conductivity. Figure 7b shows that the most influential parameter on conductivity is degree of crosslinking followed by the interaction factor and PVA MW, respectively. It can be hypothesized that degree of crosslinking enhances conductivity by interconnecting CNTs within the CNT-PVA network. Interconnections between the CNTs creates a more organized path for electrons to flow, in turn allowing for faster electron transport and thus greater conductance. This hypothesis is supported by the SEM images shown in Figure 8 which shows the thin film thickness when long chained PVA is crosslinked and uncrosslinked. As seen by Figure 8, when long chained PVA is crosslinked, the CNT layer becomes thinner. This result implies more CNT connections because it would in turn enhance CNT-CNT hydrophobic forces and allow for them to compact more tightly on the support membrane.

Further, this coincides with the interaction plot shown in Figure 7c which shows that conductivity is further enhanced when crosslinking is invoked with longer chained PVA. Since longer chained PVA can likely wrap the entirety of the CNT length, it will allow for more connections between CNTs than that seen for shorter chained PVA when crosslinked. Figure 7c also shows that without crosslinking, longer chained PVA reduces surface conductivity. This can be reasoned by the fact that more PVA will be retained within the thin film when a longer chain is used. Greater retention results in lower conductivity as this nonconductive polymer will inhibit electron flow between CNTs unless creating direct connections among them.

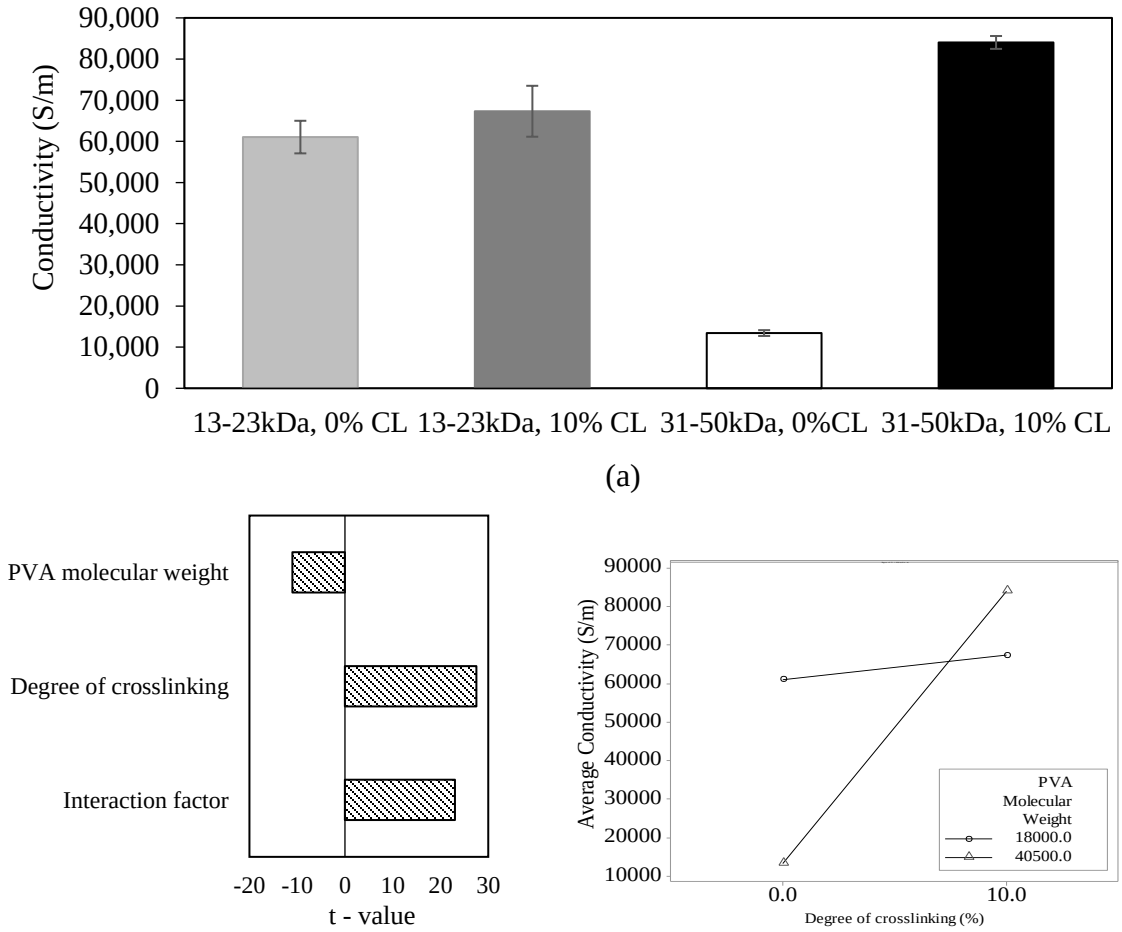

Figure 7. (a)The effect of PVA molecular weight and degree of crosslinking on the conductivity of a thin film PVA-CNT network (a), (b) the t-values found for conductivity model parameters and (c) the interaction plot depicting the influence of PVA molecular weight and degree of crosslinking has on conductivity. Error bars shown represent standard deviation.

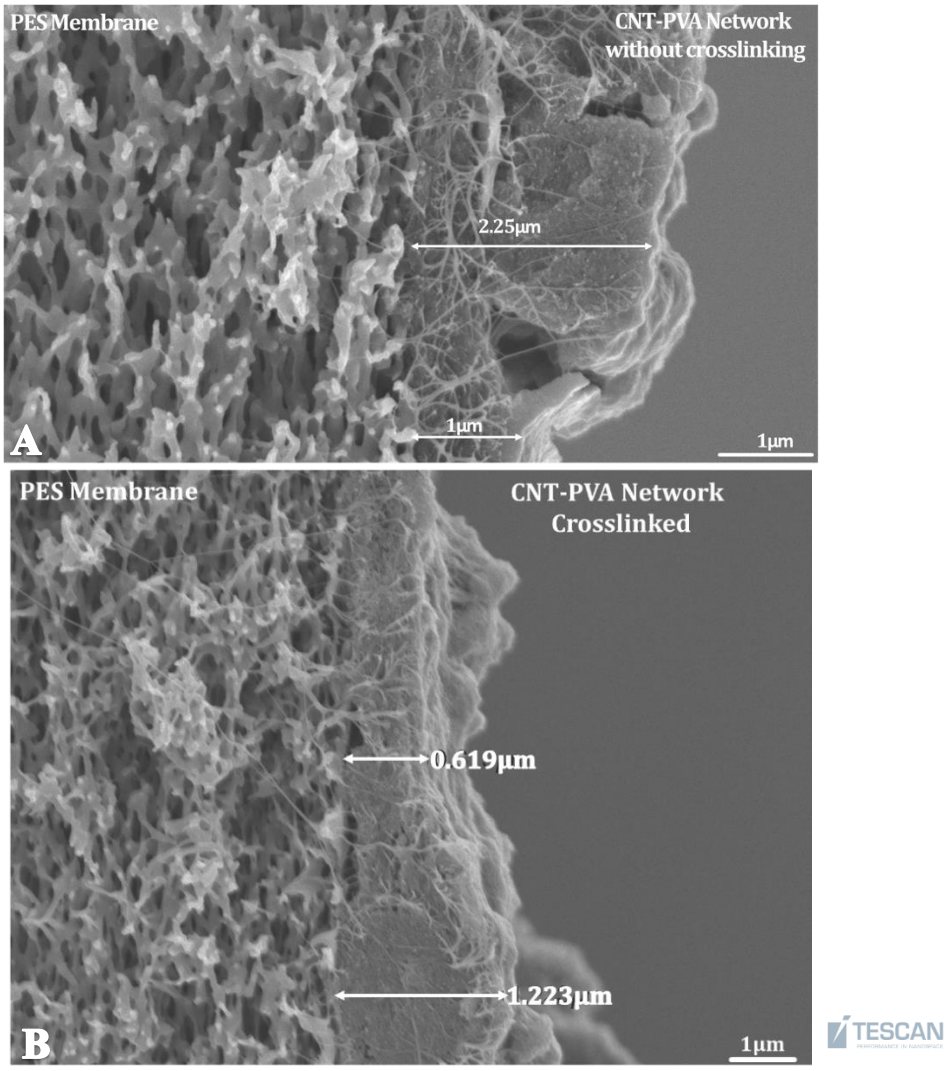

Figure 8. SEM images showing the thickness of the CNT-PVA thin film for (a) uncrosslinked 31-50kDa PVA and (b) 31-50kDa crosslinked PVA with succinic acid.

Lastly, it is interesting to note that there is a substantial difference between the influence that PVA MW and degree of crosslinking have on conductivity and permeance. Specifically, there is a logarithmic and linear relationship for permeance and conductivity, respectively. This can be attributed to the mass of CNTs used in these experiments. Specifically, the 3mg of CNTs used in this study meets the percolation threshold required for the CNTs to conduct electron flow. This means that creating connections with CNTs only enhances electron flow but is not required for the network to be conductive. However, with the relatively large mass of CNTs used, it is imperative to create an open porous network to avoid the formation of a dense CNT network that will be considerably resistant to water flow. Thus, the models may vary depending on the mass of CNTs used, where there would be a greater dependency for conductivity with a smaller mass of CNTs.

2.3.4 Rejection Tests for Pseudo-Optimal Thin Film Composite

After analyzing the three main characteristic metrics: hydrophilicity (i.e. contact angle), conductivity and water permeance, it is evident that there is a local optimum from the presented DOE using long chained PVA (31-50kDa) with 10% crosslinking. This can be concluded as this combination created a thin film with the greatest water permeance and conductivity, while improving hydrophilicity. Thus, this local optimum was selected for rejection tests. Rejection tests were carried out to investigate whether the implementation of the pseudo optimal thin film composite can aid in rejecting contaminants. The results of this experiment are presented in Figure 9.

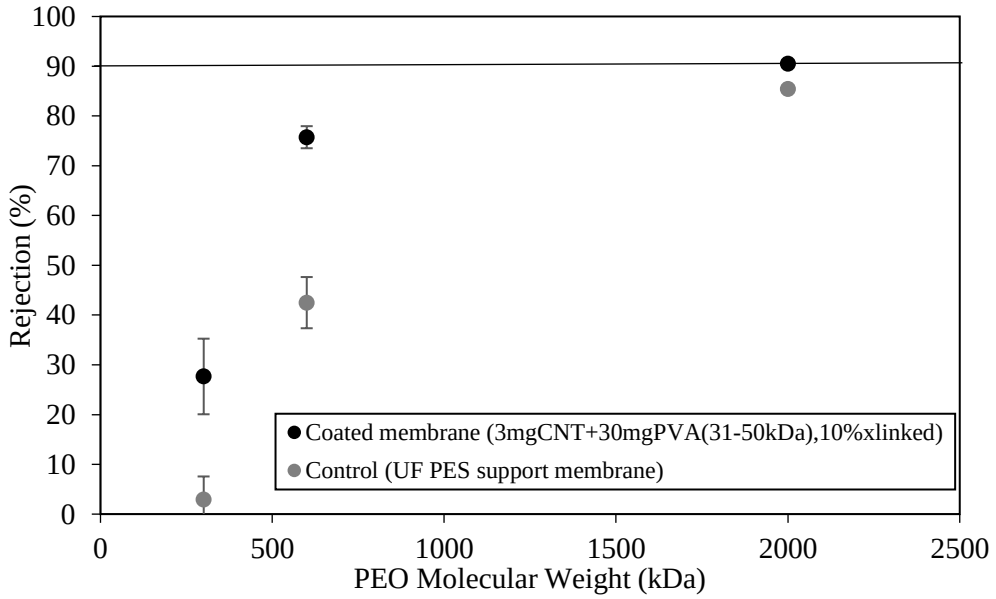

Figure 9. The rejection (%) found for local optimal thin film CNT-PVA composite (31-50kDa, 10% crosslinked) and Pristine PES membrane under different PEO molecular weights with molecular weight cut off shown at 90% rejection. Error bars shown represent standard deviation.

As seen in Figure 9, the rejection of PEO is consistently greater for the CNT-PVA thin film in comparison to the pristine PES membrane and exhibits a MW cut-off of 2000kDa. This demonstrates that the implementation of the CNT-PVA thin film composite not only mitigates fouling but can further aid in contaminant removal. This can be attributed to the fact that this composite layer introduces a secondary porous network that acts as an additional barrier for contaminants. It is further likely that the CNT network has pore sizes that are smaller than the support membrane, physically rejecting the PEO molecules via size exclusion.

2.4 Conclusions and Future Work

This study used a DOE to investigate the impact of PVA MW and degree of crosslinking on CNT-PVA thin film's permeance, hydrophilicity and conductivity. This was done in the interest of achieving a pseudo optimal thin film that exhibits the greatest antifouling

properties that may be utilized to increase membrane longevity as well as its Pb(II) regeneration abilities. The main conclusions from this work are:

- Permeance, hydrophilicity and conductivity were greatest using 31-50kDa PVA with 10% crosslinking, making this combination a local optimum in the investigated DOE.
- The predictive models for permeance and conductivity exhibited a good fit as indicated by their high R^2 values.
- Permeance exhibited a stronger dependency on PVA MW and degree of crosslinking over conductivity as indicated by its logarithmic relationship. This is likely due to the relatively high mass of CNTs used in this study.
- The model constructed for contact angle exhibited a poor correlation, likely due to its dependency on surface roughness.
- The pseudo-optimal CNT-PVA thin film composite enhanced membrane rejection compared to the pristine PES membrane.

Although this study provides insight on how CNT-PVA thin films may be optimized by different PVA MWs and degree of crosslinking, further work should look at incorporating surface roughness in the contact angle model, expanding the DOE to see if there is a more optimal combination and performing fouling studies with the different recipes to confirm that these thin films will reduce fouling on support membranes.

2.5 References

Ahmed, F., Lalia, B. S., Kochkodan, V., Hilal, N., & Hashaikeh, R. (2016). Electrically conductive polymeric membranes for fouling prevention and detection: A review. Desalination, 391, 1–15. https://doi.org/10.1016/j.desal.2016.01.030

Bai, L., Liang, H., Crittenden, J., Qu, F., Ding, A., Ma, J., Du, X., Guo, S., & Li, G. (2015). Surface modification of UF membranes with functionalized MWCNTs to control membrane fouling by NOM fractions. Journal of Membrane Science, 492, 400–411. https://doi.org/10.1016/j.memsci.2015.06.006

Bilalis, P., Katsigiannopoulos, D., Avgeropoulos, A., & Sakellariou, G. (2014). Non-covalent functionalization of carbon nanotubes with polymers. RSC Adv., 4(6), 2911–2934. https://doi.org/10.1039/c3ra44906h

de Lannoy, C. F., Jassby, D., Davis, D. D., & Wiesner, M. R. (2012). A highly electrically conductive polymer–multiwalled carbon nanotube nanocomposite membrane. Journal of Membrane Science, 415–416, 718–724. https://doi.org/10.1016/j.memsci.2012.05.061

de Lannoy, C.-F., Jassby, D., Gloe, K., Gordon, A. D., & Wiesner, M. R. (2013). Aquatic Biofouling Prevention by Electrically Charged Nanocomposite Polymer Thin Film Membranes. Environmental Science & Technology, 47(6), 2760–2768. https://doi.org/10.1021/es3045168

de Lannoy, C.-F., Soyer, E., & Wiesner, M. R. (2013). Optimizing carbon nanotube-reinforced polysulfone ultrafiltration membranes through carboxylic acid functionalization. Journal of Membrane Science, 447, 395–402. https://doi.org/10.1016/j.memsci.2013.07.023

Dudchenko, A. V., Rolf, J., Russell, K., Duan, W., & Jassby, D. (2014). Organic fouling inhibition on electrically conducting carbon nanotube–polyvinyl alcohol composite ultrafiltration membranes. Journal of Membrane Science, 468, 1–10. https://doi.org/10.1016/j.memsci.2014.05.041

Formoso, P., Pantuso, E., De Filpo, G., & Nicoletta, F. (2017). Electro-Conductive Membranes for Permeation Enhancement and Fouling Mitigation: A Short Review. Membranes, 7(3), 39. https://doi.org/10.3390/membranes7030039

Fujigaya, T., & Nakashima, N. (2015). Non-covalent polymer wrapping of carbon nanotubes and the role of wrapped polymers as functional dispersants. Science and Technology of Advanced Materials, 16(2), 024802. https://doi.org/10.1088/1468-6996/16/2/024802

Ganzoury, M. A., Chidiac, C., Kurtz, J., & de Lannoy, C.-F. (2020). CNT-sorbents for heavy metals: Electrochemical regeneration and closed-loop recycling. Journal of Hazardous Materials, 393, 122432. https://doi.org/10.1016/j.jhazmat.2020.122432

Halali, M. A., & de Lannoy, C.-F. (2019). The Effect of Cross-Linkers on the Permeability of Electrically Conductive Membranes. Industrial & Engineering Chemistry Research, 58(9), 3832–3844. https://doi.org/10.1021/acs.iecr.8b05691

Hong, S. H., Jeong, J., Shim, S., Kang, H., Kwon, S., Ahn, K. H., & Yoon, J. (2008). Effect of electric currents on bacterial detachment and inactivation. Biotechnology and Bioengineering, 100(2), 379–386. https://doi.org/10.1002/bit.21760

Lalia, B. S., Ahmed, F. E., Shah, T., Hilal, N., & Hashaikeh, R. (2015). Electrically conductive membranes based on carbon nanostructures for self-cleaning of biofouling. Desalination, 360, 8–12. https://doi.org/10.1016/j.desal.2015.01.006

Lee, N., Amy, G., Croué, J.-P., & Buisson, H. (2004). Identification and understanding of fouling in low-pressure membrane (MF/UF) filtration by natural organic matter (NOM). Water Research, 38(20), 4511–4523. https://doi.org/10.1016/j.watres.2004.08.013

Sun, X., Wu, J., Chen, Z., Su, X., & Hinds, B. J. (2012). Fouling Characteristics and Electrochemical Recovery of Carbon Nanotube Membranes. Advanced Functional Materials, 23(12), 1500–1506. https://doi.org/10.1002/adfm.201201265

Yang, Y., Qiao, S., Jin, R., Zhou, J., & Quan, X. (2018). Fouling control mechanisms in filtrating natural organic matters by electro-enhanced carbon nanotubes hollow fiber membranes. Journal of Membrane Science, 553, 54–62. https://doi.org/10.1016/j.memsci.2018.02.012

Yeung, R., Zhu, X., Gee, T., Gheen, B., Jassby, D., & Rodgers, V. G. J. (2020). Single and binary protein electroultrafiltration using poly(vinyl-alcohol)-carbon nanotube (PVA-CNT) composite membranes. PLOS ONE, 15(4), e0228973. https://doi.org/10.1371/journal.pone.0228973

Yi, G., Chen, S., Quan, X., Wei, G., Fan, X., & Yu, H. (2018a). Enhanced separation performance of carbon nanotube–polyvinyl alcohol composite membranes for emulsified oily wastewater treatment under electrical assistance. Separation and Purification Technology, 197, 107–115. https://doi.org/10.1016/j.seppur.2017.12.058

Yi, G., Chen, S., Quan, X., Wei, G., Fan, X., & Yu, H. (2018b). Enhanced separation performance of carbon nanotube–polyvinyl alcohol composite membranes for emulsified oily wastewater treatment under electrical assistance. Separation and Purification Technology, 197, 107–115. https://doi.org/10.1016/j.seppur.2017.12.058

Zhang, Q., & Vecitis, C. D. (2014). Conductive CNT-PVDF membrane for capacitive organic fouling reduction. Journal of Membrane Science, 459, 143–156. https://doi.org/10.1016/j.memsci.2014.02.017

3.0 Conductive Carbonaceous Nanomaterials as Bacterial Scaffolds for in situ Bioreduction and Biosorption for Enhanced Pb(II) Removal

Abstract

The removal of Pb(II) is imperative due to its inherent toxicity at low levels and its tendency to accumulate in ecosystems. Although biosorption has shown promise in its treatment abilities in the lab scale, its large-scale use is hindered due to the rapid saturation of their binding sites and low regeneration ability. Exoelectrogenic bacteria were proposed as reactive biosorbents that can couple biosorption with the bioreduction of Pb(II) in an attached growth reactor design. Carbon nanotubes (CNTs) and carbon nanofibers (CNFs) were proposed as bacterial scaffolds for the attached growth design where their efficacy along with Pb(II) dosage concentration was investigated. It was found that CNFs yielded optimal Pb(II) removal, maintaining Pb(II) levels ≤0.10 ppm. It was further found that Pb(II) removal was enhanced when Pb(II) dosage concentration increase from 0.5 ppm to 5 ppm, which was correlated to a higher microbial concentration. SEM-EDX analysis was carried out, where the results suggested that Pb(II) was removed as metallic Pb and subsequently oxidized to PbO through oxygen exposure. This was further supported by the found genera which is closely related to known metal reducing bacteria. Overall, these results show the removal capacity of a novel CNF attached growth reactor using exoelectrogenic bacteria for Pb(II) removal at different dosages.

3.1 Introduction

3.1.1 Background

The release of Pb(II) into the environment is inevitable due to its wide use in industries, such as metal plating, batteries, mining operations, and electrical cables (Brink et al., 2019; Colantonio and Kim, 2016). Concerns around its release stems from its level of toxicity, even at low concentrations (<10 mg/L, ppm) Pb(II) interrupts endocrine activities in vulnerable species and can eradicate entire ecosystems at >1000 ppm (Brink et al., 2019). Due to its devastating effects, the world health organization (WHO) has limited its discharge into environments to levels of <0.01ppm (Naik and Dubey, 2013).

Its inherent properties of non-biodegradability and stability make Pb(II) removal difficult from environments (Colantonio and Kim, 2016). Conventional methods that have been used to remove Pb(II) are chemical precipitation, ion-exchange, membrane filtration and electrochemical methods (Fu and Wang, 2010). Chemical precipitation can remove Pb(II) economically but produces toxic sludge that in turn creates difficulties in its disposal. Similarly, ion-exchange has the capacity to remove Pb(II) but its use is hindered due to the strong acids required for resin regeneration which is problematic in terms of secondary pollution. Membrane filtration and electrochemical methods both efficiently remove Pb(II) but are found to be too costly in terms of operational and capital costs. Thus, there is a present need to find both an economical and efficient mode to treat Pb(II) contaminated waters.

In recent years, biosorption has caught the attention of researchers as a viable and economical solution to remove Pb(II) (Hörstmann et al., 2020). Biosorption entails the use of live or reconditioned biomasses as natural adsorbents which have shown to have high sorption capacity for Pb(II) in the lab-scale (Mohapatra et al., 2019; Singh et al., 2020). However, the regeneration and pilot scale studies of these materials have been found to be problematic. For instance, the few studies conducted on biosorbents' regeneration have shown that strong acids such as HCl and HNO_3 are required to recover just 60-80% of their initial sorption capacities with diminishing returns (Martin-Lara et al., 2011; Cechinel et al., 2017; Tran and Chao, 2018; Pandey et al., 2015). Further, pilot scales have shown that biosorbents' binding sites becomes quickly saturated from the reduced retention times, eliminating further Pb(II) removal and possibly causing the desorption of Pb(II) back into treated waters (Singh et al, 2020).

The use of exoelectrogenic bacteria as live, reactive biosorbents may alleviate the challenges associated with biosorption. Exoelectrogens encompasses a class of bacteria capable of transferring electrons extracellularly onto a variety of substrates using their pili or electron shuttles (Logan et al., 2019). Typically, these bacteria are used as catalysts in microbial fuel cells (MFCs) and in microbial electrolysis cells (MECs) to drive the production of electricity or H_2 depending if operated under open circuit, aerobic conditions or under an applied voltage aerobically or anaerobically, respectively (Logan et al., 2007; Logan et al., 2008). However, it was found by Colantonio and Kim that these bacteria have the capacity to use Pb(II) as their terminal electron acceptor when operated in MECs under anaerobic, open circuit conditions (Colantonio and Kim, 2016). From the measured anode potentials, it was found that exoelectrogens have the capacity to gain energy for growth by

dumping their electrons on Pb(II) and reducing it to its elemental form metallic Pb. This is advantageous as the bioconversion of Pb(II) to metallic Pb transforms the metal to a less mobile state which inherently lowers its cytotoxic effects.

This same bioreduction phenomenon was also reported by a study conducted by Brink et al. which used Pb-resistance bacteria from industrial waste to remove 80ppm of Pb(II) in batch reactors (Brink et al., 2019). Overall, these reactors could achieve up to 76% removal of the Pb(II), and XPS confirmed the occurrence of bioreduction. It was found that the bacterial enzymes acted as catalysts to reduce the thermodynamic barrier and in turn allow for Pb(II) to be bioreduced to metallic Pb. Although there are limited studies on the bioreduction of Pb(II) itself, the occurrence of Cr(VI) and U(VI) bioreduction by the action of exoelectrogens is well reported in literature (Sukumar, 2009; Liu et al., 2002; Konishi et al., 2005; Tran and Chao, 2018; Iravani and Varma, 2020; Li et al., 2020; Wang et al., 2015; Thacher et al., 2015; Tekerlekopoulou et al., 2013).

Building on the shown bioreduction capacities of exoelectrogens, it is proposed to use these bacteria as reactive biosorbents to alleviate the challenges currently faced in the biosorption removal of Pb(II). Specifically, it is proposed to use these bacteria in an attached growth configuration utilizing conductive carbonaceous nanomaterials (CCNs). The use of CCNs such as carbon nanotubes (CNTs) and carbon nanofibers (CNFs) is proposed as their flexible structures have been shown to have high efficiency in capturing bacteria in solution (Akasaka and Watari, 2008). By these CCNs capturing bacteria, Pb(II) removal can be improved by: (1) enhancing direct electron transfer and (2) biofilm formation.

The sp^2 hybridized bonds along the CCNs structures allow for fast electron transport along their lengths. This property along with their excellent Pb(II) adsorption capabilities, will allow them to co-adsorb Pb(II) with exoelectrogens and facilitate electron transfer between them (Mahar et al., 2019),(Upadhyayula et al., 2009). This phenomenon was observed when CNTs were implemented in hydrogel beads to facilitate electron transfer between exoelectrogenic bacteria (*Geobacter*, *Pseudomonas* and *Bacillus*) and U(VI). The study conducted by Wang et al., showed that the incorporation of CNTs improved reduction rates from 53.6% to 98.4% through its promotion of electron transfer (Wang et al., 2015). The idea of electron shuttling was further realized in a study conducted by Thacher et al., which showed the electron shuttling capabilities of humic acids with the exoelectrogen, *Shewanella spp* in a Cr(VI) reduction study. Specifically, this research group showed that through the electron shuttling abilities of humic acids, the reduction rate of Cr(VI) to Cr(III) could be increased from 6.14 to 9.9 h^{-1} (Thacher et al., 2015).

Moreover, the incorporation of biofilms on CCNs have been proven to further enhance the bioremediation of metals. Biofilms form from the adsorption of bacteria onto a substrate and the subsequent production of extra polymeric substance (EPS), causing a cascade of bacterial adsorption on the surface. It has been found that this polymeric matrix keeps cells close to one another, enhancing their inter-cellular communications and allowing for them to act in a coordinated manner. This has shown to improve cells resistance to toxic metals and their removal of Pb(II) in several studies (Black et al., 2014; Igiri et al., 2018; Tekerlekopoulou et al., 2013). Thus, the use of CCNs in an attached growth configuration

with exoelectrogenic bacteria should yield a novel mode to remove Pb(II) that exhibits additional benefits compared to the conventional biosorption methods used presently.

3.1.2 Problem Statement

Exoelectrogens are proposed as reactive biosorbents that can both adsorb Pb(II) and reduce it to the less toxic form metallic Pb. Figure 10 depicts the proposed novel attached growth reactor design using CCNs. The overall objectives of this study are:

1. To determine if CCNs can enhance bioremediation removal of Pb(II) by co-adsorbing Pb(II) and exoelectrogens and in turn enhancing electron delivery between them.
2. To investigate the efficacy of different CCNs on Pb(II) removal.
3. To understand the effect Pb(II) dosage concentration has on removal.
4. To understand the mechanisms involved in removing Pb(II) within the proposed reactor

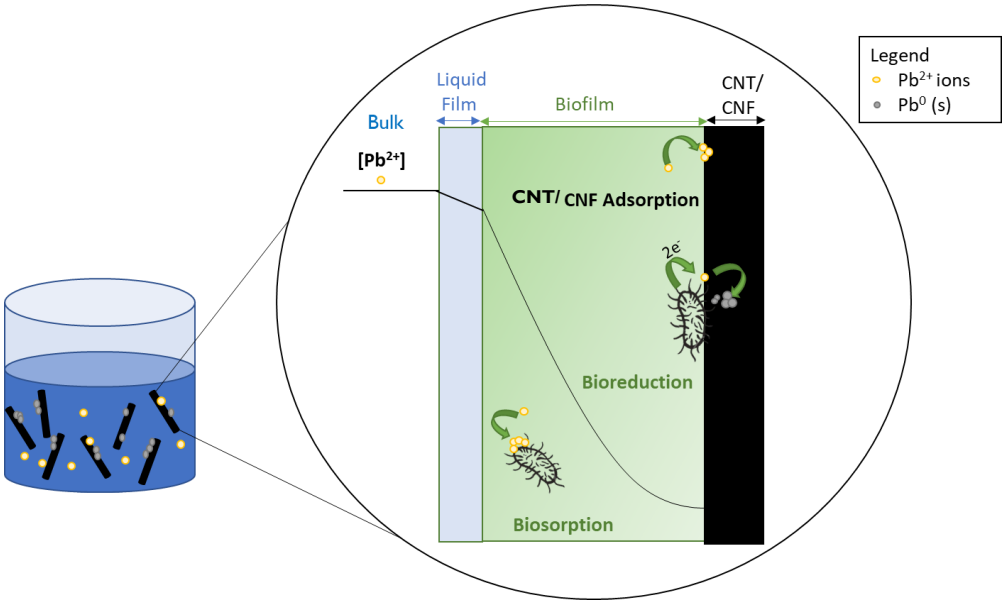

Figure 10. Schematic of the predicted Pb(II) concentration profile and associated removal mechanisms as the ion travels through the proposed attached growth reactor using conductive carbonaceous nanomaterials.

3.2 Materials and Methods

3.2.1 Materials

f-MWCNTs (CNT-COOH: functional content 1.53wt%, purity >99.9wt%, length 10-30µm and diameter 10-20nm, N-CNT: functional content 7.0 ±1.5wt%, purity>99wt%, length 3-30µm and outer diameter – 13-18nm) were purchased from Cheap Tubes (USA). Bare carbon nanofibers (CNFs, graphitized (iron-free), conical platelets diameter 100nm and length 20-200µm) were purchased from Sigma Aldrich Canada. Bare CNFs were functionalized with carboxyl groups using acid treatment with HNO_3 and H_2SO_4 as described elsewhere (Zhang et al., 2007). Glutaraldehyde for SEM fixation was purchased from Alfa Aesar (50vol%). HNO_3 (70wt%) and the 0.45µm PES syringe filters used to acidify and filter samples for ICP-OES (inductive coupled plasma-optical emission

spectrometry) were purchased from Sigma Aldrich Canada and VWR (International, USA), respectively. Reactor feed solution (i.e. synthetic wastewater) was comprised of CH_3COO^-, phosphate buffer solution (PBS, 1.73 g/L $Na_2HPO_4.7\ H_2O$, 0.43 g/L NaH_2PO_4, 0.072 g/L NH_4Cl, 0.026 g/L KCl), 10X mineral and 10X vitamin for nutrients, where $Pb(CH_3COO)_2$ was used as a Pb(II) source in all experiments. Specific dosages as well as reactor volumes can be observed in Table 2. It is important to note 3mM was chosen as the dosage for PBS to mitigate formation of Pb(II)-phosphates.

Table 2. Reactor and control specifications for high and low Pb(II) concentration conditions.

Parameter	Low [Pb(II)] Control	Low [Pb(II)] Reactors	High [Pb(II)] Control	High [Pb(II)] Reactors
[Pb(II)] (ppm)	0.5	0.5	5	5
Volume (mL)	250	250	500	500
$[CH_3COO^-]$ (g/L)	0.5	0.5	1	1
[PBS] (mM)	3	3	3	3
CNTs/CNFs mass (mg)	0	0.685	0	6.85
Inoculum Volume (mL)	3	3	18	18
10X Mineral Solution (µL)	312.5	312.5	625	625
10X Vitamin Solution (µL)	125	125	250	250
Initial COD (ppm)	428	427	947	950

3.2.2 Culture Preparation

To prepare a culture enriched with exoelectrogenic bacteria, inoculum was taken from a MEC reactor that has been operated for over one year. The MEC reactor was a single chamber reactor comprised of a carbon cloth bioanode and 316ss mesh cathode, where the reactor was operated under a constant applied voltage of 0.6V. The reactor was fed with waste activated sludge from the Woodward treatment plant and was supplemented with 1g/L CH_3COO^- and 5mM PBS. It maintained a sufficient current (>0.1mA) for over 1 year, inferring it contains healthy exoelectrogenic bacteria. Prior to taking a culture sample, mixing conditions were applied to the MEC reactor and then a volume sample was taken and dosed into the operating reactor.

3.2.3 Attached Growth Reactor Design and Mode of Operation

Figure 11 depicts the reactor setup used in the experiments. As seen by Figure 11, the reactors were constructed as batch reactors using Erlenmeyer flasks and magnetic stirrers. The magnetic stirrers were added to ensure stirring conditions were maintained at 250RPM to mitigate any concentration gradients and maintain the carbonaceous materials in suspension. To start up the reactors, the feed solution and carbonaceous materials were first added to the reactor. Rubber stoppers were then added on top of the flask and sealed with epoxy to ensure an airtight seal. The inoculum was then dosed into each reactor through the feed port and N_2 (g) was then subsequently purged throughout the reactor for 5 minutes to ensure anaerobic conditions.

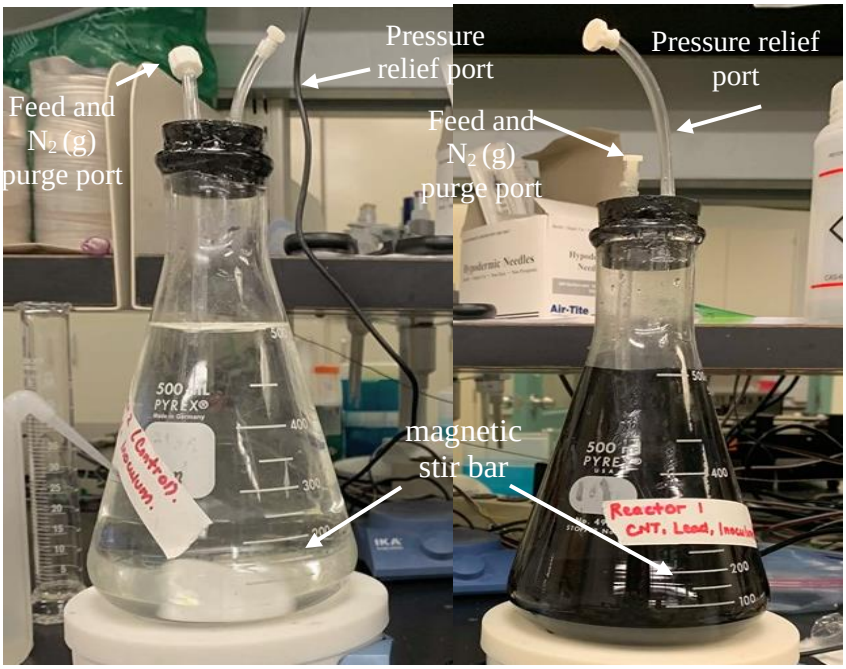

Figure 11. General reactor Design for (a) control with inoculum only and (b) reactor with carbonaceous material and inoculum.

Once the reactors were set-up, a cyclic operation would commence. Each cycle was initiated by a Pb(II) dosage through the feed port, where N_2 (g) would subsequently be bubbled through the reactor for 5 minutes. The dosed Pb(II) was retained in the reactor for approximately 48hrs before a sample would be taken for analysis, marking the end of the cycle. This cyclic pattern was repeated for 12-18 cycles. The temperature was maintained at room temperature (22 ± 0.2°C) for all cycles.

3.2.4 Analysis Measurements

Samples taken after each cycle underwent several analyses. 5mL of the samples were first acidified using HNO_3 (3vol%) prior to being filtered through a 0.45-µm poly(ether) sulfone (PES) syringe filter for ICP-OES (Vista Pro, Varian Inc., Australia) analysis. The remaining of the sample was used to measure pH, optical density (OD_{600}) and chemical oxygen demand (COD). pH was measured through the pH meter (SevenMulti, Mettler-Toledo International Inc., OH) and was carried out to maintain pH levels within 7.0 ± 0.2 to ensure exoelectrogens were healthy while mitigating Pb(II) precipitation. OD_{600} was carried out with control reactors without carbonaceous material (i.e. inoculum and synthetic wastewater) to monitor bacterial growth among cycles. Due to the difficulties of separating cells adhered onto the carbonaceous nanomaterials, the controls were used to approximate cell growth within the reactors themselves. Lastly, in each cycle, COD was measured using high range HACH test kits to ensure there were sufficient carbon sources and thus that bioreduction would not be limited from substrate depletion.

SEM-EDX (scanning electron microscopy, TESCAN SEM) analysis was carried out for some of the reactor fibers. It was performed by first washing the used fibers with DI water 3 times and then adding them onto an SEM aluminum stub in a dropwise manner. The fibers were air dried onto the stub prior to glutaraldehyde fixation, which entailed 30% glutaraldehyde being added onto the fibers' surfaces. Once the glutaraldehyde was added, the stubs were put in the fridge at 4°C for 1hr. After the 1hr, the fibers were dried out using different concentrations of ethanol (70%, 96%, 100%) for 2 minutes each. After the ethanol treatment, the fibers were rinsed once more with DI before being sputter coated with gold and imaged.

3.2.5 Adsorption Experiments Specifications

Adsorption experiments were carried out in 100mL flasks containing 5ppm of Pb(II). The CNFs were dosed at different masses of: 0, 0.00137, 0.0137, 0.137 and 1.37mg. Once the CNFs were added to the flasks, they were added to a shaker which maintained mixing conditions at 500RPM for 48hrs. After the 48hrs commenced, the flasks were taken off the shaker and the samples were filtered through a 0.45μm PES membrane. The filtrate was then acidified with HNO_3 before their Pb(II) concentrations were measured through ICP-OES.

3.2.6 DNA Sequencing

All DNA sequencing was carried out using Illumina Sequencing methods and were performed by the MOBIX Lab at McMaster University.

3.3 Results and Discussion

3.3.1 Reactor Performance Under Different Carbonaceous Materials

To understand the efficacy of using CCNs as bacterial scaffolds for Pb(II) removal, it was first imperative to investigate the performance of different CCNs and compare each to a suspended growth reactor (i.e. no conductive material). Specifically, CNTs and CNFs (CNT-COOH and CNF-COOH) were investigated as conductive materials that can be employed as bacterial scaffolds for the attached reactors. These materials were selected as they are known to have high surface area and excellent adsorbing abilities, making them excellent candidates to co-adsorb Pb(II) with exoelectrogenic bacteria. Since these materials are also comprised of sp^2 hybridized bonds, they are also able to conduct fast electron flow which could aid in the transport of electrons from exoelectrogenic bacteria onto Pb(II) when on their surfaces.

Although carboxyl functionalized CNFs and CNTs promote stable suspensions via electrostatic repulsion, it may be hypothesized that these functional groups could cause charge repulsions from the negatively charged bacteria. Thus, it was also deemed important to investigate how different functional groups may impact the reactors' performance. Thus, nitrogen doped CNTs (N-CNT) were also used in this study. The resulting Pb(II) concentration profiles after each cycle for all the investigated materials is presented in Figure 12.

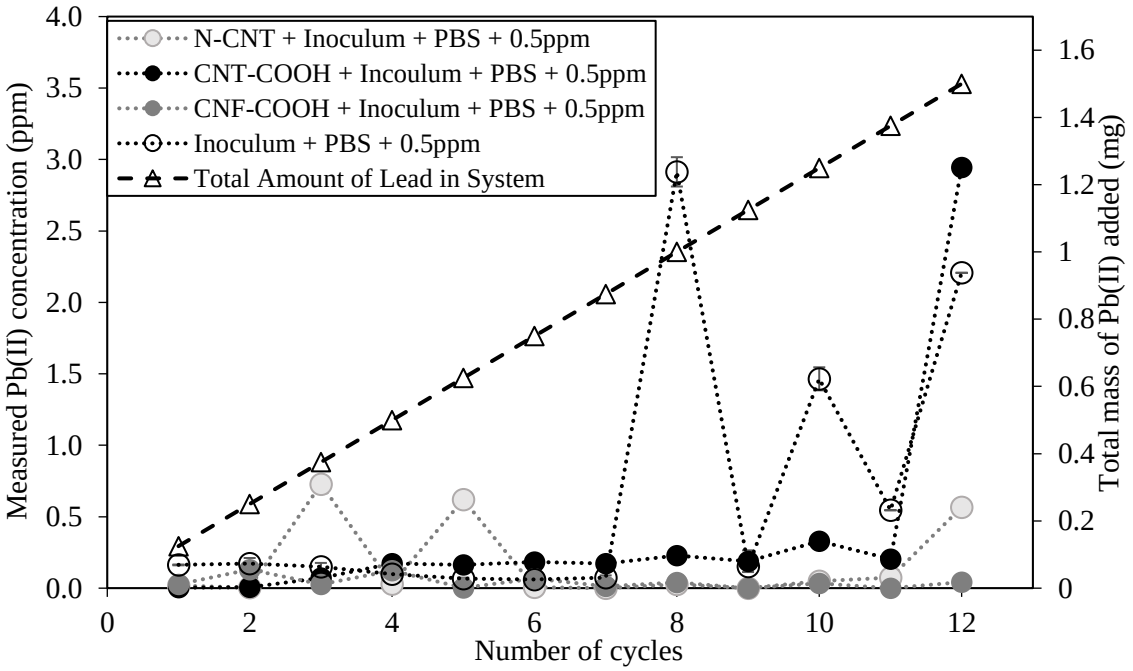

Figure 12. Pb(II) concentration (ppm) profile observed for different carbonaceous nanomaterials (N-CNT, CNT-COOH and CNF-COOH) as a function of time under multiple Pb(II) dosages (mg). Error bars shown represent standard deviation.

Figure 12 shows that CNF-COOH maintains a low Pb(II) concentration profile throughout all cycles, maintaining Pb(II) concentrations < 0.10ppm. Similarly, CNT-COOH initially maintains a low concentration profile until approximately the 4th cycle, where the Pb(II) concentration subsequently rises above 0.1ppm (0.16ppm – 0.30ppm) and then spikes up to 3ppm at the 12th cycle. N-CNT maintains a low Pb(II) concentration (<0.10ppm) for majority of cycles but experiences a multitude of sporadic spikes in Pb(II) concentration (>0.56ppm) as the cycles commence. The sporadic spikes observed for the CNT materials is comparable to the suspended growth control (i.e. inoculum only) which experiences a low Pb(II) concentration up to the 8th cycle and then subsequently experiences a multitude of spikes in Pb(II) concentration, reaching levels up to 2.9ppm.

To understand the difference in performance among the CNTs and CNFs, it is necessary to compare that with the same functional groups (i.e. CNT-COOH with CNF-COOH), where the main structural difference among these are the fibers' lengths. CNFs are approximately 10x longer in length than the CNTs used in this study, inherently making their surface more favourable for bacterial adherence. In addition, CNTs tube like structures have been known to exhibit antimicrobial properties due to their needle-like edges that can disrupt cell membranes when they encounter bacteria (Liu et al., 2018). These inherent properties of the CNTs is likely why these reactors exhibit a similar Pb(II) concentration profile to the suspended growth reactor, as if its size and morphology restricts bacterial attachment, no biofilm will form and the reactor will behave as a suspended growth reactor. Further, if there is no attachment onto the CNTs, the conductive material will not aid in electron transfer between the exoelectrogens and the Pb(II) ions and thus bioreduction will not be

enhanced. This may be the cause for the higher Pb(II) concentrations observed in the CNT-COOH reactor compared to that seen for CNF-COOH.

In terms of the efficacy of functional groups on Pb(II) removal, it is necessary to compare CNT-COOH directly with N-CNT. Figure 12 reveals that N-CNT exhibited more frequent spikes in Pb(II) concentration than CNT-COOH. This was an unexpected result as it was believed that the negative charge of the carboxyl groups may be repelling the bacteria and thus reducing their adherence. It was believed that the nitrogenous groups on the N-CNTs would not exhibit the same repellent nature and thus would be more favourable for bacterial attachment. However, due to the low functional content of the CNT-COOH material (1.53wt%), the difference in functional groups may not be a determining factor on whether bacteria adhere to their surface. Instead, the increase in Pb(II) spike frequency may instead be attributed to the fact that N-CNTs are smaller in length than the CNT-COOH (3-30µm vs. 10-30µm). This would coincide with the results observed for the CNF-COOH reactors as well. It may be worthwhile to sonicate CNTs with PBS prior to being added to the reactor, as this was found to enhance bacterial adherence to MWCNTs in precipitation assays. In theory, MWCNTs theoretically should be a better electron facilitator due to their superior electrical conductivity (Akasaka and Watari, 2008).

Further, the Pb(II) concentration profiles indicate biosorption as the main mechanism for both CNT and suspended growth reactors. In both reactors, as the number of cycles increase there is a clear increase in measured Pb(II) concentration, thereby indicating a reduction in removal. Further, both experiences large spikes in measured Pb(II) concentration to levels nearly of that added to the reactor in total. This profile indicates that their sorption sites were incrementally saturating as the cycles progressed and reached their saturation point when the Pb(II) spikes were observed. If instead bioreduction was the main removal mechanism, the conversion to metallic Pb would be irreversible and the Pb(II) concentration would maintain a low profile. This was only observed for the CNF-COOH reactors, which was theorized to promote more bacterial attachment than both groups of CNTs. Thus, the experimental data suggests that Pb(II) removal in the CNF-COOH and CNT reactors are dominated by bioreduction and biosorption, respectively.

3.3.2 Effect of Different Initial Pb(II) Concentration

To investigate how Pb(II) removal may be impacted by Pb(II) dosage concentration, the Pb(II) dosages were changed from 0.5ppm to 5ppm for the CNF-COOH reactor and the suspended growth reactors. Since the CNF-COOH outperformed both CNT reactors, it was the only reactor used for further analyses. The results for the high Pb(II) concentration and low Pb(II) concentration profiles can be observed in Figure 13a and 13b, respectively. To further understand the removal seen at different Pb(II) dosages, the OD_{600} was monitored for the suspended growth reactors and the results can be seen in Figure 13c.

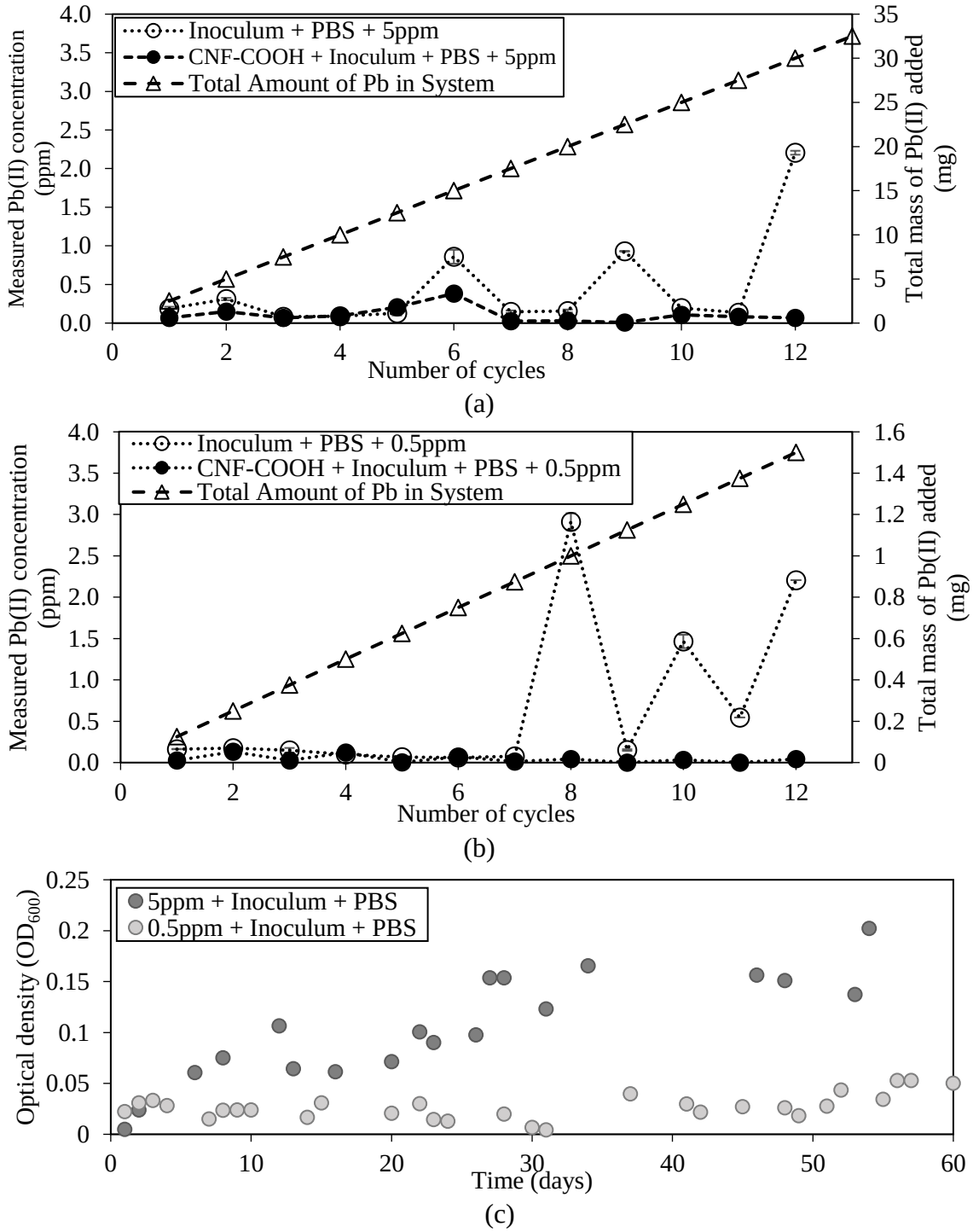

Figure 13. Pb(II) concentration profiles in CNF-COOH, CNT-COOH and Inoculum only Reactors When (a) Operated Under High Pb(II) Concentration (5ppm), (b) Operated Under Low Pb(II) Concentration (0.5ppm) and (c) optical Density found for Controls with only Inoculum when operated under low Pb(II) concentrations (0.5ppm) and high Pb(II) concentrations (5ppm). Error bars represent standard deviation.

Figure 13a and b reveals that for the CNF-COOH reactors, there is greater removal for the reactors dosed with 5ppm than that seen for those dosed with 0.5ppm. The CNF-COOH reactor dosed with 5ppm maintained a low Pb(II) concentration (<0.1ppm) except for on cycles 5 and 6 where it reached a concentration of 0.21ppm and 0.38ppm, respectively. This is comparable to that seen for the CNF-COOH reactor dosed at 0.5ppm, which maintained a Pb(II) concentration <0.1ppm for all cycles. The same trends can be observed for the suspended growth reactors which continued to maintain low Pb(II) concentration profiles under higher Pb(II) dosages and even experienced smaller spikes in Pb(II) concentration compared to the 0.5ppm dosed reactor (0.86-2.2ppm vs. 1.46-2.9ppm).The comparable Pb(II) concentration profiles observed with higher Pb(II) dosages inherently means Pb(II) removal is greater for reactors dosed with 5ppm rather than those dosed at 0.5ppm.

Figure 13c shows that the bacterial concentration initially begins at the same level for both reactors but as time progresses cell growth increases much faster and at a higher capacity for reactors fed with 5ppm. This can be attributed to the fact that these reactors are operated under anaerobic conditions with minimal nitrates and sulfates (≈ppb) which were only dosed at the beginning of operation. Thus, the only terminal electron acceptor available for these bacteria to use to gain energy for growth is the Pb(II) ions. Thus, with a greater amount of Pb(II) ions available, more bacteria can utilize them as a terminal electron acceptor to fuel their growth, which is in accordance to the hypothesis made by Colantonio and Kim (Colantonio and Kim, 2016).This trend is also in agreement to the Cr(VI) bioreduction study conducted by Tekerlekopoulou et al. which showed that Cr(VI) had an enhancing effect on microbial growth as their terminal electron acceptor when under cytotoxic levels (Tekerlekopoulou et al., 2013). Moreover, a greater concentration in bacterial population directly correlates to greater removal, as more bacteria results in more reactive biosorbents available to conduct both biosorption and bioreduction removal. This agrees with a multitude of Cr(VI) and U(VI) studies which have demonstrated greater removal with increasing initial concentrations (Sukumar, 2009; Tekerlekopoulou et al., 2013; Wang et al., 2015).

3.3.3 Investigating CNF Reactors' Removal Mechanisms

The next aspect of this study involved gaining a further understanding on the mechanisms that are governing removal in these CNF-COOH reactors. Thus, a second control was constructed with PBS and the CNF-COOHs to assess the percent removal attributed to the CNF-COOHs and the exoelectrogens themselves. The results of this second control in comparison to the CNF-COOH and the suspended growth reactors at different Pb(II) dosages can be seen in Figure 14.

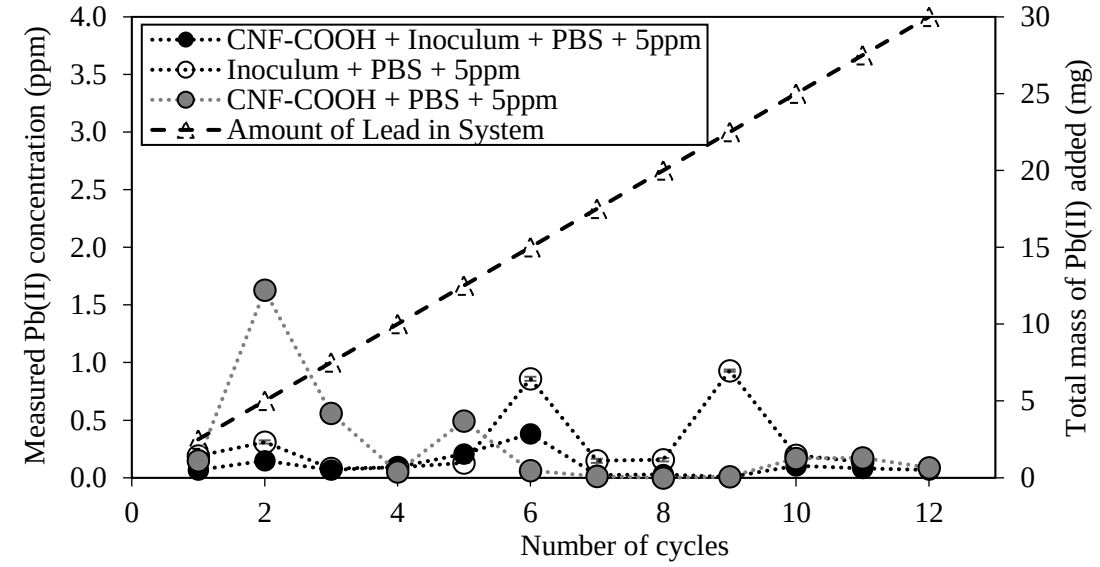

(a)

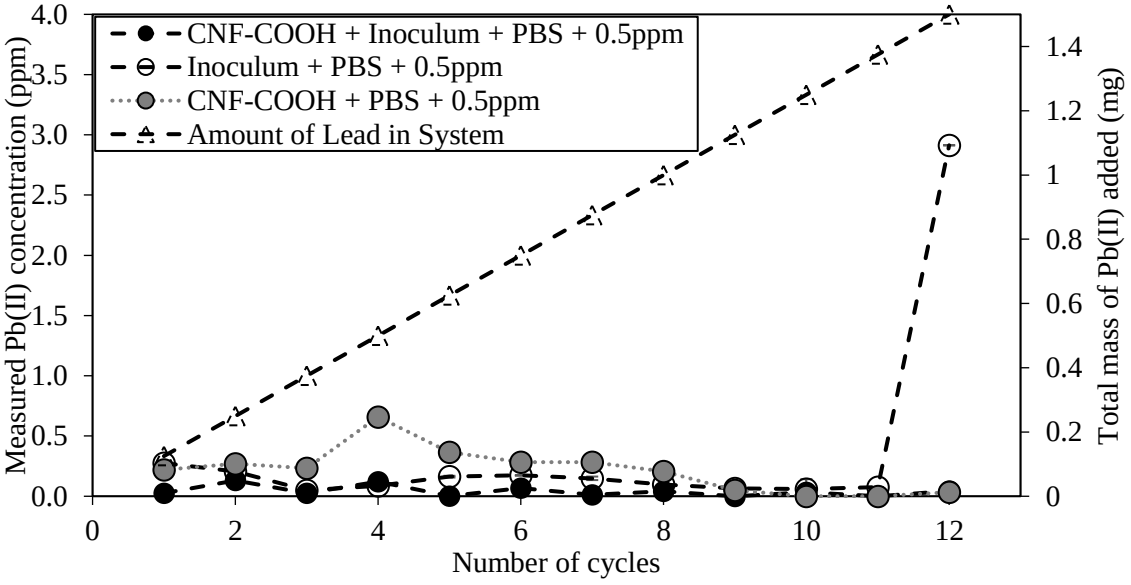

(b)

Figure 14. Comparison of Pb(II) concentration profiles for CNF-COOH reactors and their controls with inoculum and CNF-COOH only when operated under (a) high Pb(II) concentrations (5ppm) and (b) low Pb(II) concentrations (0.5ppm). Error bars shown represent standard deviation.

Figure 14 shows that under both Pb(II) dosages, the second control comprised of only PBS and Pb(II) maintained good removal. Besides the few instances where this control experienced sharp increases in Pb(II) concentration, it generally could maintain a Pb(II) concentration profile between 0.1-0.3ppm for both high and low Pb(II) dosages. This could imply that CNF-COOHs are excellent Pb(II) adsorbers and can adsorb up to approximately

30mg of Pb(II) with few instances of Pb(II) desorption. If this postulation is true, this would mean the CN-COOHFs would need a minimum sorption capacity of 4.38 x10^3 mg-Pb(II)/g-CNF-COOH, which is quite high for that reported for carbonaceous nanomaterials (Mahar et al., 2019). Therefore, another plausible cause for this removal could be due to a precipitation reaction through PBS. Specifically, insoluble Pb(II) phosphate precipitates may be forming through the reaction

$$3Pb(CH_3COO)_2(aq) + 2Na_3PO_4(aq) \rightarrow Pb_3(PO_4)_2(s) + 6Na(CH_3COO)(\text{aq}) \quad (1)$$

which has a ΔG<0, meaning the reaction occurs spontaneously.

Thus, to rule out the possibility of CNF-COOHs being excellent Pb(II) adsorbers, adsorption experiments were carried out to analyze their isotherm properties (i.e. sorption capacities). The resulting experimental data was fitted against two isotherm models, the Langmuir and the Freundlich isotherm, as these are the two isotherms commonly fitted to CCNs (Mahar et al., 2019; Upadhyayula et al., 2009). The Langmuir isotherm assumes a monolayer coverage of the sorbate and that all sorption sites are identical (i.e. identical binding energies without interference between binding sites). Using these assumptions, the Langmuir isotherm models equilibrium sorption capacity as,

$$q_{eq} = \frac{q_{max}K_L S_{eq}}{1+K_L S_{eq}} \quad (2)$$

where q_{eq} is the equilibrium sorption capacity (mg-Pb(II)/g-CNF-COOH), q_{max} is the maximum sorption capacity (mg-Pb(II)/g-CNF-COOH), K_L is the relative energy of adsorption (L/mg) and S_{eq} is the equilibrium Pb(II) concentration. Alternatively, the Freundlich isotherm model assumes that there is a distribution of adsorption sites and energies as well as multilayer adsorption on a diverse surface. Using these assumptions, the Freundlich isotherm is modelled through,

$$q_{eq} = K_F S_{eq}^{\frac{1}{N}} \quad (3)$$

where K_F represents the adsorption capacity (L/g-CNF)$^{1/N}$ and N^{-1} represents the adsorption capacity (0< N <1). To assess which model's isotherm is a better fit for the CNF-COOH experimental data, the experimental data was plotted along both isotherms in Figure S.2.
Figure S.2 shows that both Freundlich and Langmuir isotherm models fit the experimental data well with R^2 values of 0.95 and 0.96, respectively. To better understand the CNF-COOH's maximum sorption capacity, the Langmuir model was used. It was found that the maximum capacity of the CNF-COOH are 61.4 mg-Pb(II)/g-CNF-COOH. This only allows for a maximum of 0.042mg and 0.42mg of Pb(II) to be adsorbed in the 0.5 and 5ppm Pb(II) concentrated reactors, respectively. This means Pb(II) precipitation is the main removal mechanism in the second control.
To ensure this was not the dominating removal mechanism of the reactors themselves, PBS was no longer added to the reactors and they were operated for 6 more Pb(II) dosages. The results of this experiment can be observed in Figure S.3. Figure S.3 shows that reactors containing both CNF-COOHs and exoelectrogens can maintain the same degree of Pb(II) removal without PBS, thus supporting that Pb(II) precipitation does not govern its Pb(II) removal. This does not hold true for the control reactors which experienced a great reduction of Pb(II) removal, especially those simply comprised of CNF-COOHs and PBS. It was observed that the Pb(II) concentration increased to levels 10x that experienced

without PBS, demonstrating their dependency on Pb(II) precipitation as the dominant removal mechanism. Suspended growth controls also experienced a reduction in performance, especially those dosed with 0.5ppm, insinuating that chemical precipitation aided their removal of Pb(II). However, since the Pb(II) concentration did not rise to the same levels as the second control, it can be concluded that bioremediation methods also played a role in its Pb(II) removal.

To further investigate the governing removal mechanisms in the CNF-COOH reactors, the CNF-COOH with inoculum reactor and the CNF-COOH without inoculum control operated under 5ppm were analyzed using SEM-EDX. Figure 15 shows the different SEM images taken for the reactor and control CNF fibers with PBS under mapping analysis and point spectra.

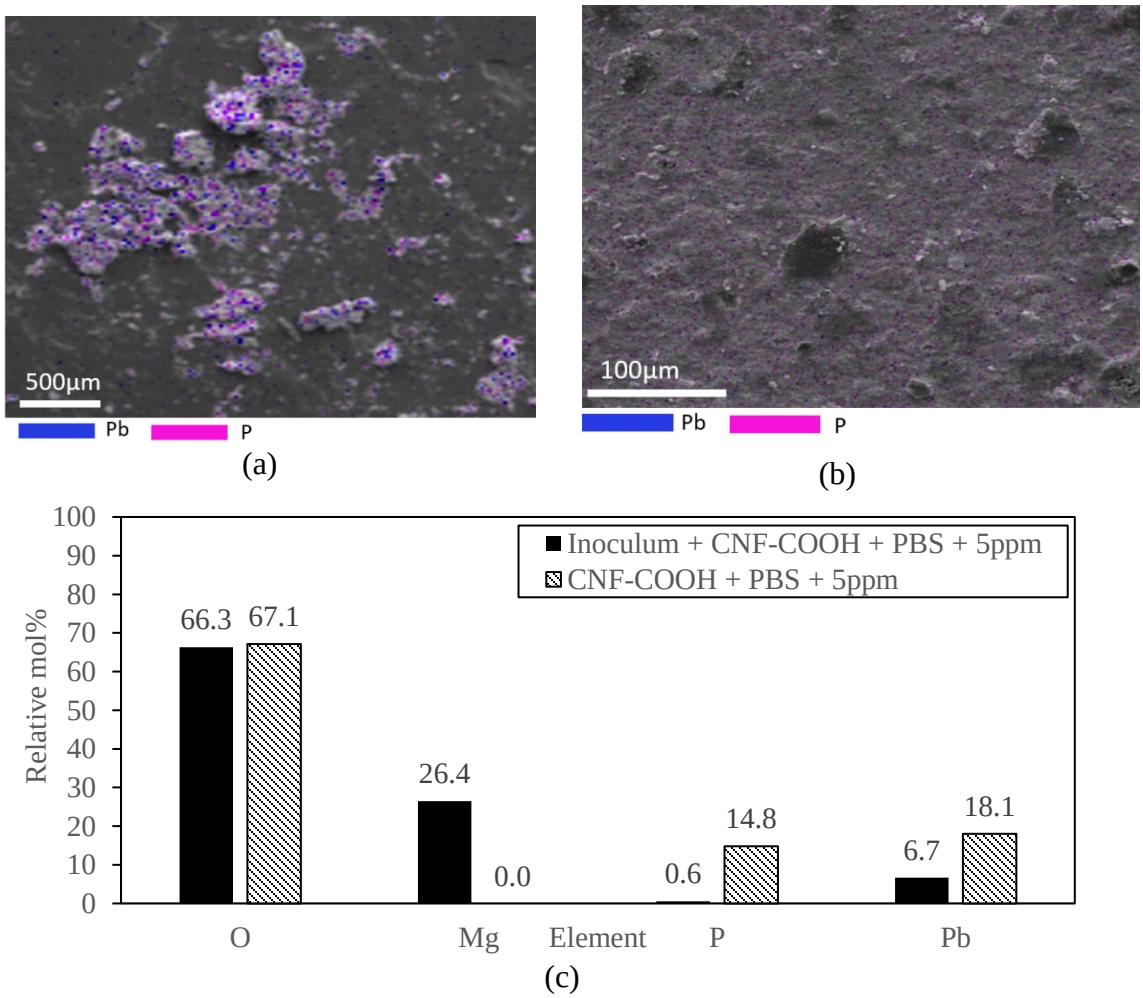

Figure 15. SEM-EDX images from (a) mapping of CNF Reactor operated under high Pb(II) concentration, and (b) mapping of CNF control without inoculum dosed with high Pb(II) and (c) Point spectra results from the CNF reactor and CNF control without inoculum that were operated under high Pb(II) concentration, where carbon mol% was excluded.

The mapping images reveal that the distribution of Pb(II) and P-ions vary greatly between reactors operated with and without inoculum. The mapping images for CNF-COOH with inoculum show that in the presence of inoculum, Pb is deposited in distinct locations along the fiber. The same phenomenon was observed for Colantonio and Kim who found that metallic Pb deposited in distinct locations of graphite fibers when operating an MEC under open circuit conditions (Colantonio and Kim, 2016). If Pb(II) removal was dominated by CNF-COOH adsorption, the CNF-COOHs would likely exhibit a monolayer coverage of the Pb(II) ions and further would have likely been washed by the washing steps that were put in place. Conversely, the control fibers without inoculum have a distribution of ions that are uniform, insinuating Pb(II) has complexation with P. Therefor, the data suggests that Pb(II) has been removed as $Pb_3(PO4)_2$ in the control and likely as metallic Pb in the reactor with inoculum. To support this hypothesis, EDX point spectra analysis was carried out for both samples.

EDX is a semi-quantitative analysis that provides an estimate of ion ratios within each sample, providing further insight on ion complexation. In terms of the control without inoculum, the relative mol ratios support the hypothesis that Pb(II) is complexed with PO_4^{3-} to form $Pb_3(PO_4)_2$. Specifically, the Pb:P ratio of 1.24:1 and the P:O ratio of 4.5:1 closely resembling the theoretical ion ratios of $Pb_3(PO_4)_2$ which is 1.5 and 4:1, respectively. The ratios of the respective ions drastically changed once inoculum was added to the reactors. For instance, the Pb:P ratio increased from 1.24:1 to 11.2:1, indicating that other forms of Pb exist other than $Pb_3(PO_4)_2$. Prior to analyzing mol ratios with Pb, it is important to consider the complexation the mineral Mg(II) may form. $Mg(SO_4)$ was added to the reactor with inoculum to aid in bacterial growth and it seems that the cation of the mineral has adsorbed onto the fibers themselves. $Mg(SO_4)$ is extremely soluble in water, dissociating into its ionic form and subsequently forming the complexation $Mg(OH)_2$. If it is assumed that all Mg is present in this form, then 52.8mols of O will be consumed, leaving 13.5mols left to react with other ions. If we further assume that P forms PO_4^{3-} with oxygen 2.4 more mols of O will be complexed and 11.1 mols will be remaining to form complexation with Pb.

O was considered to be complexed with Pb as it has been found in literature that metallic Pb nanoparticles spontaneously oxidize in aerobic conditions, transforming them to PbO (Brink et al., 2019). It is likely that through the different feeds and Pb(II) dosages, oxygen was introduced into the reactor and thus oxidizing the present metallic Pb nanoparticles. Thus, after the consideration of the aforementioned complexations the Pb:O mol ratio was calculated at 0.6:1 which is close to the theoretical approximation of 1:1 of PbO. The deviation from the theoretical prediction can be associated with O ions present on CNF-COOH fibers as carboxyl and carbonyl functional groups. Moreover, the yellow/brown colour formed in the control reactor with only inoculum seen in Figure S.4 further support this, as PbO has been reported to exhibit this colour (Brink et al., 2019). This could not be seen in the CNF-COOH reactors themselves due to the black colour the carbonaceous material yields

The postulation that majority of Pb(II) was converted to metallic Pb is further supported by the found genus types in the CNF-COOH reactor seen in Figure 16.

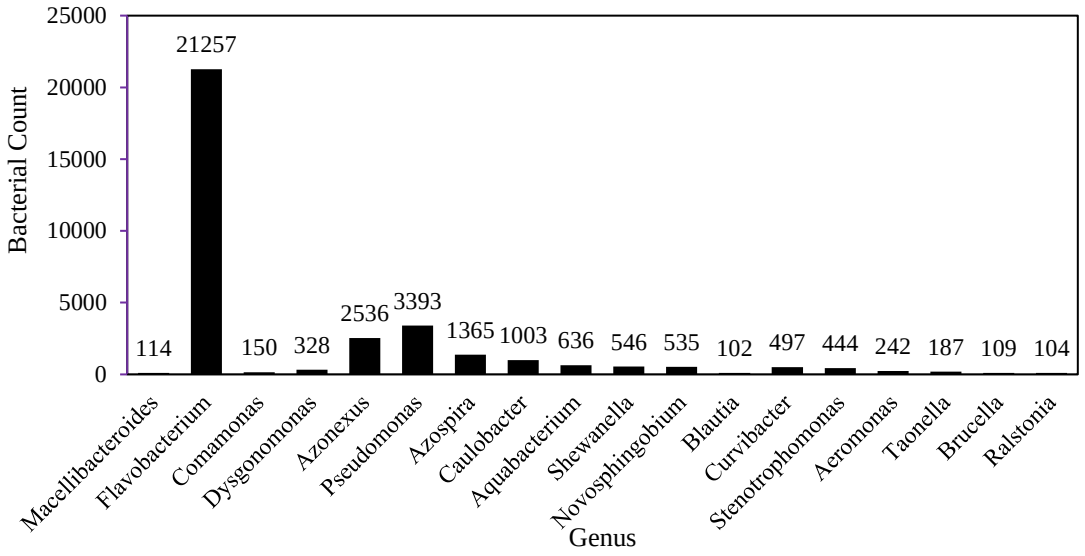

Figure 16. Bacterial count found for dominant genus types in the CNF reactor with inoculum dosed at 5ppm. Genus types found with less than 100 counts were not included.

As shown in Figure 16, the reactor was mainly comprised of the *flavobacterium* spp. This genus type has been reported by Chen et al. and Lovley to be able to transfer electrons to dye compounds and Se(IV), in turn degrading dyes and reducing the metal to its elemental form, respectively (Chen et al., 2017; Lovely, 1993). Although, this genus has not been investigated in Pb(II) bioreduction, it shows its capacity to extracellularly transfer electrons to different substrates. Further, *Shewanella spp.* are well reported in literature as dissimilarity metal reducing bacteria, capable of simultaneously reducing Fe(III), Co(III), U(VI) Cr(VI) and Tc(VII), exemplifying its capacity to bioreduce various metals (Liu et al., 2002) *Shewanella spp.* was further reported by Logan et al. to have the capacity of bioreducing Cr(VI) to Cr(III) at >90% removals (Logan et al., 2019).

Additionally, *Pseudomonas spp.* was confirmed by Wang et al. to have the capacity of bioreducing Cr(VI) to Cr(III) through XPS analysis (Li et al., 2020). In another study the same genera *Pseudomonas spp.* was used in the reduction of U(VI) utilizing CNT hydrogel beads (Wang et al., 2015). The genera were found to have bioreducing capabilities, removing 90% of the metal via bioreduction. This just highlights a few examples of well-documented exoelectrogenic bacteria found in the CNF-COOH reactor to demonstrate that the consortium found in the reactor has high bioreducing capacities. Using the found consortium along with the mass balances from the EDX spectra, it is likely that the reactor containing inoculum removed Pb(II) as metallic Pb and was in turn oxidized to PbO. To conclude these results, XPS and XRD experiments should be carried out to confirm the valence state and crystallinity of the Pb(II) forms.

3.4 Conclusions and Recommendations

This study looked at the efficacy of different conductive nanomaterials as bacterial scaffolds for the reactive biosorbents, exoelectrogenic bacteria. Specifically, it investigated the efficacy of different conductive carbonaceous nanomaterials, Pb(II) dosage

concentrations and attempted to understand the main removal mechanisms present in the reactors. The main conclusions that resulted from this study are:

1. CNF-COOH was the optimal conductive material in removing Pb(II), maintaining Pb(II) concentrations < 0.1ppm over 18 cycles
2. Pb(II) removal was enhanced with higher Pb(II) concentration dosages as it promotes higher bacterial concentrations in the reactors
3. Experimental data suggest that Pb(II) bioreduction is the dominant Pb(II) removal mechanism in the CNF-COOH reactors

Future studies should look at using XPS and XRD analyses to confirm if Pb(II) bioreduction is the dominant removal mechanism in the CNF-COOH reactors. In addition, further studies should look at optimizing operational conditions (i.e. mixing conditions, temperature, pH, feed composition etc.) in a design of experiment format in the interest of improving the efficacy of the attached growth reactor in Pb(II) removal. Further, it would also be advantageous to look at specific isolates' ability to bioreduce Pb(II) in the found attached growth configuration to gain a better understanding of individual microorganisms' capacity to remove Pb(II).

3.5 References

Akasaka, T., & Watari, F. (2009). Capture of bacteria by flexible carbon nanotubes. Acta Biomaterialia, 5(2), 607–612. https://doi.org/10.1016/j.actbio.2008.08.014

Black, R., Sartaj, M., Mohammadian, A., & Qiblawey, H. A. M. (2014). Biosorption of Pb and Cu using fixed and suspended bacteria. Journal of Environmental Chemical Engineering, 2(3), 1663–1671. https://doi.org/10.1016/j.jece.2014.05.023

Brink, H. G., Hörstmann, C., & Peens, J. (2019). Microbial Pb(II)-precipitation: the influence of oxygen on Pb(II)-removal from aqueous environment and the resulting precipitate identity. International Journal of Environmental Science and Technology, 17(1), 409–420. https://doi.org/10.1007/s13762-019-02502-4

Cechinel, M. A. P., Mayer, D. A., Mazur, L. P., Silva, L. G. M., Girardi, A., Vilar, V. J. P., de Souza, A. A. U., & Guelli U. de Souza, S. M. A. (2018). Application of ecofriendly cation exchangers (Gracilaria caudata and Gracilaria cervicornis) for metal ions separation and recovery from a synthetic petrochemical wastewater: Batch and fixed bed studies. Journal of Cleaner Production, 172, 1928–1945. https://doi.org/10.1016/j.jclepro.2017.11.235

Chen, C.-Y., Tsai, T.-H., Wu, P.-S., Tsao, S.-E., Huang, Y.-S., & Chung, Y.-C. (2017). Selection of electrogenic bacteria for microbial fuel cell in removing Victoria blue R from wastewater. Journal of Environmental Science and Health, Part A, 53(2), 108–115. https://doi.org/10.1080/10934529.2017.1377580

Colantonio, N., & Kim, Y. (2016). Lead(II) Removal at the Bioanode of Microbial Electrolysis Cells. ChemistrySelect, 1(18), 5743–5748. https://doi.org/10.1002/slct.201601539

Feng, C., Li, J., Qin, D., Chen, L., Zhao, F., Chen, S., Hu, H., & Yu, C.-P. (2014). Characterization of Exoelectrogenic Bacteria Enterobacter Strains Isolated from a Microbial Fuel Cell Exposed to Copper Shock Load. PLoS ONE, 9(11), e113379. https://doi.org/10.1371/journal.pone.0113379

Fu, F., & Wang, Q. (2011). Removal of heavy metal ions from wastewaters: A review. Journal of Environmental Management, 92(3), 407–418. https://doi.org/10.1016/j.jenvman.2010.11.011

Hörstmann, C., Brink, H. G., & Chirwa, E. M. N. (2020). Pb(II) Bio-Removal, Viability, and Population Distribution of an Industrial Microbial Consortium: The Effect of Pb(II) and Nutrient Concentrations. Sustainability, 12(6), 2511. https://doi.org/10.3390/su12062511

Igiri, B. E., Okoduwa, S. I. R., Idoko, G. O., Akabuogu, E. P., Adeyi, A. O., & Ejiogu, I. K. (2018). Toxicity and Bioremediation of Heavy Metals Contaminated Ecosystem from Tannery Wastewater: A Review. Journal of Toxicology, 2018, 1–16. https://doi.org/10.1155/2018/2568038

Iravani, S., & Varma, R. S. (2020). Bacteria in Heavy Metal Remediation and Nanoparticle Biosynthesis. ACS Sustainable Chemistry & Engineering, 8(14), 5395–5409. https://doi.org/10.1021/acssuschemeng.0c00292

Jangir, Y., French, S., Momper, L. M., Moser, D. P., Amend, J. P., & El-Naggar, M. Y. (2016). Isolation and Characterization of Electrochemically Active Subsurface

Delftia and Azonexus Species. Frontiers in Microbiology, 7, 3130–3137. https://doi.org/10.3389/fmicb.2016.00756

Kim, H. J. (2009). Book Review: Microbial Fuel Cells. By Bruce E. Logan. Chemical Engineering & Technology, 32(6), 858. https://doi.org/10.1002/ceat.200990026

Konishi, Y., Tsukiyama, T., Ohno, K., Saitoh, N., Nomura, T., & Nagamine, S. (2006). Intracellular recovery of gold by microbial reduction of AuCl4− ions using the anaerobic bacterium Shewanella algae. Hydrometallurgy, 81(1), 24–29. https://doi.org/10.1016/j.hydromet.2005.09.006

Li, Y., Wang, H., Wu, P., Yu, L., Rehman, S., Wang, J., Yang, S., & Zhu, N. (2020). Bioreduction of hexavalent chromium on goethite in the presence of Pseudomonas aeruginosa. Environmental Pollution, 265, 114765. https://doi.org/10.1016/j.envpol.2020.114765

Liu, C., Gorby, Y. A., Zachara, J. M., Fredrickson, J. K., & Brown, C. F. (2002). Reduction kinetics of Fe(III), Co(III), U(VI), Cr(VI), and Tc(VII) in cultures of dissimilatory metal-reducing bacteria. Biotechnology and Bioengineering, 80(6), 637–649. https://doi.org/10.1002/bit.10430

Liu, D., Mao, Y., & Ding, L. (2018). Carbon nanotubes as antimicrobial agents for water disinfection and pathogen control. Journal of Water and Health, 16(2), 171–180. https://doi.org/10.2166/wh.2018.228

Logan, B. E., Call, D., Cheng, S., Hamelers, H. V. M., Sleutels, T. H. J. A., Jeremiasse, A. W., & Rozendal, R. A. (2008). Microbial Electrolysis Cells for High Yield Hydrogen Gas Production from Organic Matter. Environmental Science & Technology, 42(23), 8630–8640. https://doi.org/10.1021/es801553z

Logan, B. E., Rossi, R., Ragab, A., & Saikaly, P. E. (2019). Electroactive microorganisms in bioelectrochemical systems. Nature Reviews Microbiology, 17(5), 307–319. https://doi.org/10.1038/s41579-019-0173-x

Lovley, D. R. (1993). Dissimilatory Metal Reduction. Annual Review of Microbiology, 47(1), 263–290. https://doi.org/10.1146/annurev.mi.47.100193.001403

Madhavan, A., Prasad, M., Girish, S., Shetty, K., & Nair, B. (2017). Caulobacter Crescentus as a Novel Exoelectricigen in a Dual Chambered Microbial Fuel Cell (MFC). International Conference on Technological Advancements in Power and Energy (TAP Energy), 6905–6909. https://doi.org/10.1109/TAPENERGY.2017.8397199

Mahar, F. K., He, L., Wei, K., Mehdi, M., Zhu, M., Gu, J., Zhang, K., Khatri, Z., & Kim, I. (2019). Rapid adsorption of lead ions using porous carbon nanofibers. Chemosphere, 225, 360–367. https://doi.org/10.1016/j.chemosphere.2019.02.131

Martín-Lara, M. A., Blázquez, G., Ronda, A., Rodríguez, I. L., & Calero, M. (2012). Multiple biosorption–desorption cycles in a fixed-bed column for Pb(II) removal by acid-treated olive stone. Journal of Industrial and Engineering Chemistry, 18(3), 1006–1012. https://doi.org/10.1016/j.jiec.2011.11.150

Mohapatra, R. K., Parhi, P. K., Pandey, S., Bindhani, B. K., Thatoi, H., & Panda, C. R. (2019). Active and passive biosorption of Pb(II)using live and dead biomass of marine bacterium Bacillus xiamenensis PbRPSD202: Kinetics and isotherm studies. Journal of Environmental Management, 247, 121–134. https://doi.org/10.1016/j.jenvman.2019.06.073

Naik, M. M., & Dubey, S. K. (2013). Lead resistant bacteria: Lead resistance mechanisms, their applications in lead bioremediation and biomonitoring. Ecotoxicology and Environmental Safety, 98, 1–7. https://doi.org/10.1016/j.ecoenv.2013.09.039

Narayani, M., & Vidya Shetty, K. (2013). Reduction of hexavalent chromium by a novelOchrobactrumsp. - microbial characteristics and reduction kinetics. Journal of Basic Microbiology, 54(4), 296–305. https://doi.org/10.1002/jobm.201200183

Pandey, A., Bera, D., Shukla, A., & Ray, L. (2007). Studies on Cr(VI), Pb(II) and Cu(II) adsorption–desorption using calcium alginate as biopolymer. Chemical Speciation & Bioavailability, 19(1), 17–24. https://doi.org/10.3184/095422907x198031

Singh, S., Kumar, V., Datta, S., Dhanjal, D. S., Sharma, K., Samuel, J., & Singh, J. (2020). Current advancement and future prospect of biosorbents for bioremediation. Science of The Total Environment, 709, 135895. https://doi.org/10.1016/j.scitotenv.2019.135895

Sun, Y., Zuo, J., Cui, L., Deng, Q., & Dang, Y. (2010). Diversity of microbes and potential exoelectrogenic bacteria on anode surface in microbial fuel cells. The Journal of General and Applied Microbiology, 56(1), 19–29. https://doi.org/10.2323/jgam.56.19

Tekerlekopoulou, A. G., Tsiflikiotou, M., Akritidou, L., Viennas, A., Tsiamis, G., Pavlou, S., Bourtzis, K., & Vayenas, D. V. (2013). Modelling of biological Cr(VI) removal in draw-fill reactors using microorganisms in suspended and attached growth systems. Water Research, 47(2), 623–636. https://doi.org/10.1016/j.watres.2012.10.034

Thacher, R., Hsu, L., Ravindran, V., Nealson, K. H., & Pirbazari, M. (2015). Modeling the transport and bioreduction of hexavalent chromium in aquifers: Influence of natural organic matter. Chemical Engineering Science, 138, 552–565. https://doi.org/10.1016/j.ces.2015.08.011

Tran, H. N., & Chao, H.-P. (2018). Adsorption and desorption of potentially toxic metals on modified biosorbents through new green grafting process. Environmental Science and Pollution Research, 25(13), 12808–12820. https://doi.org/10.1007/s11356-018-1295-9

Upadhyayula, V. K. K., Deng, S., Mitchell, M. C., & Smith, G. B. (2009). Application of carbon nanotube technology for removal of contaminants in drinking water: A review. Science of The Total Environment, 408(1), 1–13. https://doi.org/10.1016/j.scitotenv.2009.09.027

Venkidusamy, K., & Megharaj, M. (2016). Identification of Electrode Respiring, Hydrocarbonoclastic Bacterial Strain Stenotrophomonas maltophilia MK2 Highlights the Untapped Potential for Environmental Bioremediation. Frontiers in Microbiology, 7, 1965–1971. https://doi.org/10.3389/fmicb.2016.01965

Wang, W., Feng, Y., Tang, X., Li, H., Du, Z., Yi, A., & Zhang, X. (2015). Enhanced U(VI) bioreduction by alginate-immobilized uranium-reducing bacteria in the presence of carbon nanotubes and anthraquinone-2,6-disulfonate. Journal of Environmental Sciences, 31, 68–73. https://doi.org/10.1016/j.jes.2014.11.005

Xing, D., Cheng, S., Logan, B. E., & Regan, J. M. (2009). Isolation of the exoelectrogenic denitrifying bacterium Comamonas denitrificans based on dilution to extinction. Applied Microbiology and Biotechnology, 85(5), 1575–1587. https://doi.org/10.1007/s00253-009-2240-0

Yoshida, N., Miyata, Y., Doi, K., Goto, Y., Nagao, Y., Tero, R., & Hiraishi, A. (2016). Graphene oxide-dependent growth and self-aggregation into a hydrogel complex of exoelectrogenic bacteria. Scientific Reports, 6(1), 6. https://doi.org/10.1038/srep21867

Zhang, G., Sun, S., Yang, D., Dodelet, J.-P., & Sacher, E. (2008). The surface analytical characterization of carbon fibers functionalized by H2SO4/HNO3 treatment. Carbon, 46(2), 196–205. https://doi.org/10.1016/j.carbon.2007.11.002

Zhang, Y., Min, B., Huang, L., & Angelidaki, I. (2009). Generation of Electricity and Analysis of Microbial Communities in Wheat Straw Biomass-Powered Microbial Fuel Cells. Applied and Environmental Microbiology, 75(11), 3389–3395. https://doi.org/10.1128/aem.02240-08

Zuo, Y., Xing, D., Regan, J. M., & Logan, B. E. (2008). Isolation of the Exoelectrogenic Bacterium Ochrobactrum anthropi YZ-1 by Using a U-Tube Microbial Fuel Cell. Applied and Environmental Microbiology, 74(10), 3130–3137. https://doi.org/10.1128/aem.02732-07

4.0 Modelling of Carbon Nanofiber Attached Growth Reactors as a Predictive Tool for Pb(II) Removal in Biofilms

Abstract

The removal of Pb(II) is paramount due to its tendency to accumulate in ecosystems, creating devastating effects at concentrations <10ppm. In recent years, biosorption has gained the attention of researchers due to biosorbents' high sorption capacity for Pb(II) at the lab-scale. However, its large-scale use has been hindered from sorption site saturation, reducing its overall removal capacity and possibly causing the recontamination of treated waters. Exoelectrogens are proposed as reactive sorbents in a carbon nanofiber (CNF) attached growth design to alleviate the current hurdle faced by biosorption. This study showed the efficacy of CNF attached growth reactors for long term removal under multiple Pb(II) dosages, demonstrating its robustness in maintaining removal at approximately 80% over 10 cycles with 1.5ppm Pb(II) dosages. A numerical model was further proposed to assess which removal mechanisms dominated Pb(II) removal. The model fit the experimental data well with an R^2 of 0.92 and confirmed the prediction that bioreduction governed removal. A sensitivity analysis further revealed that Pb(II) removal is most sensitive to Monod kinetic parameters and biofilm thickness in the reactor. Overall, this study was successful in demonstrating the efficacy of a CNF-attached growth reactor in long term Pb(II) removal while using numerical modelling to understand the removal mechanisms involved as well as the main influential parameters on Pb(II) removal.

4.1 Introduction

4.1.1 Background

Environmental exposure to Pb(II) remains a ubiquitous issue through its use in metal plating, pesticides, mining, electrical cables, and storage battery plating (Fu and Wang, 2011; Brink et al., 2019; Colantonio and Kim, 2016). Concerns around its environmental release stems from its level of toxicity. It was found that even at small concentrations, Pb(II) can disrupt endocrine activities in susceptible species (<10ppm) and even destroy ecosystems (>100ppm). Due to its devastating effects, the United States Environmental Protection Agency (EPA) has created stringent regulations limiting its release to 0.01ppm (Rodriguez et al., 2019). Pb(II) removal from wastewater faces a multitude of challenges due to its fundamental properties of physical stability and non-biodegradability.

Conventional methods used to remove Pb(II) from wastewater include chemical precipitation, ion-exchange, adsorption, membrane filtration and electrochemical methods. Although these processes have the capacity to remove Pb(II) to meet regulations, each method possesses its own limitations and challenges. For instance, chemical precipitation requires the continual addition of chemicals as well as subsequent removal of toxic chemical precipitants (Fu and Wang, 2011). Ion exchange often lacks selectivity and requires the regeneration of resins which in turn needs the addition of harmful chemicals (Brink et al., 2019). Adsorption requires acid-treatment for adsorbent regeneration and often suffers from low efficiency. Moreover, membrane filtration and electrochemical methods require high capital and operating costs. Thus, there remains a present need to find both an efficient and economical approach for Pb(II) removal.

Recently, researchers have looked towards bioremediation as an economical method to remove Pb(II) from wastewater. One bioremediation strategy that has been extensively researched is biosorption. Biosorption entails the adsorption of Pb(II) onto a variety of biological masses including algal, dead, and reconditioned biomass and has shown promise in its removal efficiency (Rodriguez et al., 2019). However, its large-scale use is hindered due to the occurrence of rapid saturation of metal binding sites that causes Pb(II) removal efficiency to decrease and possibly cause the occurrence of Pb(II) desorption (Martin-Lara et al., 2011). The use of exoelectrogens as reactive biosorbents may alleviate this hurdle through the coupling of biosorption with bioreduction.

Exoelectrogenic bacteria are naturally found in wastewater and are used in both microbial electrolysis cells (MECs) and microbial fuel cells (MFCs). These bacteria are the main catalysts for these systems as they have the capacity to oxidize organics and subsequently produce and extracellularly transfer electrons. In the presence of an electrode – these bacteria will dump their electrons to the anode which in turn either reduces the energy requirements for H_2 production or produces electricity depending on if the reactor is operated under an applied potential or under aerobic, open circuit conditions, respectively. However, Colantonio and Kim discovered that in the absence of an applied potential – the bacteria can dump their electrons onto Pb(II) ions, leading to enhanced Pb(II) removal under open circuit conditions (Colantonio and Kim, 2016). It is believed that without another substrate acting as an electron acceptor, exoelectrogenic bacteria can use Pb(II) as a terminal electron acceptor to fuel their growth. This phenomenon has also been reported

for Pb(II) in a bio-precipitation study and is well reported in Cr(VI) and U(VI) bioreduction studies (Brink et al., 2019; Thacher et al., 2015; Tekerlekopoulou et al, 2013; Chirwa and Wang, 2004).

Cr(VI) and U(VI) bioreduction studies have revealed that removal can be enhanced through attached growth reactors via biofilm formation (Liu et al., 2002). Biofilms not only reduce cytotoxic effects induced from metals but are also believed to enhance microbial-reduction by keeping cells in close proximity. This in turn allows for enhanced metabolic interactions and inter-cellular communications, allowing them to behave in a coordinated manner (Tekerlekopoulou et al, 2013). Carbon nanofibers (CNFs) are excellent candidates for bacterial scaffolds as they not only exhibit a large surface area for bacterial attachment, but they also contain sp^2 hybridized bonds. The presence of sp^2 hybridized bonds means there are delocalized electrons along the fiber that can act as an electron facilitator between exoelectrogens and Pb(II). This phenomenon was observed in Cr(VI)-reduction studies that used carbon nanotubes and humic acids as electron facilitators, where removal was enhanced in both cases (Thacher et al., 2015; Wang et al., 2015). Further, the adsorption properties of CNFs can also act as in situ metallic Pb collectors during the bioreduction process to mitigate saturation on bacterial cell walls and therefor reduce cytotoxic effects. Overall, it is predicted that this mode of operation will allow for a robust method for long term Pb(II) removal.

Although the proposed CNF attached growth reactor can yield an efficient mode to remove Pb(II), it convolutes the removal mechanisms involved. This can be problematic for the full understanding of the system at hand which in turn is necessary for its optimization. The construction of a model that captures the transport and removal of Pb(II) as it propagates through the biofilm may be a viable solution to understand the mechanisms involved. Similar approaches have been carried out in Cr(VI) and U(VI) bioreduction studies for understanding removal trends, kinetics, and system optimization. For instance, Lin used a predictive model to investigate the causes for temporal variations in Cr(VI) removal when using *E.coli* grown on ceramic beads. The model further realized the reactor's kinetics which is necessary when considering its upscale (Lin, 2013). Similarly, Chirwa and Wang modelled the prevalence of cell inactivation in a pure culture biofilm when subjected to high Cr(VI) loading (Chirwa and Wang, 2004). This allowed the researchers to understand the removal capacity and kinetics of the reactor under different operational conditions.

Thacher et al. modelled Cr(VI) bioreduction using *Shewanella spp.* in aquifers. A sensitivity analysis identified the main influential parameters that determined the dynamic removal of Cr(VI) in the system (Thacher et al., 2015). Specifically, it revealed the significance of biomass concentration and Monod kinetics, while uncovering the insignificant role biofilm thickness had on its removal. Further, a reactive model constructed for an aquifer in Oak ridge, allowed researchers to establish the significance of sorption and desorption effects on U(VI) removal on site (Luo et al, 2007). By revealing the significance of this phenomenon, the removal of U(VI) may be better controlled. Overall, predictive models have aided in researchers understanding of their designed reactors' kinetics and removal mechanisms that is useful in their optimization and upscale. It is therefor proposed to construct a model from a theoretical standpoint as a predictive

tool for understanding the removal mechanisms of Pb(II) and the key parameters involved. This model can be further advantageous in predicting the fate and removal of Pb(II) as it propagates in the biofilm, yielding a further understanding of the inherent mechanisms involved.

4.1.2 Objectives

The overall objectives of this study are:

1. To show the efficacy of the proposed CNF attached growth design for long term removal of Pb(II) when compared to suspended growth reactors.
2. To use numerical modelling to understand the removal mechanisms involved in the attached growth reactor.
3. Use the fitted model to predict the fate and removal of Pb(II) as it transports through the biofilm in the short and long term.
4. Perform a sensitivity analysis on model parameters to gain a further understanding on key parameters that can aid in the system's optimization.

4.2 Materials and Methods

4.2.1 Materials

Bare carbon nanofibers (CNFs, graphitized (iron-free), conical platelets diameter 100nm and length 20-200μm) were purchased from Sigma Aldrich Canada. Bare CNFs were functionalized with carboxyl groups using acid treatment with HNO_3 and H_2SO_4 as described elsewhere (Zhang et al., 2007). HNO_3 (70wt%) and the 0.45μm poly(ether) sulfone (PES) syringe filters were purchased from Sigma Aldrich Canada and VWR (International, USA), respectively. Luria Bertani HiVeg Broth (LB) and CH_3COO^- were purchased from Sigma Aldrich Canada and HIMEDIA, respectively. $Pb(CH_3COO)_2$ and $Ca(OH)_2$ were purchased from ThermoFisher and Sigma Aldrich Canada, respectively.

4.2.2 Culture preparation and attached growth reactor design

Inoculum was taken from a MEC reactor that was operated for two years under a constant applied voltage of 0.6V, where it produced sufficient current (>0.5mA). It was batch fed with waste activated sludge from the Woodward wastewater treatment plant and supplemented with 1g/L CH_3COO^-. To climatize the bacteria to a Pb(II)-enriched environment, it was continuously dosed with Pb(II) in increments of 0.5ppm until toxicity was reached. Toxicity levels were deemed to be reached once current production halted in the MEC reactor for over 24hrs. This current data can be seen in Figure S.5.

1mL of the bacterial culture was then dosed into a 1L flask containing 1g/L LB media-broth supplemented with 2g/L CH_3COO^-. 13mg of CNFs were then aliquoted into the 1L flask, where 13mg was chosen to ensure adsorption did not dominate Pb(II) removal. The reactor and control design can be seen in Figure 17 where triplicates of the reactor were run to capture performance variability. $N_2(g)$ was then sparged throughout for 5 minutes to ensure anaerobic conditions. Continuous stirring was then supplied overnight to ensure bacterial attachment. Subsequently, 1.5ppm of $Pb(CH_3COO)_2$ was dosed into the reactor for a retention time of approximately of 48hrs. 1.5ppm was chosen as the Pb(II) dosage concentration as it was the highest concentration without toxicity. Samples were then taken for analyses prior to another 1.5ppm Pb(II) dose, marking the beginning of another cycle.

This procedure was repeated for 13 cycles, where the temperature was maintained at 22 ± 0.2°C and the pH was maintained around 7.0 ± 0.2 using $Ca(OH)_2$.

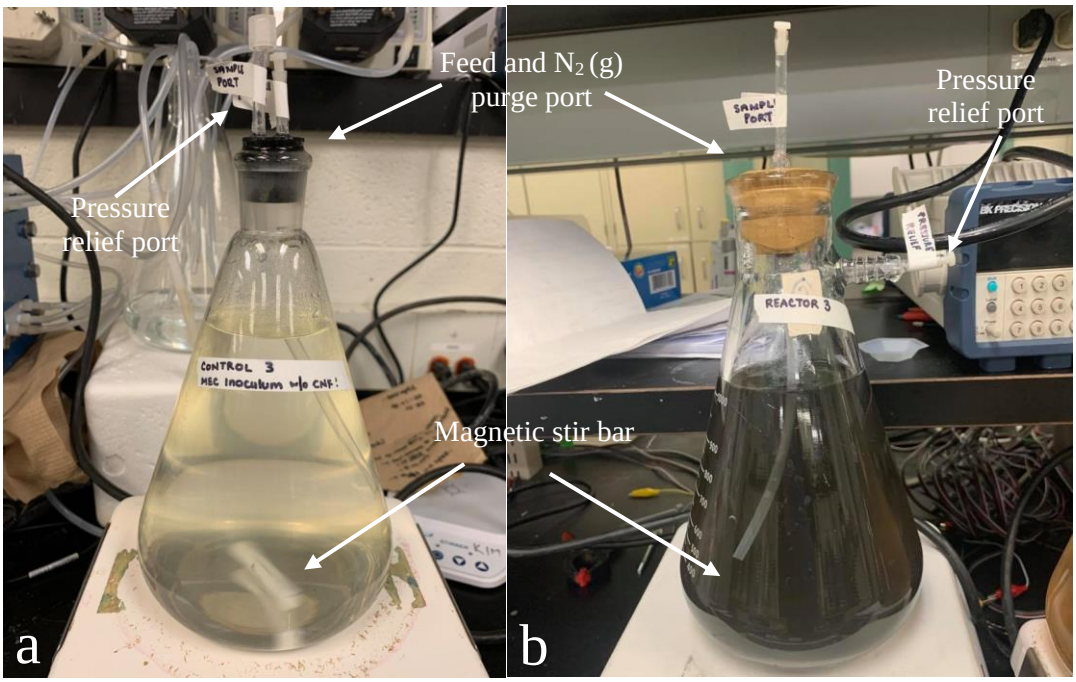

Figure 17. Experimental set-up used for the (a) the control reactor with inoculum only and (b) the CNF reactors with inoculum operated in triplicates.

4.2.3 Sample Preparation and Measurements

4.2.3.1 Sulfuric Acid Treatment

Acid treatment using H_2SO_4 was considered for the dissolution of formed precipitants. To validate the treatment, small metallic strips (1mm x 1mm) and Pb(II)-phosphate samples (5ppm Pb(II) with 3mM PBS) were immerged into H_2SO_4 at different pH levels (0-5). In the Pb(II)-phosphate samples, CNFs were added in separate batches to ensure adsorption would also not be affected by this treatment. The results of this experiment confirmed that H_2SO_4 at a pH of 2 could dissolve the Pb(II) precipitates without dissolving metallic Pb nor interfering with CNF Pb(II) adsorption. The repeatability of this pre-treatment was also verified through triplicate experiments. Thus, H_2SO_4 at a pH of 2 was used to acidify half of the samples' volumes. For the interested reader, the results of this experiment can be seen in the Figure S.6.

4.2.3.2 Analyses Measurements

5mL of the samples were first acidified using HNO_3 (3vol%) prior to being filtered through a 0.45µm PES syringe filter for ICP-OES (Inductively couple plasma atomic emission spectrometry, Vista Pro, Varian Inc., Australia) analysis. A separate 5mL sample underwent H_2SO_4 treatment prior to ICP-OES analysis as well, where the remaining sample was used to measure pH and chemical oxygen demand (COD). pH was measured through the pH meter (SevenMulti, Mettler-Toledo International Inc., OH) and was carried out to maintain levels within 7.0 ± 0.2 to ensure exoelectrogens were healthy while

mitigating Pb(II) precipitation. COD was also measured after each cycle using high range HACH test kits to ensure there were sufficient carbon sources and thus that bioreduction would not be limited from substrate depletion.

4.2.3.3 CNF Adsorption Measurements

To capture CNF removal in the model, it was imperative to study its isotherm properties. Adsorption experiments were carried out in 100mL flasks containing 5ppm of Pb(II). The CNFs were dosed at different masses ranging from: 0.00137, 0.0137, 0.137 and 1.37mg. Once the CNFs were added to the flasks, they were added to a shaker which maintained mixing conditions at 500RPM for 48hrs. After the 48hrs commenced, the samples were filtered through a 0.45µm PES membrane and acidified with HNO_3 for ICP-OES. Freundlich and Langmuir isotherms were both fitted to the experimental data where their model predictions along with the experimental data can be observed in Figure 18.

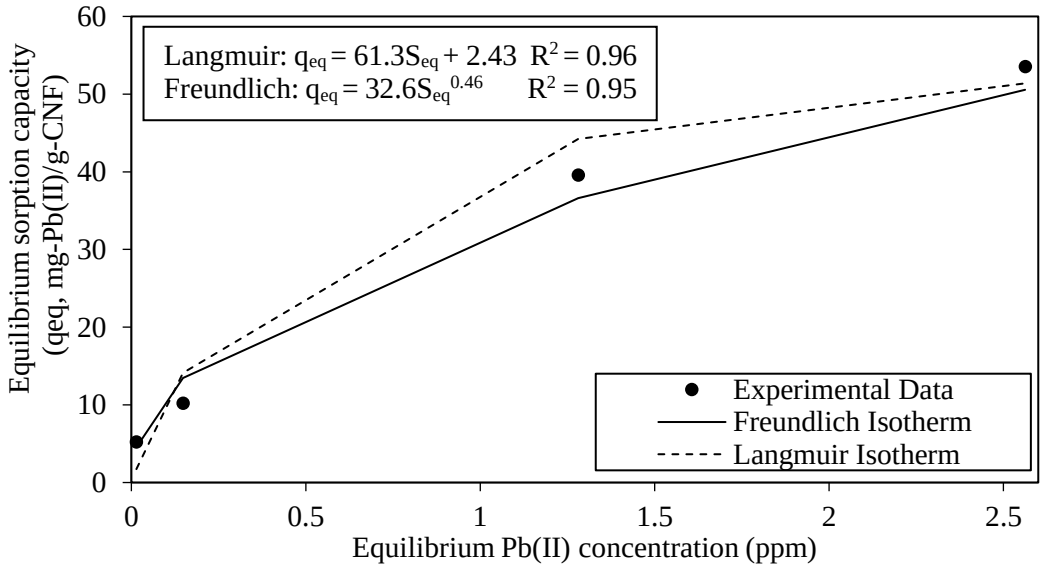

Figure 18. Equilibrium sorption capacity (q_{eq}, mg-Pb(II)/g-CNF) as a function of equilibrium Pb(II) concentration (S_{eq}, ppm) for CNFs fitted with Langmuir and Freundlich isotherms. The fitted Langmuir isotherm was found to be $q_{eq} = 61.34$ Seq + 2.43 with an R^2 of 0.96 and the fitted Freundlich isotherm was found to be $q_{eq} = 32.6S_{eq}^{0.46}$ with an R^2 of 0.95.

4.2.3.4 DNA Sequencing

All DNA sequencing was carried out using Illumina Sequencing methods and were performed by the MOBIX Lab at McMaster University.

4.3 Model Development

The reactor was subdivided into three regions: the bulk, the liquid film, and the biofilm to capture the different phenomenon in the reactor. Figure 19 depicts the predicted Pb(II) concentration and the associated removal mechanisms as the ion diffuses through the different modelled regions. The following sections will discuss how each region captures the transport and removal of Pb(II) as it propagates through the biofilm.

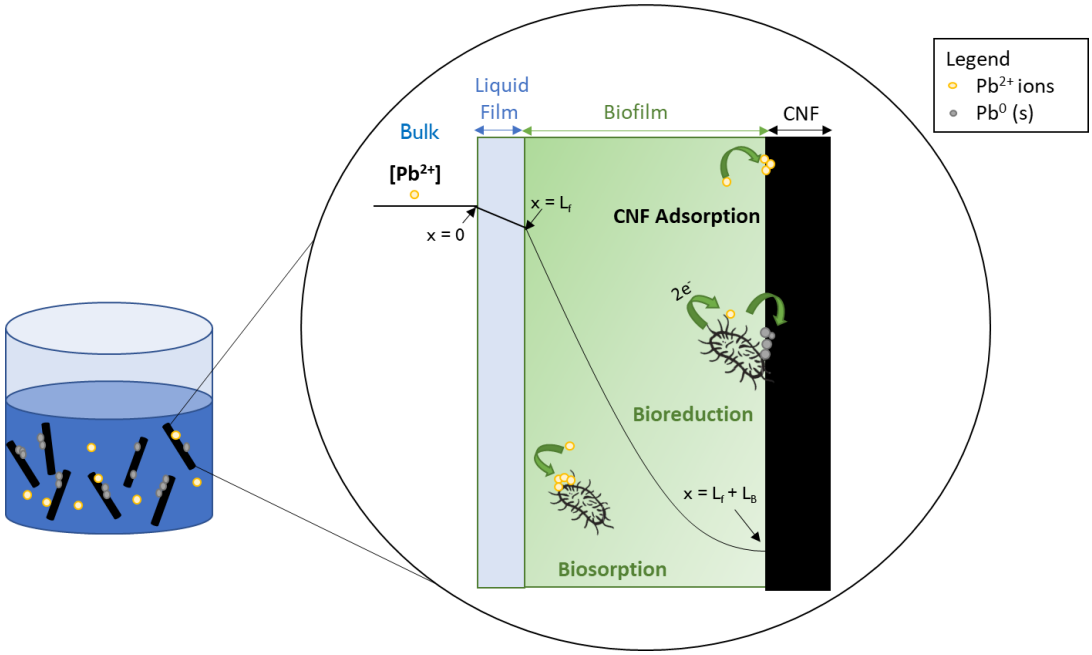

Figure 19. Schematic of CNF attached growth reactor and predicted Pb(II) concentrations with the respective bounds as it moves from the bulk to the CNF surface.

4.3.1 The Bulk

To model the removal of Pb(II) from the bulk it was necessary to account for its diffusive transport into the liquid film interface. To accomplish this, 1-D diffusive transport was considered using the following Fick's first law equation,

$$\frac{\partial S_b(t)}{\partial t} = -D_L \times A_{CNF} \times \frac{\Delta S(t)}{\Delta x} \times \frac{1}{V_{reactor}} \times \frac{1000L}{m^3} \quad (1)$$

where $S_b(t)$ (mg/L) is the temporal Pb(II) bulk concentration, t is time (hr) D_L is the free ion diffusivity of Pb(II) (m^2/hr), A_{CNF} is the total CNF surface area, $\frac{\Delta S}{\Delta x}$ is the Pb(II) concentration gradient between the bulk and the liquid film (mg/m^4) and $V_{reactor}$ is the reactor's volume (m^3). Although CNFs are approximately cylindrical in shape, axial dimension were used because Pb(II) ions are significantly smaller than the lengths of the CNFs, inferring that Pb(II) ions will never feel their edge-effects. Further, since the reactor was continuously mixed, it was assumed the Pb(II) bulk concentration would remain uniform, eliminating the occurrence of advective transport. The initial and boundary condition shown in Table 3 were used to solve for the Pb(II) bulk concentration.

Table 3. Initial and boundary conditions used to solve for bulk Pb(II) concentration profile

Initial Condition	at t = 0, ∀ x, S = S_o
Boundary Condition 1	at x = 0, ∀ t, S = S_{Bulk}

4.3.2 The Liquid Film

Pb(II) transport in the liquid film was depicted by the following 1-D diffusive transport equation,

$$\frac{\partial S(t,x)}{\partial t} = -D_L \frac{\partial^2 S(t,x)}{\partial x^2} \quad (2)$$

where S(t,x) is the temporal and axial Pb(II) concentration in the liquid film (mg/m^3) and x is the axial position (m). To solve for the liquid film Pb(II) concentration, the initial and boundary conditions seen in Table 4 were used.

Table 4. Initial and boundary conditions used to solve for the liquid film Pb(II) concentration profile

Initial Condition	at t = 0, ∀ x, S = 0
Boundary Condition 1	at x = L_F, S = S_{Bulk} ∀ t
Boundary Condition 2	at x = 0, S = S_{Lf} ∀ t

4.3.3 The Biofilm

To model the biofilm Pb(II) concentration, 1-D diffusive transport was used with Monod kinetics and first order biosorption kinetics in the following equation,

$$\frac{\partial S(t,x)}{\partial t} = -D_B \frac{\partial^2 S(t,x)}{\partial x^2} - \frac{k \times S(t,x)}{K_s + S(t,x)} X - k_b(S(t,x) - S_{eq,b}(t,x)) \quad (3)$$

where S(t,x) represents the axial and temporal Pb(II) concentration in the biofilm (mg/m^3), D_B represents Pb(II) diffusivity in the biofilm (m^2/hr), k is the specific substrate utilization rate (hr^{-1}), X is microbial concentration (mg/m^3), k_b represents the first order biosorption kinetic constant (hr^{-1}) and $S_{eq,b}$ represents the temporal and axial equilibrium biosorbed phase concentration (mg/m^3).

The first term on the right-hand side accounts for the 1-D diffusive transport of Pb(II) as it diffuses through the biofilm. The second term represents the Monod kinetics used to depict the bioreduction removal of Pb(II). Monod kinetics was used as it has been shown to capture bioreduction kinetics well for Cr(VI) (Lin, 2013; 2015; Pandey et al., 2015; Martin-Lara et al., 2011; Tang et al., 2006; Thacher et al.). Inhibition terms were not considered due to the relatively low Pb(II) concentrations used and due to the reduction of inhibitory effects observed in biofilm studies (Liu et al., 2002; Tran and Chao, 2018; Logan et al., 2008). It is important to note that the substrate under consideration in this expression is Pb(II) due to the excess supply of CH_3COO^-. Further, the last term depicts the biosorption kinetics in the biofilm while accounting for the occurrence of desorption in the biosorbed phase.

To model the biosorbed phase of the biofilm, it was necessary to capture the transient behavior of the sorption capacity through the following equation,

$$\frac{\partial q_b(t,x)}{\partial t} = \frac{k_b\left(S(t,x) - S_{eq,b}(t,x)\right)}{\rho_{biofilm}} \quad (4)$$

where q_b represents the temporal and axial biofilm sorption capacity (mg-Pb(II)/g-biofilm) and $\rho_{biofilm}$ is the biofilm density (g/m^3). This equation models the sorption capacity by accounting for the fact that the biosorbed phase will gain the same mass of Pb(II) that is removed from the biofilm's aqueous phase by biosorption. To solve equation 4, it is still necessary to account for the isotherm properties of the biofilm which relates the sorption capacity to the equilibrium Pb(II) biosorbed phased concentration. Since the Langmuir isotherm was found to capture biosorption well in literature it was used in the following equation (Aryal and Kyriakides, 2015; Singh et al., 2020).

$$S_{eq,b}(t,x) = \frac{q_b(t,x)}{K_{L,b} \times (q_{max,b} - q_b(t,x))} \quad (5)$$

where $q_{max,b}$ represents the maximum sorption capacity of the biofilm (mg-Pb(II)/g-biofilm) and $K_{L,b}$ represents the saturation coefficient (m^3/mg-Pb(II)). By utilizing Equation 5, it is inherently assumed that at each time step the biosorbed phase reaches equilibrium with the aqueous phase. To solve Equations 3-5 the initial and boundary conditions used in Table 5 were used.

Table 5. Initial and boundary conditions used to solve for the biofilm Pb(II) concentration profile

Initial Condition	at t = 0, ∀ x, S = 0
Boundary Condition 1	at $x = L_F$, $S = S_{Lf}$ ∀ t
Boundary Condition 2	at $x = L_F + L_B$, *refer to CNF surface subsection*

To capture CNF adsorption on the second biofilm boundary, additional equations that captured its isotherm properties had to be used, which is summarized in the following section.

4.3.4 The CNF surface

To model CNF adsorption as the second boundary condition, it was assumed that there would be strictly diffusive transport onto the CNF surface and the Pb(II) that encountered its surface would directly enter the adsorbed phase of the CNFs (i.e. immediate adsorption). This was accomplished by coupling Fick's first law with the sorption capacity definition in the following equation,

$$\frac{\partial q_c(t)}{\partial t} = \frac{-D_B \times A_{CNF} \times \frac{\Delta S(t)}{\Delta x}}{m_{CNF}} \quad (6)$$

where q_c represents the CNF sorption capacity (mg-Pb(II)/g-CNF) as a function of time (hr), D_B is the Pb(II) diffusivity in the biofilm (m^2/hr), A_{CNF} represents the CNF surface area, $\frac{\Delta S(t)}{\Delta x}$ represents the Pb(II) concentration gradient between the last biofilm grid and the CNF surface (mg/m^4) as a function of time and m_{CNF} represents the mass of CNFs (g). To account for the maximum sorption capacity, it was required to use an isotherm to relate the temporal sorption capacity to the equilibrium aqueous phase concentration. The following Langmuir isotherm relationship was used to relate these due to its excellent fit to the CNF experimental data

$$S_{eq,CNF} = \frac{q_c(t)}{K_{L,C} \times (q_{max,c} - q_c)} \quad (7)$$

where $S_{eq,CNF}$ represents the equilibrium aqueous Pb(II) concentration on the CNFs (mg/m^3), q_c is the CNF sorption capacity (mg-Pb(II)/g-CNF) as a function of time (hr), $q_{max,c}$ is the maximum sorption capacity of the CNFs and $K_{L,C}$ is the saturation coefficient (m^3/mg). By using Equation 7, the model is assuming that the adsorbed phase and the aqueous phase Pb(II) reach equilibrium instantaneously.

4.3.5 Biomass Concentration and Biofilm Thickness Considerations

Two types of models were attempted for the data set, where one considered a constant biofilm thickness with a transient biomass concentration and the other assumed constant biomass concentration with a transient biofilm thickness. In the first model, biomass

concentration was held constant over each cycle and allowed to undergo step changes after a cycle commenced. The following mass balance was used to estimate its step growth after each cycle,

$$\Delta X|_{cycle} = \Delta X|_{growth,cycle} - \Delta X|_{decay,cycle} \quad (8).$$

It was further assumed that microbial growth was limited to Pb(II) availability as their terminal electron acceptor, thereby inferring that bioreduction governs microbial growth. Therefore, the microbial yield coefficient was used as a conversion factor between the Pb(II) mass removed via bioreduction and the amount of biomass produced in the following equation,

$$\Delta X|_{growth,cycle} = \frac{Y_{X/S}(m_i - m_f)_{bioreduction}}{V_{BIOFILM}} \quad (9)$$

where $Y_{X/S}$ represents the microbial yield coefficient (mg-X/mg-Pb(II)), $(m_i - m_f)_{red}$ is the mass of Pb(II) removed by bioreduction and $V_{biofilm}$ is the biofilm volume (m^3). To further model the decay portion of the microbial biomass, it was assumed it followed first order kinetics proportional to the biomass concentration as dictated by the following,

$$\Delta X|_{decay,cycle}\, b\Delta t_{cycle} X \quad (10)$$

where b represents the endogenous decay coefficient (h^{-1}) and Δt_{cycle} is cycle time. By using equation 10, it is assumed that microorganisms simply disappear under decay in the biofilm. This assumption was found to be suitable for the problem at hand, as generally when biomass decays it is assumed it either forms decay or inert particulates. These formed particulates in turn would have negligible impact on Pb(II) removal via sorption.

In the second model, biomass concentration was held constant and the biofilm grew in a stepwise manner after each cycle by the relationship,

$$\Delta L|_{cycle} = \frac{\Delta X|_{cycle}}{\rho_{cell} A_{CNF}} \quad (11)$$

where ρ_{cell} is cell density (mg/m^3). Equation 11 inherently assumes that biofilm growth is determined by microbial growth which is further normalized by the cross-sectional area available. However, it was found that the second model grossly overestimated removal regardless of the model parameters used due to its overestimation of adsorption removal. For the interested reader, the results of this model fitting can be seen in Figure S.7. Thus, the following sections will only focus on the first model constructed with constant biofilm thickness and a transient biomass concentration.

4.3.6 Additional Model Assumptions and Computational Methods

To solve the equations shown in the previous subsections the following assumptions were made:

1. CNFs are uniform in size and that there would be 1% of total CNF surface area available initially. This was approximated from a CNF bundling study (Peigney et al., 2000)
2. After 3 cycles, CNFs were assumed to experience a further 15% loss in surface area due to aggregation.
3. Initial biomass concentration was assumed to be 1000mg/L. This initial biomass concentration was approximated from the initial biomass dosage of 0.1vol% assuming that ρ_{cell} is the same as water.

4. CH_3COO^- is in excess and thus does not limit microbial growth.
5. Fixed biofilm length at 264µm.
6. Fixed liquid film thickness of 6 µm.
7. Biosorption kinetics is independent of microbial concentration (i.e. biosorbent dosage)
8. Pb(II) is the only present electron acceptor.
9. Pb(II) bioreduction follows the same biokinetic behaviour as Cr(VI).
10. Pb(II) concentration only varies in the axial direction.
11. Pb(II) transport is diffusion controlled.
12. P(II) is consumed in the biofilm
13. Pb(II) diffusivity drops by 75% in the biofilm as that predicted in literature (Lin, 2013; Thacher et al., 2015)
14. There is a maximum cell concentration of 1.03×10^6 mg/L. Please refer to supporting information for the sample calculation of this maximum.
15. Pb(II) removed as precipitates is removed instantaneously and thus is not available for removal at the beginning of each cycle

Using the listed assumptions, Equations 4.1-4.10 were solved using finite difference modelling coupled with Euler methods in VBA. The time steps were minimized until a stable solution was found in the simulations.

4.3 Results and Discussion

4.3.1 Experimental Results and Discussion

To investigate the removal mechanisms and the efficacy of the CNF attached growth reactor, precipitate and non-precipitate removal were decoupled through H_2SO_4 treatments. Figure 20 shows the total Pb(II) removal achieved from three CNF attached growth reactors and the control with only inoculum along with the contributions from precipitation and non-precipitation removal as time progressed.

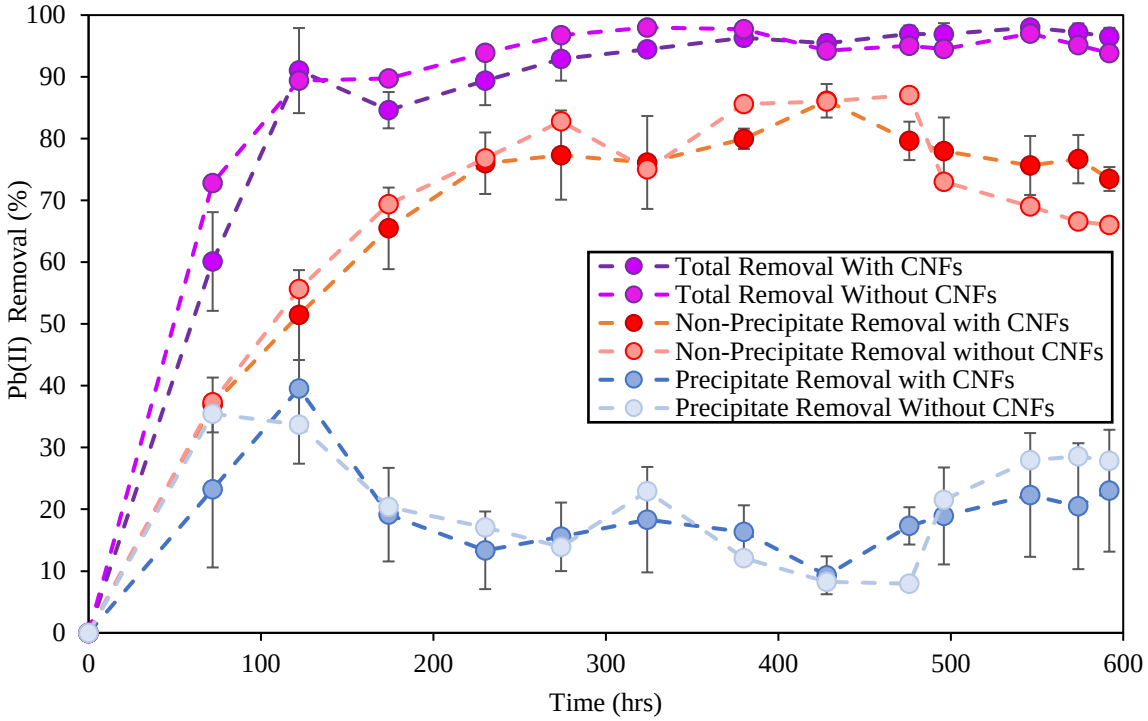

Figure 20. Pb(II) removal (%) found for total removal, non-precipitate removal and precipitate removal with CNF reactors and control with only inoculum as a function of time (hrs). Error bars represent standard deviation found from removal from three reactors.

Figure 20 reveals that precipitation initially dominates removal in the reactors and control (<120hrs), reaching levels between approximately 40-50%. Surpassed this 120hr period, precipitation maintains approximately the same level of removal, ranging from 10-20% throughout the remaining cycles. Non-precipitate removal experiences an initial linear increase up until approximately 230hrs and subsequently experiences a nearly constant removal at around 85% for the reactors. Similarly, the control experiences the same removal up until approximately 480hrs, where a subsequent decline is experienced.

The initial large precipitation removal is likely due to the fast kinetics associated with Pb(II) phosphate formation. Due to the initial low dose of bacteria (0.1vol%) in the reactor, there will not be enough present to utilize a large portion of these phosphates for growth. Surpassed this, it is apparent that the biomass enters their log phase of growth, which entails a period in which bacteria uptake nutrients and phosphates for cell division. This marks the period in which the biomass begins to dominate removal in the reactors. The subsequent constant removal is likely due to the biomass entering their stationary phase, meaning a constant biomass within the reactor. Due to the continual dosing of CH_3COO^- and the terminal electron acceptor Pb(II), the occurrence of their death phase seems to have been minimized.

This removal curve insinuates that bioreduction is the dominant removal mechanism in the CNF reactors. If biosorption or CNF adsorption governed removal, you would likely see a decline in removal performance rather than its maintenance. Since this experiment dosed a

large amount of Pb(II) (19.5mg), it is likely their sorption sites would have become saturated over the long-term test. The saturation of sorption sites infers that there will be a reduction or possibly the elimination of active sites, causing a reduction in removal and possibly the desorption of Pb(II).

Further, all three CNF reactors exhibited nearly the same removal capacity, as indicated by the relatively small standard deviation found among them. The similarities among the reactors' removal likely stems from their similar bacterial genera as indicated in Figure S.8. Figure S.8 also demonstrates that both the control and CNF reactors are composed of a mixture of known exoelectrogenic bacteria (*Acinetobacter spp., Klebsiella spp., Comamomnas spp., Citrobacter spp., Exiguobacterium spp., Dysgonomonas spp., Desulfovibrio spp.*) which further supports that bioreduction is playing an integral role in each (Kumar et al., 2015; Wu et al., 2017; Xu and Liu, 2011).

Moreover, the found genera and removal trend insinuates that the control experiences substantial removal via bioreduction. Due to the incorporation of riboflavin within the LB media, it is likely that there was electron shuttling occurring in the control up until 480hrs (Hsueh et al., 2019). The decline in removal could be from the depletion of riboflavin or possibly from the accumulation of Pb that is creating a cytotoxic effect. The robustness observed in the CNFs could be due to the CNFs providing additional electron shuttling, or that the biofilm improves the microbial Pb resistance or possibly that the cytotoxic effects are alleviated from the CNFs acting as Pb collectors. Nonetheless, the reactor comprised of CNF and biomass was shown to be superior to the control in the long run.

4.3.2 Model Results and Discussion

4.3.2.1 Model Fitting

To confirm the hypothesis that bioreduction governs removal in the CNF reactors, it was first necessary to fit the model to the experimental data. To accomplish this, a collection of the model parameters' values were found from literature and are summarized in Table 6.

Table 6. Collection of model parameters' average values and spread found from literature

	Model Parameter	Average Value	Tested Range (±σ)	Unit	Number of observations (N)
Bioreduction	μ_{max}	1.49	(0, 6.79)	hr^{-1}	79
	$Y_{x/s}$	0.38	(0.1, 0.66)	-	30
	Ks	49.52	(0.5, 156.14)	mg/L	70
	b	0.022	(0, 0.15)	d^{-1}	20
Biosorption	q_{max}	126.49	(0, 336.71)	mg/g	106
	K_L	2.03	(1×10^{-5}, 9.01)	L/mg	52
	k_b	2.68	(0, 6.72)	h^{-1}	26
CNF Adsorption	q_{max}	61.34	(55.21, 67.47)	mg/g	Experimental
	K_L	2.43	(2.19, 2.67)	L/mg	Experimental

*CNF parameters found experimentally and tested ±10%.

*Lower limit restricted to 0 or lowest physically possible value.

Abdulaziz and Musayev, 2017; Ahmed et al., 2015; Areco and Alfonso, 2010; Banerhee et al., 2007; Bautista-Hernández et al., 2011; Black et al., 2014; Bolte and Hill, 1990; Bueno et al., 2008; Bueno et al., 2011; Cai et al, 2018; Chang et al., 2007; Çolak et al., 2011; Edris et al., 2013; Evans and Wang, 2004; Fan et al., 2008; Gabr et al., 2008; Gallardo-Rodriguez et al., 2019; Guha et al., 2001; Halttunen et al., 2007; Hlihor et al., 2017; Jacob et al., 2018; Jeong et al., 2019; Kumari et al., 2017; Leung et al., 2001; Li et al, 2018; Lin, 2013; Lin et al., 2017; Liu et al., 2002; Lu et al., 2006; Mahar et al., 2019; Mamun et al., 2015;Manasi et al., 2014; Mohamed and Hatflied, 2005; Mohapatra et al., 2019; Muñoz et al., 2015; Preetha and Viruthagiri, 2007; Schmeiman et al., 1998; Selatnia et al., 2004; Seo et al., 2019; Somasundaram et al., 2009; Sulaymon et al., 2012; Sulaymon et al., 2014; Tekerlekopoulou et al., 2013; Thacher et al., 2015; Wang et al., 2016; Xue-jiang et al., 2006; Yin et al., 2019; Zhang and Bishop, 1994; Zhang et al., 1998

Due to the nature of the proposed attached growth design, it is difficult to decouple the kinetics of biosorption from bioreduction. Thus, this study looked at using these average reported values and adjusting these values until the following sum of squared error was minimized,

$$R^2 = 1 - \frac{RSS}{TSS} = 1 - \frac{\sum(\hat{y}_i - \bar{y})^2}{\sum(y_i - \bar{y})^2} \quad (12).$$

Using this method, the following model parameters were found to make a good fit with an R^2 of 0.92: $k = 3.92h^{-1}$, $K_s = 49.52$ mg/L, $b = 0.15d^{-1}$, $Y_{X/S} = 0.6$, $q_{max,b} = 126.5$mg/g, $K_{L,b} = 2.03$mg/L, $k_b = 2.68\ h^{-1}$ and $q_{max,c} = 61.34$mg/g and $K_{L,c} = 2.43$ mg/L. Figure 21a displays the fitted model to the experimental data with the percent removal found for each removal mechanism along with the predicted biomass concentration.

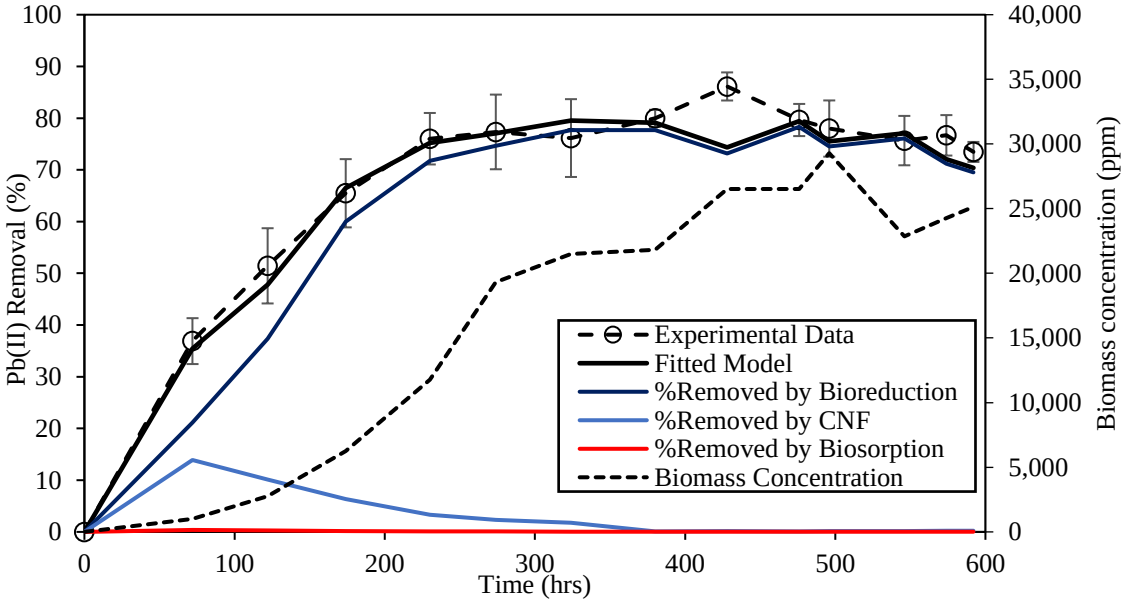

Figure 21. Average Pb(II) removal achieved by attached growth reactors as a function of time (hrs) with its fitted model ($R^2 = 0.92$) and percent contributions of individual removal mechanisms. Biomass concentration (ppm) is also presented as a function of time (hrs). Error bars represent standard deviation.

Figure 21a shows that overall, the model fits the experimental data well where there is a slight deviation around 428hrs. In terms of percent removal from individual mechanisms, it shows that biosorption does not play a significant role, accounting for <1% overall for all 13 cycles. This can be attributed to biosorption's relatively slow kinetics. Further, it also shows that initially CNF adsorption plays an integral role in removal, but as time progresses its removal drops off accounting for <1% after 380hrs. This can be explained by the fact that CNF adsorption sites are fixed and thus as time progresses the Pb(II) will infiltrate these active until it reaches a saturation point. CNF adsorption contributed to greater removal compared to biosorption due to the model's assumption that there is instantaneous adsorption onto the CNFs.

As predicted the model shows that bioreduction plays an integral role in removal throughout all cycles. Specifically, there is a linear increase in bioreduction removal up until approximately 230hrs (i.e. 4th cycle) where it then subsequently maintains the same extent of removal (≈75%) for the remaining time. The model reveals that the linear increase in bioreduction removal is the result of an increase in biomass concentration. Once the biomass concentration reaches a relatively large concentration, the bioreduction removal becomes independent and thus is maintained.

Further, this study shows the model's capability of predicting which mechanisms are dominant without knowledge of individual parameters. As shown, the only removal mechanism that has the capacity to have this initial linear trend proportional to the microorganism concentration is bioreduction. This proportionality is predicted from Monod kinetics which has been found to accurately model metal bioreduction (Lin, 2013; Martin-Lara et al., 2011; Pandey et al., 2015; Tang et al., 2016; Thacher et al., 2015). Additionally, the model confirms that is the only removal mechanism that can sustain removal over 13 Pb(II) dosages (19.5mg) without experiencing a decline in removal. Thus, this model confirms that bioreduction is the governing removal mechanism in the CNF attached growth reactors.

4.3.2.2 Pb(II) concentration profiles in the biofilm

Tracking the fate and removal of Pb(II) in the CNF attached growth reactor provides further insight on the system's removal mechanisms and thus was deemed important in this study. Figure 22a and b shows the transient behaviour of Pb(II) as it diffuses through the biofilm over the first cycle and over several cycles, respectively.

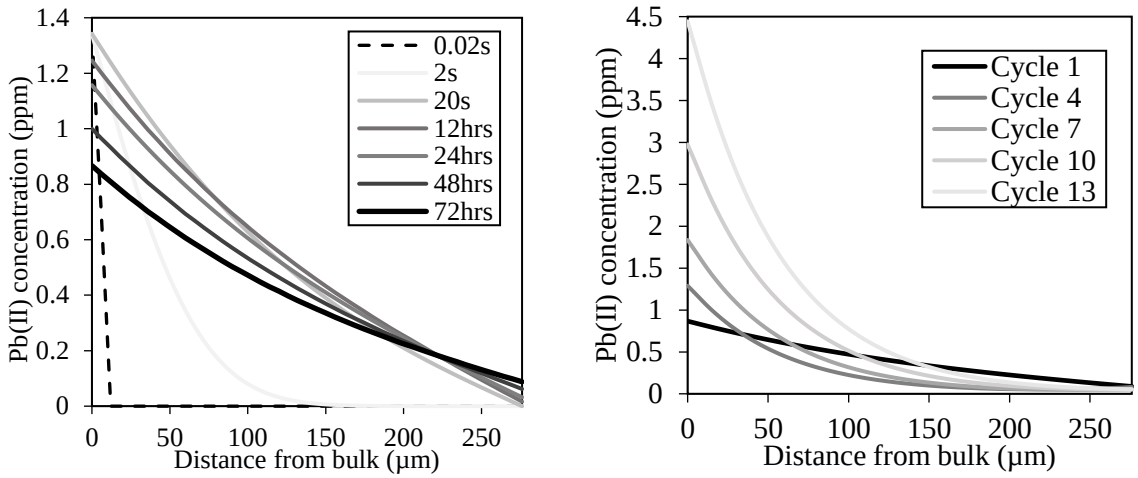

Figure 22. Pb(II) concentration profile throughout the biofilm over (a) cycle 1 and (b) several cycles.

Figure 22a shows that initially Pb(II) transport in the biofilm is diffusion controlled. This is seen by time periods 0.02s – 200s, which shows the infiltration of Pb(II) in the biofilm. At around 12hrs, Pb(II) removal begins to commence as dictated by the drop in the bulk concentration. Within this removal at around 12-24hrs, a substantial portion is attributed to CNF adsorption. This can be concluded from the linear trend that forms toward the CNF surface. A transition of this linear profile to a flat profile at approximately 48hrs marks the saturation point of the CNFs. Further, the removal rate throughout the biofilm remains relative the same as time progressed as indicated by the curves' slopes. This can be attributed to the fact that it was assumed that the biomass concentration remains the same throughout each cycle.

Figure 22b reveals the difference in removal rates within the biofilm as the cycles commence. Specifically, cycle 1 reveals a relatively flat profile with a linear region towards the CNF surface. This is due to the relatively low microbial concentration and initial substantial removal observed within the CNFs. As the cycles commence the CNFs no longer contribute to removal as indicated by the flat profile at the CNF surfaces. Although it shows CNFs do not hold a significant role in removal it does not indicate that Pb(II) desorption is occurring on the interface. If this were true, there would be an incline in the Pb(II) concentration at that interface. Pb(II) saturation was likely avoided due to the increase in bioreduction removal rates as the cycles commence, as indicated continual increase in the biofilm Pb(II) concentration gradients. This trend coincides with the increase in biomasses observed in Figure 21.

4.3.2.3 Model Sensitivity Analysis

The last portion of this study investigated the sensitivity of the model to individual model parameters to give insight on the most influential parameters on Pb(II) removal and its robustness to influent conditions. Figure 23a-d shows the removal curve's sensitivity to biofilm properties, microbial growth rate parameters, Monod kinetics and Pb(II) dosage

concentration, respectively. The model's sensitivity to biosorption and CNF parameters was neglected due to the model's insensitivity to the parameters.

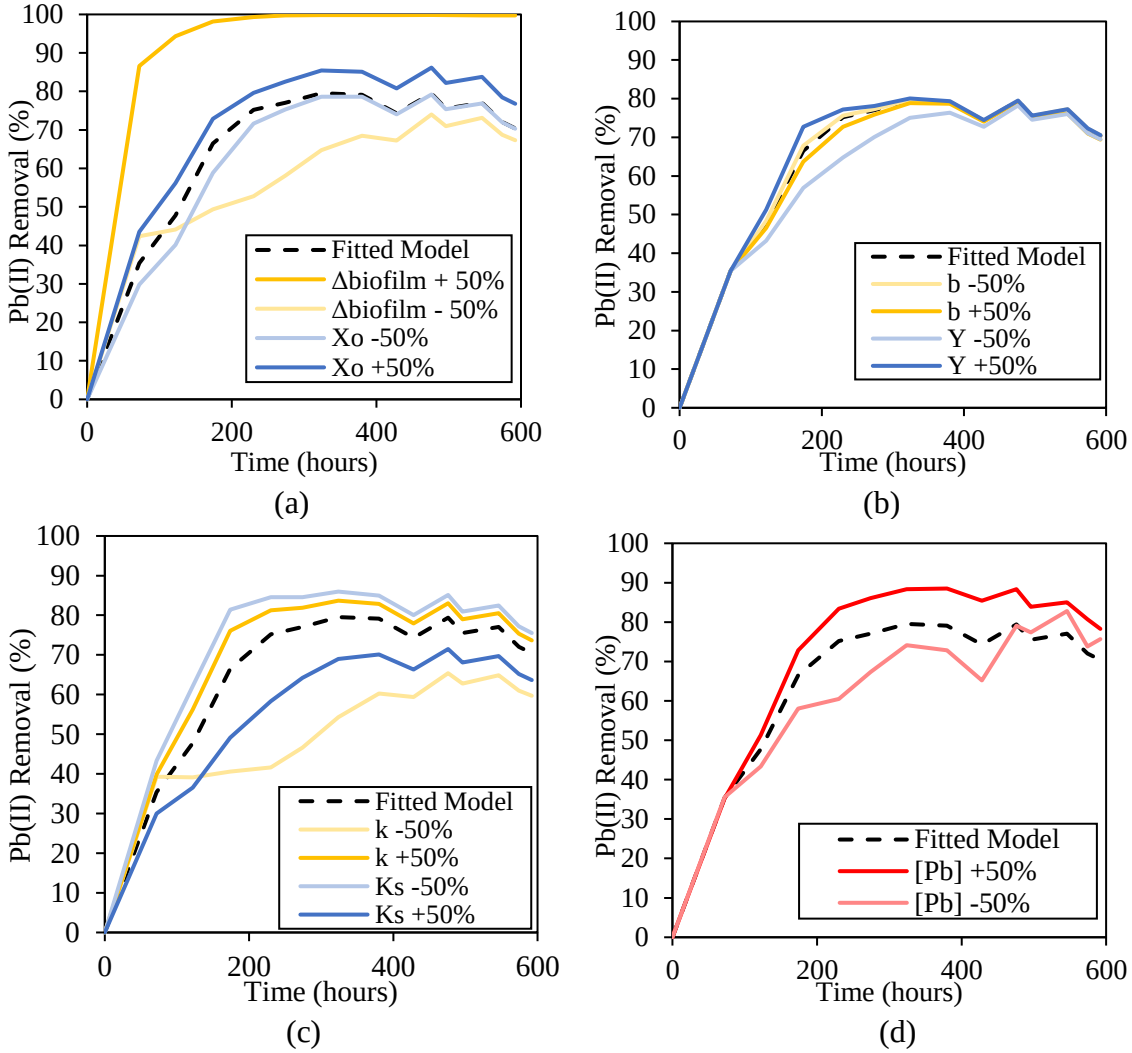

Figure 23. Model's sensitivity on (a) biofilm length and initial biomass (Xo), (b) yield and decay coefficient (Y, b), (c)bioreduction kinetic parameters k and Ks and (d)Pb dosage concentration in terms of Pb(II) removal (%).

Figure 23a demonstrates the model's sensitivity to changing biofilm length and initial biomass concentration. The model is shown to be sensitive to biofilm length, where the removal curves indicate an initial shift toward adsorption removal with smaller biofilms and an overall smaller Pb(II) removal capacity. Conversely, larger biofilms substantially improved removal due to the overall larger amount of biomass available to bioreduce Pb(II). Moreover, the model is shown to be less sensitive to initial biomass. This likely is attributed to the fact this parameter only substantially reduces the initial amount of Pb(II) bioreduced. This propagates through the removal curve as this affects microbial yield in the first cycle but overall has diminishing effects as the biomass growth progresses.

Further, the model was found to be insensitive to the endogenous decay coefficient. This can be attributed to the fact that bioreduction governs removal, meaning microbial growth would be too large to feel the effects of the microbial decay invoked by the changing endogenous decay coefficient. In accordance, the model was more sensitive to the microbial yield coefficient. Moreover, the model was found to be sensitive to both Monod kinetic parameters. In terms of specific substrate utilization rate, a decline in its value resulted in an initial shift towards adsorption removal where its overall removal capacity was substantially reduced. Conversely, an increase in its value resulted in a fairly small increase in Pb(II) removal, insinuating bioreduction kinetics was near its maximum given the half saturation coefficient used. However, the model was sensitive to an increase and decrease in the half saturation coefficient. An increase and decrease in the parameter resulted in an equal downward and upward shift in the removal curve, respectively. The trends observed are attributed to the fact that this value determines at what Pb(II) concentration the specific substrate utilization rate will reach half its maximum value. Therefor, this parameter governs the overall bioreduction kinetics of the reactor.

Lastly, the effect of Pb(II) dosage concentration was investigated. It was found that an increase in Pb(II) concentration improved removal and vise versa. This is likely from the positive influence it would have on microbial biomass concentration which in turn affects the kinetics of bioreduction. This same phenomenon was observed in Cr(VI) studies which showed an increase in its concentration provided had an enhancing effect on microbial biomass at low concentrations (Tekerlekopoulou et al., 2013). Overall, this sensitivity analysis provides further insight on the main influential parameters on Pb(II) removal and its robustness to changing Pb(II) concentration.

4.4 Conclusions

This study investigated the efficacy of CNF attached growth reactors on long term Pb(II) removal under multiple dosages and attempted to understand the intrinsic mechanisms using numerical modeling. The main outcomes from this investigation were:

- CNF attached growth reactors can remove Pb(II) long term under multiple Pb(II) dosages with approximately 80% removal and outperformed the suspended growth reactor in the long run.
- The constructed model accurately predicted Pb(II) removal with an R^2 of 0.92 and supported the theoretical prediction that bioreduction governs removal in the CNF reactors.
- The model captured the transient behaviour of Pb(II) as it transports through the biofilms, yielding a better understand of its fate among different cycles.
- The performed sensitivity analysis revealed the significance of Monod kinetics and biofilm thickness on Pb(II) removal as well as the positive correlation Pb(II) removal has with Pb(II) concentration.

Overall, this study was successful in exemplifying the robustness of CNF attached growth reactors on long term Pb(II) removal and used numerical modelling to gain a better understanding of the system at hand that may aid in its further optimization.

4.5 References

Abdulaziz, M., & Musayev, S. (2017). Multicomponent Biosorption of Heavy Metals from Aqueous Solutions: A Review. Polish Journal of Environmental Studies, 26(4), 1433–1441. https://doi.org/10.15244/pjoes/67975

Ahmed, Y. M., Al-Mamun, A., Al Khatib, M. F. R., Jameel, A. T., & AlSaadi, M. A. H. A. R. (2015). Efficient lead sorption from wastewater by carbon nanofibers. Environmental Chemistry Letters, 13(3), 341–346. https://doi.org/10.1007/s10311-015-0509-3

Al Mamun, A., Ahmed, Y. M., AlKhatib, M. F. R., Jameel, A. T., & AlSaadi, M. A. H. A. R. (2015). Lead Sorption by Carbon Nanofibers Grown on Powdered Activated Carbon — Kinetics and Equilibrium. Nano, 10(02), 1550017. https://doi.org/10.1142/s1793292015500174

Areco, M. M., & dos Santos Afonso, M. (2010). Copper, zinc, cadmium and lead biosorption by Gymnogongrus torulosus. Thermodynamics and kinetics studies. Colloids and Surfaces B: Biointerfaces, 81(2), 620–628. https://doi.org/10.1016/j.colsurfb.2010.08.014

Aryal, M., & Liakopoulou-Kyriakides, M. (2014). Bioremoval of heavy metals by bacterial biomass. Environmental Monitoring and Assessment, 187(1), 187. https://doi.org/10.1007/s10661-014-4173-z

Banerjee, S., Joshi, S. R., Mandal, T., & Halder, G. (2017). Insight into Cr6+ reduction efficiency of Rhodococcus erythropolis isolated from coalmine waste water. Chemosphere, 167, 269–281. https://doi.org/10.1016/j.chemosphere.2016.10.012

Bautista-Hernández, D. A., Ramírez-Burgos, L. I., Duran-Páramo, E., & Fernández-Linares, L. (2012). Zinc and Lead Biosorption by Delftia tsuruhatensis: A Bacterial Strain Resistant to Metals Isolated from Mine Tailings. Journal of Water Resource and Protection, 04(04), 207–216. https://doi.org/10.4236/jwarp.2012.44023

Black, R., Sartaj, M., Mohammadian, A., & Qiblawey, H. A. M. (2014). Biosorption of Pb and Cu using fixed and suspended bacteria. Journal of Environmental Chemical Engineering, 2(3), 1663–1671. https://doi.org/10.1016/j.jece.2014.05.023

Bolte, J. P., & Hill, D. T. (1990). A Monod-based model of attached-growth anaerobic fermenters. Biological Wastes, 31(4), 275–289. https://doi.org/10.1016/0269-7483(90)90085-7

Brink, H. G., Hörstmann, C., & Peens, J. (2019). Microbial Pb(II)-precipitation: the influence of oxygen on Pb(II)-removal from aqueous environment and the resulting precipitate identity. International Journal of Environmental Science and Technology, 17(1), 409–420. https://doi.org/10.1007/s13762-019-02502-4

Bueno, B. Y. M., Torem, M. L., de Carvalho, R. J., Pino, G. A. H., & de Mesquita, L. M. S. (2011). Fundamental aspects of biosorption of lead (II) ions onto a Rhodococcus opacus strain for environmental applications. Minerals Engineering, 24(14), 1619–1624. https://doi.org/10.1016/j.mineng.2011.08.018

Bueno, B. Y. M., Torem, M. L., Molina, F., & de Mesquita, L. M. S. (2008). Biosorption of lead(II), chromium(III) and copper(II) by R. opacus: Equilibrium and kinetic studies. Minerals Engineering, 21(1), 65–75. https://doi.org/10.1016/j.mineng.2007.08.013

Cai, Y., Li, X., Liu, D., Xu, C., Ai, Y., Sun, X., Zhang, M., Gao, Y., Zhang, Y., Yang, T., Wang, J., Wang, L., Li, X., & Yu, H. (2018). A Novel Pb-Resistant Bacillus subtilis Bacterium Isolate for Co-Biosorption of Hazardous Sb(III) and Pb(II): Thermodynamics and Application Strategy. International Journal of Environmental Research and Public Health, 15(4), 702. https://doi.org/10.3390/ijerph15040702

Chang, J.-S., Law, R., & Chang, C.-C. (1997). Biosorption of lead, copper and cadmium by biomass of Pseudomonas aeruginosa PU21. Water Research, 31(7), 1651–1658. https://doi.org/10.1016/s0043-1354(97)00008-0

Çolak, F., Atar, N., Yazıcıoğlu, D., & Olgun, A. (2011). Biosorption of lead from aqueous solutions by Bacillus strains possessing heavy-metal resistance. Chemical Engineering Journal, 173(2), 422–428. https://doi.org/10.1016/j.cej.2011.07.084

Colantonio, N., & Kim, Y. (2016). Lead(II) Removal at the Bioanode of Microbial Electrolysis Cells. ChemistrySelect, 1(18), 5743–5748. https://doi.org/10.1002/slct.201601539

Edris, G., Alhamed, Y., & Alzahrani, A. (2013). Biosorption of Cadmium and Lead from Aqueous Solutions by Chlorella vulgaris Biomass: Equilibrium and Kinetic Study. Arabian Journal for Science and Engineering, 39(1), 87–93. https://doi.org/10.1007/s13369-013-0820-x

Fan, T., Liu, Y., Feng, B., Zeng, G., Yang, C., Zhou, M., Zhou, H., Tan, Z., & Wang, X. (2008). Biosorption of cadmium(II), zinc(II) and lead(II) by Penicillium simplicissimum: Isotherms, kinetics and thermodynamics. Journal of Hazardous Materials, 160(2–3), 655–661. https://doi.org/10.1016/j.jhazmat.2008.03.038

Gabr, R. M., Hassan, S. H. A., & Shoreit, A. A. M. (2008). Biosorption of lead and nickel by living and non-living cells of Pseudomonas aeruginosa ASU 6a. International Biodeterioration & Biodegradation, 62(2), 195–203. https://doi.org/10.1016/j.ibiod.2008.01.008

Gallardo-Rodríguez, J. J., Rios-Rivera, A. C., & Von Bennevitz, M. R. (2019). Living biomass supported on a natural-fiber biofilter for lead removal. Journal of Environmental Management, 231, 825–832. https://doi.org/10.1016/j.jenvman.2018.11.004

Guha, H., Jayachandran, K., & Maurrasse, F. (2001). Kinetics of chromium (VI) reduction by a type strain Shewanella alga under different growth conditions. Environmental Pollution, 115(2), 209–218. https://doi.org/10.1016/s0269-7491(01)00108-7

Halttunen, T., Salminen, S., & Tahvonen, R. (2007). Rapid removal of lead and cadmium from water by specific lactic acid bacteria. International Journal of Food Microbiology, 114(1), 30–35. https://doi.org/10.1016/j.ijfoodmicro.2006.10.040

Hlihor, R. M., Roşca, M., Tavares, T., & Gavrilescu, M. (2017). The role of Arthrobacter viscosus in the removal of Pb(II) from aqueous solutions. Water Science and Technology, 76(7), 1726–1738. https://doi.org/10.2166/wst.2017.360

Hsueh, C.-C., Wu, C.-C., & Chen, B.-Y. (2019). Polyphenolic compounds as electron shuttles for sustainable energy utilization. Biotechnology for Biofuels, 12(1), 1391. https://doi.org/10.1186/s13068-019-1602-9

Jacob, J. M., Karthik, C., Saratale, R. G., Kumar, S. S., Prabakar, D., Kadirvelu, K., & Pugazhendhi, A. (2018). Biological approaches to tackle heavy metal pollution: A survey of literature. Journal of Environmental Management, 217, 56–70. https://doi.org/10.1016/j.jenvman.2018.03.077

Jeong, S.-W., Kim, H., Yang, J., & Choi, Y. (2019). Removal of Pb(II) by Pellicle-Like Biofilm-Producing Methylobacterium hispanicum EM2 Strain from Aqueous Media. Water, 11(10), 2081. https://doi.org/10.3390/w11102081

Kumar, R., Singh, L., Wahid, Z. A., & Din, M. F. M. (2015). Exoelectrogens in microbial fuel cells toward bioelectricity generation: a review. International Journal of Energy Research, 39(8), 1048–1067. https://doi.org/10.1002/er.3305

Kumari, S., Mahapatra, S., & Das, S. (2017). Ca-alginate as a support matrix for Pb(II) biosorption with immobilized biofilm associated extracellular polymeric substances of Pseudomonas aeruginosa N6P6. Chemical Engineering Journal, 328, 556–566. https://doi.org/10.1016/j.cej.2017.07.102

Leung, W. C., Chua, H., & Lo, W. (2001). Biosorption of Heavy Metals by Bacteria Isolated from Activated Sludge. Applied Biochemistry and Biotechnology, 91–93(1–9), 171–184. https://doi.org/10.1385/abab:91-93:1-9:171

Li, X., Liu, X., Bao, H., Wu, T., Zhao, Y., Liu, D., Li, X., Yang, T., & Yu, H. (2017). A Novel High Biosorbent of Pb-resistant Bacterium Isolate for the Removal of Hazardous Lead from Alkaline Soil and Water: Biosorption Isotherms In Vivo and Bioremediation Strategy. Geomicrobiology Journal, 35(3), 174–185. https://doi.org/10.1080/01490451.2017.1348405

Li, X., Xu, H., Gao, B., Shi, X., Sun, Y., & Wu, J. (2018). Efficient biosorption of Pb(II) from aqueous solutions by a PAH-degrading strain Herbaspirillum chlorophenolicum FA1. Journal of Industrial and Engineering Chemistry, 57, 64–71. https://doi.org/10.1016/j.jiec.2017.08.008

Lin, D., Ji, R., Wang, D., Xiao, M., Zhao, J., Zou, J., Li, Y., Qin, T., Xing, B., Chen, Y., Liu, P., Wu, Z., Wang, L., Zhang, Q., Chen, H., Qin, W., Wu, D., Liu, Y., Liu, Y., & Li, S. (2017). The research progress in mechanism and influence of biosorption between lactic acid bacteria and Pb(II): A review. Critical Reviews in Food Science and Nutrition, 59(3), 395–410. https://doi.org/10.1080/10408398.2017.1374241

Lin, Y.-H. (2013a). Modeling chromium(VI) reduction by Escherichia coli 33456 using ceramic pearl as a supporting medium. International Journal of Environmental Science and Technology, 11(7), 1887–1896. https://doi.org/10.1007/s13762-013-0392-z

Liu, C., Gorby, Y. A., Zachara, J. M., Fredrickson, J. K., & Brown, C. F. (2002a). Reduction kinetics of Fe(III), Co(III), U(VI), Cr(VI), and Tc(VII) in cultures of dissimilatory metal-reducing bacteria. Biotechnology and Bioengineering, 80(6), 637–649. https://doi.org/10.1002/bit.10430

Lu, W.-B., Shi, J.-J., Wang, C.-H., & Chang, J.-S. (2006). Biosorption of lead, copper and cadmium by an indigenous isolate Enterobacter sp. J1 possessing high heavy-metal resistance. Journal of Hazardous Materials, 134(1–3), 80–86. https://doi.org/10.1016/j.jhazmat.2005.10.036

Luo, J., Weber, F.-A., Cirpka, O. A., Wu, W.-M., Nyman, J. L., Carley, J., Jardine, P. M., Criddle, C. S., & Kitanidis, P. K. (2007). Modeling in-situ uranium(VI) bioreduction by sulfate-reducing bacteria. Journal of Contaminant Hydrology, 92(1–2), 129–148. https://doi.org/10.1016/j.jconhyd.2007.01.004

Mahar, F. K., He, L., Wei, K., Mehdi, M., Zhu, M., Gu, J., Zhang, K., Khatri, Z., & Kim, I. (2019). Rapid adsorption of lead ions using porous carbon nanofibers. Chemosphere, 225, 360–367. https://doi.org/10.1016/j.chemosphere.2019.02.131

Manasi, Rajesh, V., & Rajesh, N. (2014). Adsorption isotherms, kinetics and thermodynamic studies towards understanding the interaction between a microbe immobilized polysaccharide matrix and lead. Chemical Engineering Journal, 248, 342–351. https://doi.org/10.1016/j.cej.2014.03.022

Martín-Lara, M. A., Blázquez, G., Ronda, A., Rodríguez, I. L., & Calero, M. (2012). Multiple biosorption–desorption cycles in a fixed-bed column for Pb(II) removal by acid-treated olive stone. Journal of Industrial and Engineering Chemistry, 18(3), 1006–1012. https://doi.org/10.1016/j.jiec.2011.11.150

Mohamed, M. M., & Hatfield, K. (2005). Modeling microbial-mediated reduction in batch reactors. Chemosphere, 59(8), 1207–1217. https://doi.org/10.1016/j.chemosphere.2004.12.013

Mohapatra, R. K., Parhi, P. K., Pandey, S., Bindhani, B. K., Thatoi, H., & Panda, C. R. (2019). Active and passive biosorption of Pb(II)using live and dead biomass of marine bacterium Bacillus xiamenensis PbRPSD202: Kinetics and isotherm studies. Journal of Environmental Management, 247, 121–134. https://doi.org/10.1016/j.jenvman.2019.06.073

Muñoz, A. J., Espínola, F., & Ruiz, E. (2017). Removal of heavy metals by Klebsiella sp. 3S1. Kinetics, equilibrium and interaction mechanisms of Zn(II) biosorption. Journal of Chemical Technology & Biotechnology, 93(5), 1370–1380. https://doi.org/10.1002/jctb.5503

Nkhalambayausi-Chirwa, E. M., & Wang, Y.-T. (2004a). Modeling hexavalent chromium removal in aBacillus sp. fixed-film bioreactor. Biotechnology and Bioengineering, 87(7), 874–883. https://doi.org/10.1002/bit.20196

Pandey, A., Bera, D., Shukla, A., & Ray, L. (2007). Studies on Cr(VI), Pb(II) and Cu(II) adsorption–desorption using calcium alginate as biopolymer. Chemical Speciation & Bioavailability, 19(1), 17–24. https://doi.org/10.3184/095422907x198031

Peigney, A., Laurent, C., Flahaut, E., Bacsa, R. R., & Rousset, A. (2001). Specific surface area of carbon nanotubes and bundles of carbon nanotubes. Carbon, 39(4), 507–514. https://doi.org/10.1016/s0008-6223(00)00155-x

Preetha, B., & Viruthagiri, T. (2007). Bioaccumulation of chromium(VI), copper(II) and nickel(II) ions by growing Rhizopus arrhizus. Biochemical Engineering Journal, 34(2), 131–135. https://doi.org/10.1016/j.bej.2006.11.022

Schmieman, E. A., Yonge, D. R., Rege, M. A., Petersen, J. N., Turick, C. E., Johnstone, D. L., & Apel, W. A. (1998). Comparative Kinetics of Bacterial Reduction of Chromium. Journal of Environmental Engineering, 124(5), 449–455. https://doi.org/10.1061/(asce)0733-9372(1998)124:5(449)

Selatnia, A., Boukazoula, A., Kechid, N., Bakhti, M. Z., Chergui, A., & Kerchich, Y. (2004). Biosorption of lead (II) from aqueous solution by a bacterial dead Streptomyces rimosus biomass. Biochemical Engineering Journal, 19(2), 127–135. https://doi.org/10.1016/j.bej.2003.12.007

Seo, J. H., Kim, N., Park, M., Lee, S., Yeon, S., & Park, D. (2019). Evaluation of metal removal performance of rod-type biosorbent prepared from sewage-sludge. Environmental Engineering Research, 25(5), 700–706. https://doi.org/10.4491/eer.2019.201

Singh, S., Kumar, V., Datta, S., Dhanjal, D. S., Sharma, K., Samuel, J., & Singh, J. (2020). Current advancement and future prospect of biosorbents for bioremediation. Science of The Total Environment, 709, 135895. https://doi.org/10.1016/j.scitotenv.2019.135895

Somasundaram, V., Philip, L., & Bhallamudi, S. M. (2009). Experimental and mathematical modeling studies on Cr(VI) reduction by CRB, SRB and IRB, individually and in combination. Journal of Hazardous Materials, 172(2–3), 606–617. https://doi.org/10.1016/j.jhazmat.2009.07.043

Sulaymon, A. H., Ebrahim, S. E., & Mohammed-Ridha, M. J. (2012). Equilibrium, kinetic, and thermodynamic biosorption of Pb(II), Cr(III), and Cd(II) ions by dead anaerobic biomass from synthetic wastewater. Environmental Science and Pollution Research, 20(1), 175–187. https://doi.org/10.1007/s11356-012-0854-8

Sulaymon, A. H., Ebrahim, S. E., & M-Ridha, M. J. (2013). Competitive biosorption of Pb(II), Cr(III), and Cd (II) from synthetic wastewater onto heterogeneous anaerobic biomass in single, binary, and ternary batch systems. Desalination and Water Treatment, 52(28–30), 5629–5638. https://doi.org/10.1080/19443994.2013.813008

Tang, Y. J., Meadows, A. L., & Keasling, J. D. (2006). A kinetic model describingShewanella oneidensis MR-1 growth, substrate consumption, and product secretion. Biotechnology and Bioengineering, 96(1), 125–133. https://doi.org/10.1002/bit.21101

Tekerlekopoulou, A. G., Tsiflikiotou, M., Akritidou, L., Viennas, A., Tsiamis, G., Pavlou, S., Bourtzis, K., & Vayenas, D. V. (2013a). Modelling of biological Cr(VI)

removal in draw-fill reactors using microorganisms in suspended and attached growth systems. Water Research, 47(2), 623–636. https://doi.org/10.1016/j.watres.2012.10.034

Thacher, R., Hsu, L., Ravindran, V., Nealson, K. H., & Pirbazari, M. (2015a). Modeling the transport and bioreduction of hexavalent chromium in aquifers: Influence of natural organic matter. Chemical Engineering Science, 138, 552–565. https://doi.org/10.1016/j.ces.2015.08.011

Tran, H. N., & Chao, H.-P. (2018). Adsorption and desorption of potentially toxic metals on modified biosorbents through new green grafting process. Environmental Science and Pollution Research, 25(13), 12808–12820. https://doi.org/10.1007/s11356-018-1295-9

Wang, L., Yang, J., Chen, Z., Liu, X., & Ma, F. (2013). Biosorption of Pb(II) and Zn(II) by Extracellular Polymeric Substance (Eps) of Rhizobium Radiobacter: Equilibrium, Kinetics and Reuse Studies. Archives of Environmental Protection, 39(2), 129–140. https://doi.org/10.2478/aep-2013-0020

Wang, W., Feng, Y., Tang, X., Li, H., Du, Z., Yi, A., & Zhang, X. (2015). Enhanced U(VI) bioreduction by alginate-immobilized uranium-reducing bacteria in the presence of carbon nanotubes and anthraquinone-2,6-disulfonate. Journal of Environmental Sciences, 31, 68–73. https://doi.org/10.1016/j.jes.2014.11.005

WANG, X., XIA, S., CHEN, L., ZHAO, J., CHOVELON, J., & NICOLE, J. (2006). Biosorption of cadmium(II) and lead(II) ions from aqueous solutions onto dried activated sludge. Journal of Environmental Sciences, 18(5), 840–844. https://doi.org/10.1016/s1001-0742(06)60002-8

Wei, W., Wang, Q., Li, A., Yang, J., Ma, F., Pi, S., & Wu, D. (2016). Biosorption of Pb (II) from aqueous solution by extracellular polymeric substances extracted from Klebsiella sp. J1: Adsorption behavior and mechanism assessment. Scientific Reports, 6(1), 1282–1290. https://doi.org/10.1038/srep31575

Wu, L.-C., Tsai, T.-H., Liu, M.-H., Kuo, J.-L., Chang, Y.-C., & Chung, Y.-C. (2017). A Green Microbial Fuel Cell-Based Biosensor for In Situ Chromium (VI) Measurement in Electroplating Wastewater. Sensors, 17(11), 2461. https://doi.org/10.3390/s17112461

Xu, S., & Liu, H. (2011). New exoelectrogen Citrobacter sp. SX-1 isolated from a microbial fuel cell. Journal of Applied Microbiology, 111(5), 1108–1115. https://doi.org/10.1111/j.1365-2672.2011.05129.x

Yin, K., Wang, Q., Lv, M., & Chen, L. (2019). Microorganism remediation strategies towards heavy metals. Chemical Engineering Journal, 360, 1553–1563. https://doi.org/10.1016/j.cej.2018.10.226

Zhang, G., Sun, S., Yang, D., Dodelet, J.-P., & Sacher, E. (2008). The surface analytical characterization of carbon fibers functionalized by H2SO4/HNO3 treatment. Carbon, 46(2), 196–205. https://doi.org/10.1016/j.carbon.2007.11.002

Zhang, L., Zhao, L., Yu, Y., & Chen, C. (1998). Removal of lead from aqueous solution by non-living rhizopus nigricans. Water Research, 32(5), 1437–1444. https://doi.org/10.1016/s0043-1354(97)00348-5

Zhang, T. C., & Bishop, P. L. (1994). Density, porosity, and pore structure of biofilms. Water Research, 28(11), 2267–2277. https://doi.org/10.1016/0043-1354(94)90042-6

5.0 Conclusions

This study assessed the efficacy of CCNs as electrically conductive coatings in membrane filtration as well as the bacterial scaffolds in the bioremediation of Pb(II). First, CNTs were proposed to reduce membrane fouling while utilized in a CNT-PVA thin film composite. The focus of this was to establish the effects of PVA chain length and degree of crosslinking on the overall antifouling properties of the thin film. It was found that water permeance, hydrophilicity and conductivity were greatest using long chained PVA with crosslinking, making this combination a local optimum in the investigated DOE. The predictive models from the DOE exhibited a goodness of fit water permeance and conductivity, which further realized the stronger dependency permeance has on PVA MW and degree of crosslinking when compared to conductivity. Lastly, the pseudo-optimal CNT-PVA thin film composite further enhanced membrane rejection compared to the pristine PES membrane. Future work should look towards expanding the DOE to assess if there's a more optimal combination of PVA properties and to assess its antifouling properties through fouling studies.

The second portion of this study investigated the efficacy of different CCNs as bacterial scaffolds to enhance the bioremediation removal of Pb(II). CNF-COOH was the optimal conductive material in removing Pb(II), maintaining Pb(II) concentrations $\leq$0.1ppm over 18 cycles. Pb(II) removal was found to be further enhanced with higher Pb(II) concentration dosages and the experimental data suggested that Pb(II) bioreduction is the dominant Pb(II) removal mechanism in the CNF-COOH reactors. Future studies should look at using XPS and XRD to confirm this speculation and look towards optimizing operational conditions. (i.e. mixing conditions, temperature, pH, feed composition etc.) in a design of experiment format in the interest of improving the efficacy of the attached growth reactor in Pb(II) removal.

The last portion of this study looked at the efficacy of CNF attached growth reactors on long term Pb(II) removal under multiple dosages. A tangential goal was to construct a numerical model that can aid in the understanding of reactor's intrinsic mechanisms. The study showed that CNF attached growth reactors can remove Pb(II) long term under multiple Pb(II) dosages and outperformed control with only inoculum in the long run. The constructed model accurately predicted removal with an R^2 of 0.92 and supported the theoretical prediction that bioreduction governs removal in the CNF reactors. The model further captured the transient behaviour of Pb(II) as it transports through the biofilms, yielding a better understand of its fate among different cycles, and sensitivity analysis further realized the importance of Monod kinetics and biofilms thickness of Pb(II) removal. Overall, this study was successful in exemplifying the robustness of CNT attached growth reactors on long term Pb(II) removal and used numerical modelling to gain a better understanding of the system at hand that may aid in its further optimization.

Appendix A.1 – Supporting information for Optimizing a Carbon-Nanotube Poly(vinyl) Alcohol Thin Film Composite Through a Design of Experiments

The following section incorporates the results supporting the findings found in Section 2 of the thesis.

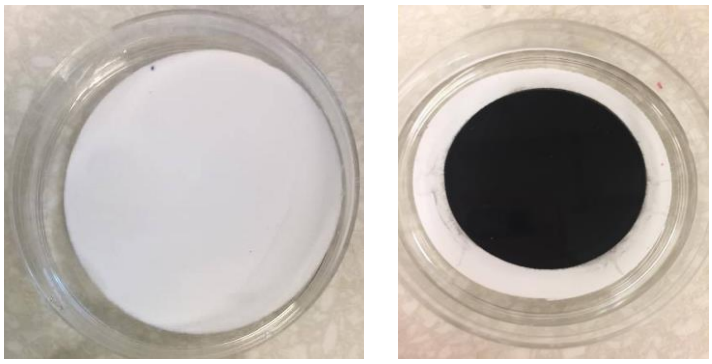

(a) (b)

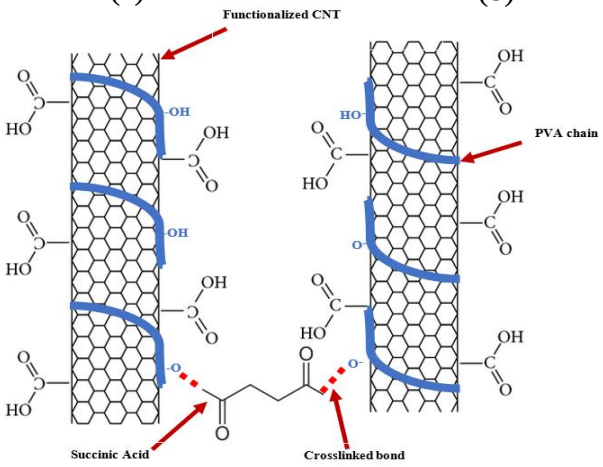

(c)

Figure S.1. (a) Pristine PES membrane, (b) PES membrane with a thin composite layer of CNT-PVA and (c) a schematic of the crosslinked CNT-PVA network with succinic acid.

Appendix A.2 – Supporting information for Conductive Carbonaceous Nanomaterials as Bacterial Scaffolds for in situ Bioreduction and Biosorption for Enhanced Pb(II) Removal

The following section incorporates the results supporting the findings found in Section 3 of the thesis.

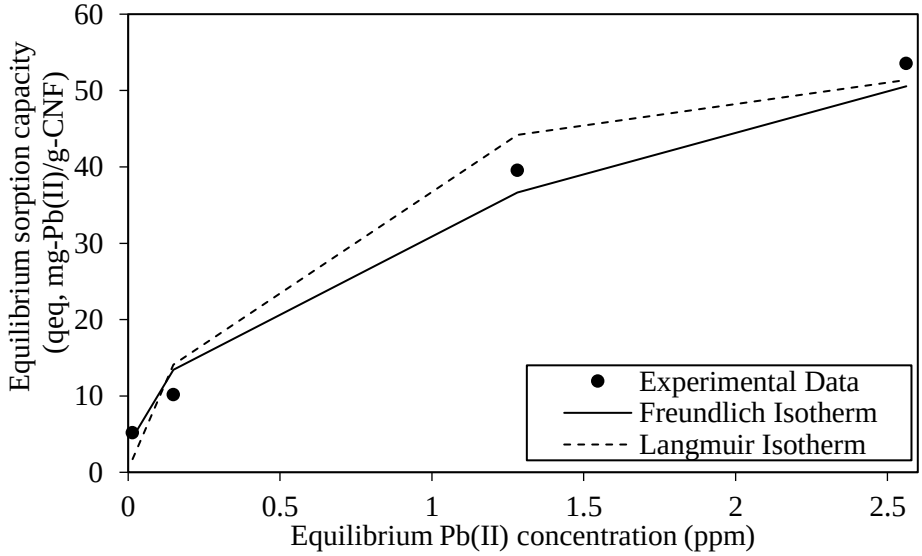

Figure S.2. Equilibrium sorption capacity (q_{eq}, mg-Pb(II)/g-CNF) as a function of equilibrium Pb(II) concentration (S_{eq}, ppm) for CNFs fitted with Langmuir and Freundlich isotherms.

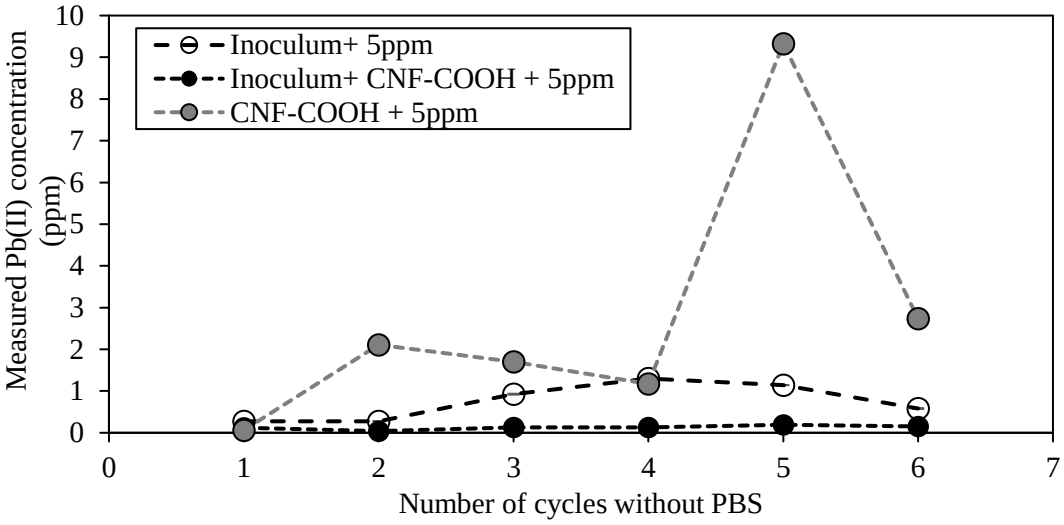

(a)

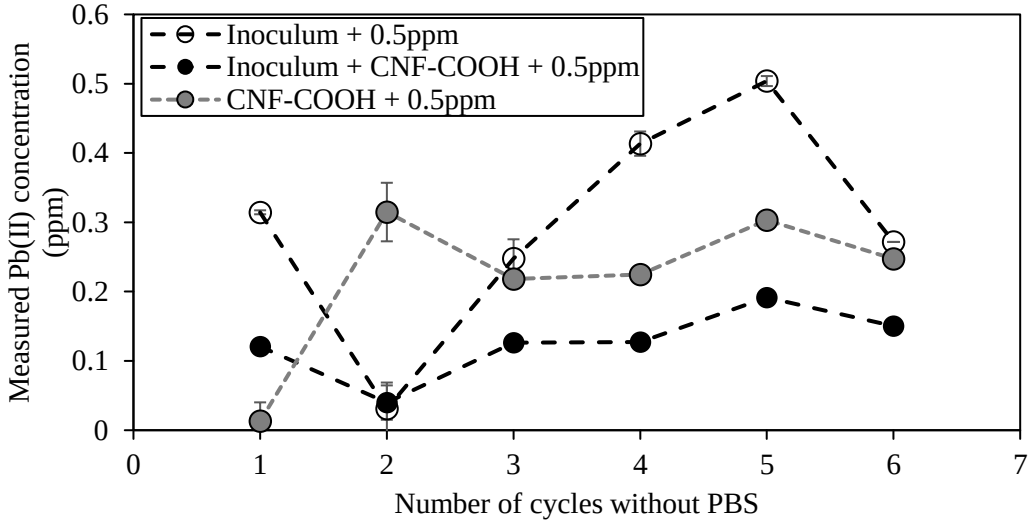

(b)

Figure S.3. Pb(II) concentration profile CNF reactors and controls without inoculum and without CNFs for (a) high Pb(II) concentration (5ppm) and (b) low Pb(II) concentration (0.5ppm). Error bars represent standard deviation.

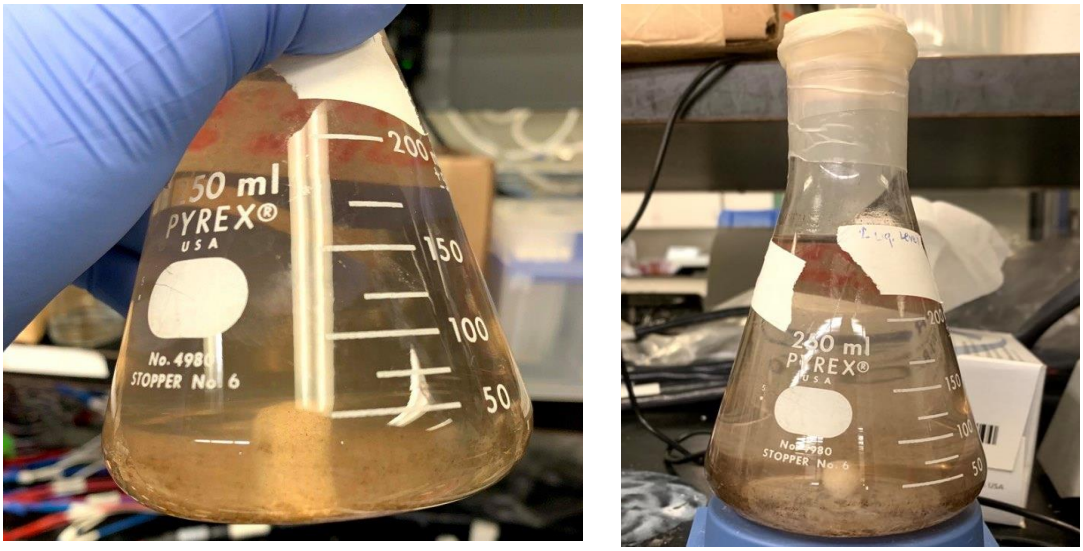

Figure S.4. The yellow and brown precipitates observed in the controls without CCNs.

Appendix A.3 – Supporting information for Modelling of Carbon Nanofiber Attached Growth Reactors as a Predictive Tool for Pb(II) Removal in Biofilms

The following section outlines supporting information generated for Chapter 4 of the thesis.

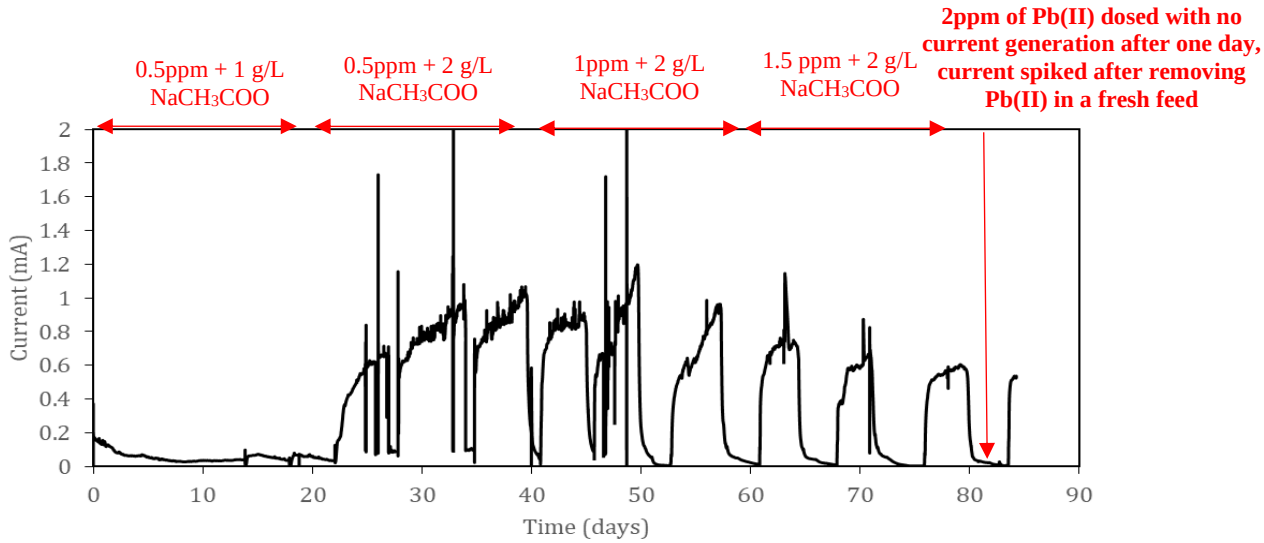

Figure S.5. Current generation in MEC reactor under different Pb dosages.

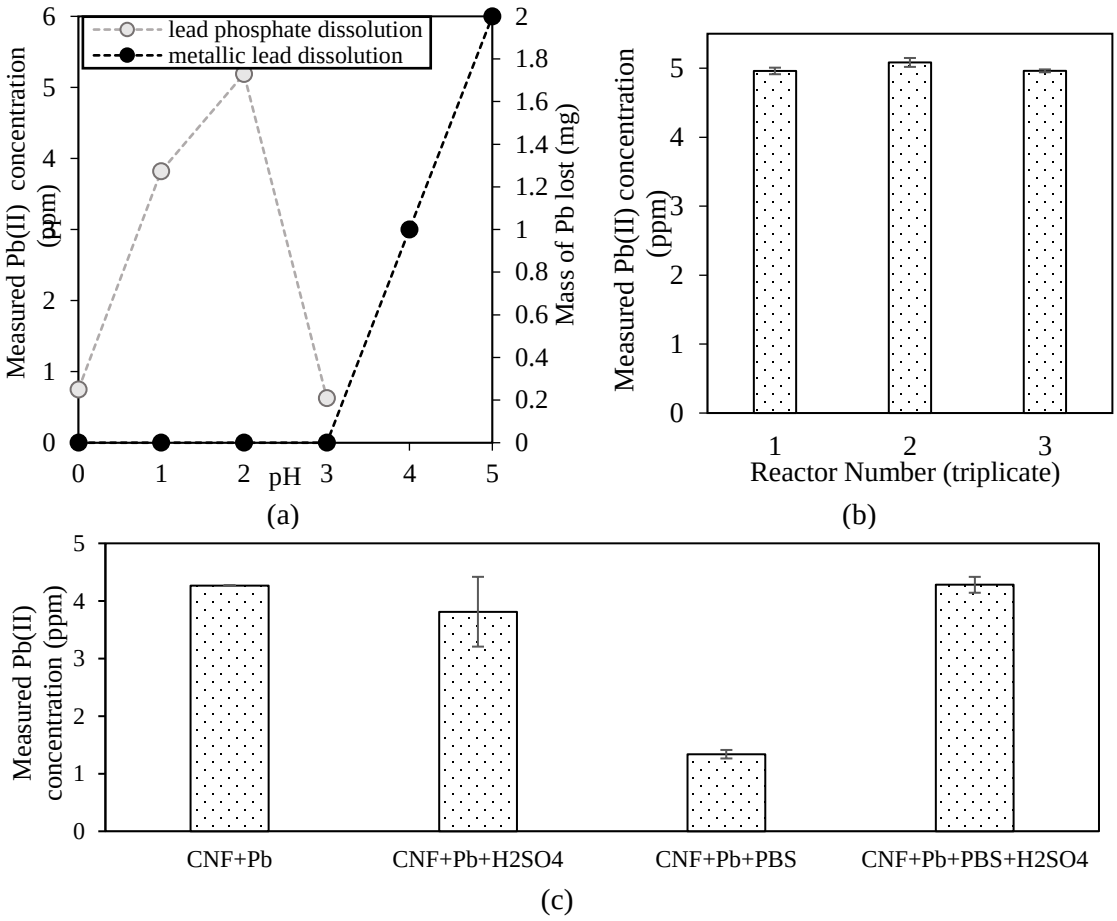

Figure S.6. (a) metallic lead and lead phosphate dissolution in sulfuric acid under different pH conditions, (b) measured lead concentration in triplicate reactors composed of lead and PBS and (c) lead concentration in reactors composed of different combinations Pb(II), CNF, PBS and sulfuric acid (pH = 2).

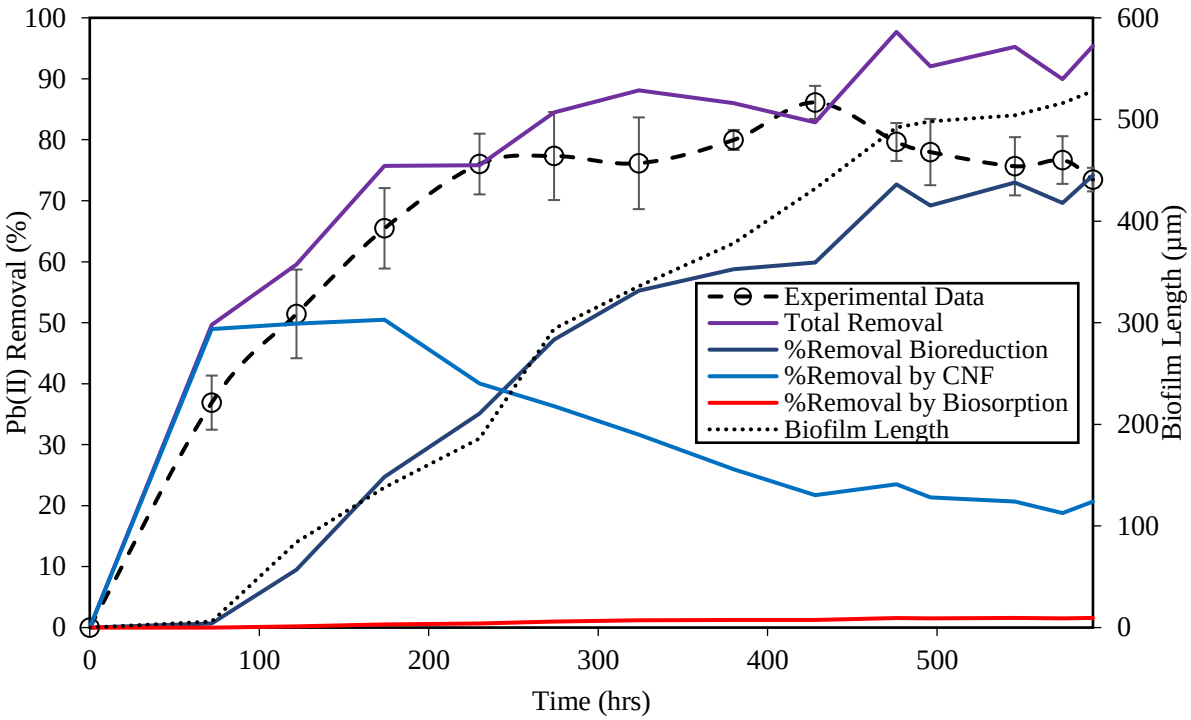

Figure S.7. Total removal found for CNF attached growth reactor and the associated theoretical prediction using a growing biofilm model and the percentage removal of individual mechanisms as a function of time (hrs).

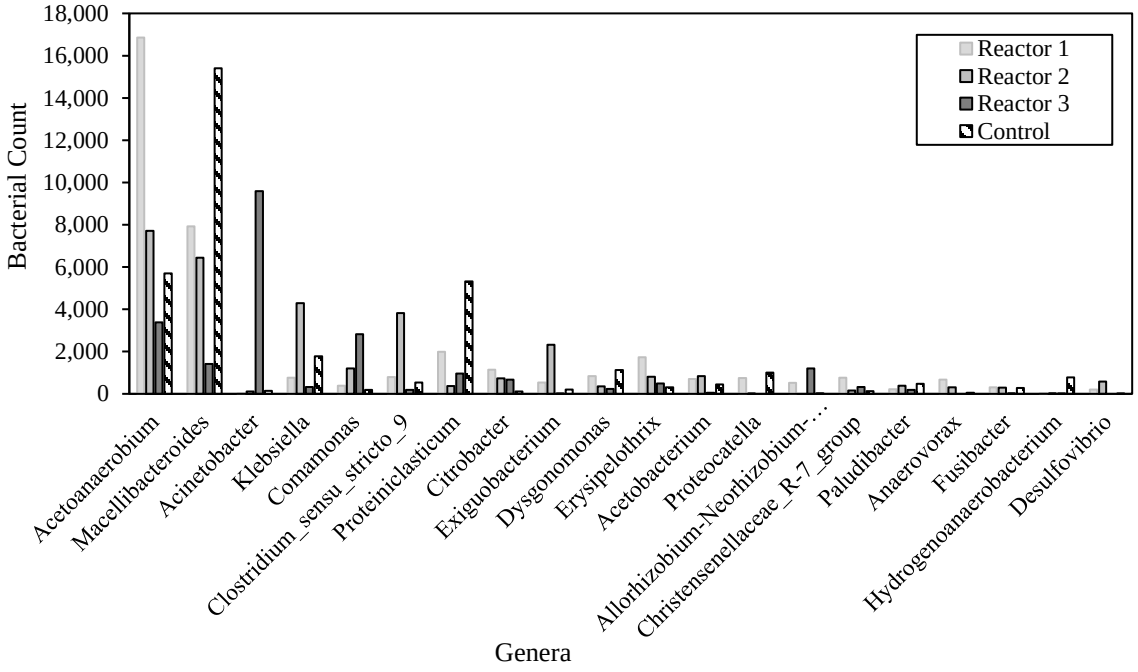

Figure S.8. The bacterial counts found for different genera found in the triplicate CNF reactor and the control with only inoculum.

Sample calculation for maximum cell concentration:

Assuming that a cell is a cube of a side length of1µm (L_{cell}), then the number of cells (n_{cell}) that can fit in the biofilm are:

$$n_{cell} = \frac{V_{biofilm}}{V_{cell}} = \frac{A_{CNF} \times L_{biofilm}}{L_{cell}^3} \quad \text{(A1)}$$

where $L_{biofilm}$ is the biofilm thickness (m) and A_{CNF} is the CNF surface area (m^2). By using the density of the cell (ρ_{cell}) the mass of an individual cell can be approximated as,

$$m_{cell} = \rho_{cell} \times L_{cell}^3 \quad \text{(A2)}$$

which can further me correlated to the total cell mass via using the number,

$$m_{cell,total} = \rho_{cell} \times L_{cell}^3 \times n_{cell} \quad \text{(A3)}$$

$$m_{cell,total} = \rho_{cell} \times L_{cell}^3 \times \frac{A_{CNF} \times L_{biofilm}}{L_{cell}^3} = \rho_{cell} \times A_{CNF} \times L_{biofilm} \quad \text{(A4).}$$

Using this total mass of cells, the maximum microbial concentration ($X_{maximum}$) simply reduces to the following,

$$X_{maximum} = \frac{m_{cell,total}}{V_{biofilm}} = \rho_{cell} \approx 1.03 \frac{g}{mL} \approx 1.03 \times 10^6 \frac{mg}{L} \quad \text{(A5).}$$